NASA CR-168134

ELECTRIC THRUSTER RESEARCH

Prepared for

LEWIS RESEARCH CENTER

NATIONAL AERONAUTICS AND SPACE ADMINISTRATION

GRANT NSG 3011

December 1982

Harold R. Kaufman and Raymond S. Robinson
Department of Mechanical Engineering
Colorado State University
Fort Collins, Colorado

1 Report No	2 Government Accession No	3 Recipient's Catalog No
NASA CR-168134		

4 Title and Subtitle	5 Report Date
Electric Thruster Research (U)	December 1982
	6 Performing Organization Code

7 Author(s)	8 Performing Organization Report No
Harold R. Kaufman and Raymond S. Robinson	
	10 Work Unit No

9 Performing Organization Name and Address	11 Contract or Grant No
Department of Mechanical Engineering Colorado State University Fort Collins, Colorado 80523	NSG 3011
	13 Type of Report and Period Covered
12 Sponsoring Agency Name and Address	Contr. Report
National Aeronautics and Space Administration Washington, DC 20546	14 Sponsoring Agency Code

15 Supplementary Notes

Contr. Manager, Vincent K. Rawlin
NASA Lewis Research Center
Cleveland, Ohio 44135

16 Abstract

It has been customary to assume that ions flow nearly equally in all directions from the ion production region within an electron-bombardment discharge chamber. In general, the electron current through a magnetic field can alter the electron density, and hence the ion density, in such a way that ions tend to be directed away from the region bounded by the magnetic field. When this mechanism is understood, it becomes evident that many past discharge chamber designs have operated with a preferentially directed flow of ions.

Thermal losses were calculated for an oxide-free hollow cathode At low electron emissions, the total of the radiation and conduction losses agreed with the total discharge power. At higher emissions, though, the plasma collisions external to the cathode constituted an increasingly greater fraction of the discharge power.

Experimental performance of a Hall-current thruster was adversely affected by nonuniformities in the magnetic field, produced by the cathode heating current The technology of closed-drift thrusters was reviewed. The experimental electron diffusion in the acceleration channel was found to be within about a factor of 3 of the Bohm value for the better thruster designs at most operating conditions Thruster efficiencies of about 0.5 appear practical for the 1000 to 2000 s range of specific impulse. Lifetime information is limited, but values of several thousands of hours should be possible with anode-layer thrusters operated ≤2000 s.

Several electric thrusters have been compared to chemical rockets for orbit-raising and in-orbit maneuvering applications. A performance gap exists between the specific impulse of an arcjet (∿1000 sec) and the minimum practical specific impulse of an electrostatic thruster (∿2000 sec). A high performance ($\eta \geq 0.5$) thruster in this specific impulse range, with minimal power processing requirements, would offer time-payload compromises intermediate of those possible with either the arcjet or the electrostatic thruster This gap could presumably be filled with a closed-drift thruster

17 Key Words (Suggested by Author(s))	18 Distribution Statement
Electric propulsion Ion sources Plasma physics	Unclassified - Unlimited

19 Security Classif (of this report)	20 Security Classif (of this page)	21 No of Pages	22 Price*
Unclassified	Unclassified		

* For sale by the National Technical Information Service Springfield Virginia 22161

NASA-C-168 (Rev 10-75)

N83-32843#

PREFACE

This annual report is divided into five sections. Each section is complete in itself. Most of these sections have been, or will be, presented as papers at conferences.

The first section is on ion flow in a multipole discharge chamber. Most of this section is identical to a paper presented previously.[1] A short appendix (Appendix A) has been added to show a more detailed mathematical basis for some of the statements in the paper. This section is believed to be of fundamental importance in explaining the variation of ion arrival rates at different discharge-chamber boundaries. Although the experiments were conducted with a multipole design, the ion-flow conclusions reached can be applied to many other configurations.

The second section is on hollow cathodes. A paper containing much of the information presented here was also presented elsewhere.[2] Because some of the information presented in the paper was also included in the last annual report of this grant,[3] this section was rewritten to emphasize the most recent work. In this work, the thermal evaluation of oxide-free hollow-cathode operation was carried out. The results presented also have application to operation of other hollow cathodes. That is, with emissive oxides present, there has always been considerable uncertainty regarding the work function of the emissive surfaces. With only relatively pure metals used, this uncertainty is essentially eliminated in the oxide-free design.

The third section covers an experimental investigation of a Hall-current thruster, which was also covered in a conference paper.[4] Although certain aspects of the performance presented can be compared favorably with the performance of gridded ion thrusters, the main conclusions concern the need for much greater circumferential uniformity, as well as other detailed changes.

The fourth section is a technology review of closed-drift thrusters, which is expected to be presented at an upcoming conference. Closed-drift is a currently used name for a class of electric thrusters that includes the Hall-current type. The information presented in this section supports the general conclusion that about 50% efficiency is possible in the 1000 to 2000 s range of specific impulse, with high thrust densities compared to gridded electrostatic thrusters, and with useful lifetimes of at least several thousands of hours.

In the fifth and last section a mission analysis is presented for near-earth orbit raising and maneuvering missions. This work was presented originally as a conference paper, and was only incidentally supported by this grant. The subject matter, however, is believed to be central to the electric thruster research presented herein, and it is therefore included. In general, a shift of emphasis from interplanetary to near-earth missions results in a corresponding decrease in the range of interest for specific impulses. The range of most interest in the near-earth environment appears to be about 1000 to 2000 sec.

This range is below what can be readily achieved with gridded ion thrusters. It is also above what can be achieved with electrothermal thrusters, except with hydrogen propellant at about 1000 s. Comparison of this performance need with the technology review of the previous section, indicates that closed-drift thrusters, or something similar, may dominate near-earth applications.

References

1. H. R. Kaufman, R. S. Robinson, and L. E. Frisa, "Ion Flow Experiments in a Multipole Discharge Chamber," AIAA Paper No. AIAA-82-1930, Nov. 1982.

2. R. P. Stillwell, R. S. Robinson, H. R. Kaufman, and R. K. Cupp, "Experimental Investigation of an Argon Hollow Cathode," AIAA Paper No. AIAA-82-1890, Nov. 1982.

3. H. R. Kaufman and R. S. Robinson, "Electric Thruster Research," NASA Contr. Rep. CR-165603, Dec. 1981.

4. G. M. Plank, H. R. Kaufman, and R. S. Robinson, "Experimental Investigation of a Hall-Current Thruster," AIAA Paper No. AIAA-82-1920, Nov. 1982.

5. H. R. Kaufman and R. S. Robinson, "Electric Thruster Performance for Orbit Raising and Maneuvering," AIAA Paper No. AIAA-82-1247, June 1982.

TABLE OF CONTENTS

ION FLOW EXPERIMENTS IN A MULTIPOLE DISCHARGE CHAMBER

Abstract

It has been customary to assume that ions flow nearly equally in all directions from the ion production region within an electron-bombardment discharge chamber. Ion flow measurements in a multipole discharge chamber have shown that this assumption is not true. In general, the electron current through a magnetic field can alter the electron density, and hence the ion density, in such a way that ions tend to be directed away from the region bounded by the magnetic field. When this mechanism is understood, it becomes evident that many past discharge chamber designs have operated with a preferentially directed flow of ions.

Introduction

The efficiency of an ion thruster used for electric space propulsion is an important parameter. The discharge loss (the power used to generate beam ions) is the major loss involved in this efficiency. A reduction of discharge loss, then, can be translated directly into an increase in thruster efficiency.

Discharge loss correlations have indicated that, for similar utilization conditions, the volume production cost for ions is roughly constant.[1] This means that discharge losses can be reduced by extracting a larger fraction of the ions produced. It has been generally assumed that, for normal operation, ions tend to flow nearly equally in all directions. According to this assumption, the fraction of ions that is extracted into the ion beam is determined by the ratio of the extraction area to the total surface area surrounding the ion production region. The fraction of ions that is extracted can therefore be enhanced by using a discharge chamber with a depth that is small compared to the beam diameter. A reduction in discharge-chamber depth, however, can be constrained by a need for high propellant utilization.

The fraction of ions extracted could be increased without compromising the propellant utilization if the discharge chamber walls could be configured so that the ion flow to the walls were reduced. A larger chamber depth could then be used to increase the probability of ionization, without a corresponding increase in ion loss to the walls.

An ion containment mechanism has been proposed in the past, and sufficiently low discharge losses were obtained in some designs to

indicate that some form of ion containment might have been obtained.[2,3] But the mechanism proposed depended on anodes being biased positive of the plasma to "reflect" ions. Further, subsequent experiments have failed to show any significant decrease in discharge losses for a multipole design when the anodes were biased positive relative to the discharge plasma.[4]

A detailed study is presented herein of the effects of various operating parameters on the ion flow within a multipole discharge chamber. Although a multipole chamber is used, some of the results are applicable to more general containment configurations.

Apparatus and Procedure

The thruster used herein is rectangular in shape and has been described in previous publications.[5,6] The rectangular shape of this thruster made it well suited to changes of the anode and magnetic pole-piece configuration. The description herein will be limited to those aspects directly involved in the experiments.

A cross section of the thruster used is shown in Fig. 1. The internal dimensions of the discharge chamber (circumscribed by the screen grid and pole pieces) were 7.5 cm deep, 10 cm wide, and 45 cm long. (The 45 cm dimension is normal to the page in Fig. 1.) There were no pole pieces at the ends of the discharge chamber. The ion beam extraction area was 5 × 40 cm, with a 58% open screen grid within this area. The small size of the extraction area, relative to the overall length and width of the chamber, resulted in a large discharge loss per extracted ion. But the distribution of the various losses within the chamber were of more interest in this investigation than the actual magnitudes of the measured discharge losses per extracted ion. The design, although not optimized for efficiency was well suited to the types of experiments required.

The magnetic field integrals for the back anodes were tested at mean values from about 70-240 × 10^{-6} T-m (70-240 Gauss-cm). The side anodes (three on each side in Fig. 1) were operated at mean values from 50-60 × 10^{-6} T-m in all tests.

Several anode bias arrangements were tested. The arrangement of most interest herein was with the six side anodes connected directly to the discharge power supply, and the four back anodes operated at various degrees of positive bias relative to the side anodes. Some tests were also conducted with two of the back anodes held at cathode potential so that they were not conducting discharge current.

A variety of probes was used to determine properties of the discharge plasma and ion arrival rates at each class of surfaces within the discharge plasma. Bulk plasma properties were obtained with a Langmuir probe, while a planar probe was used to independently evaluate Bohm current density within the bulk discharge plasma. Because the planar

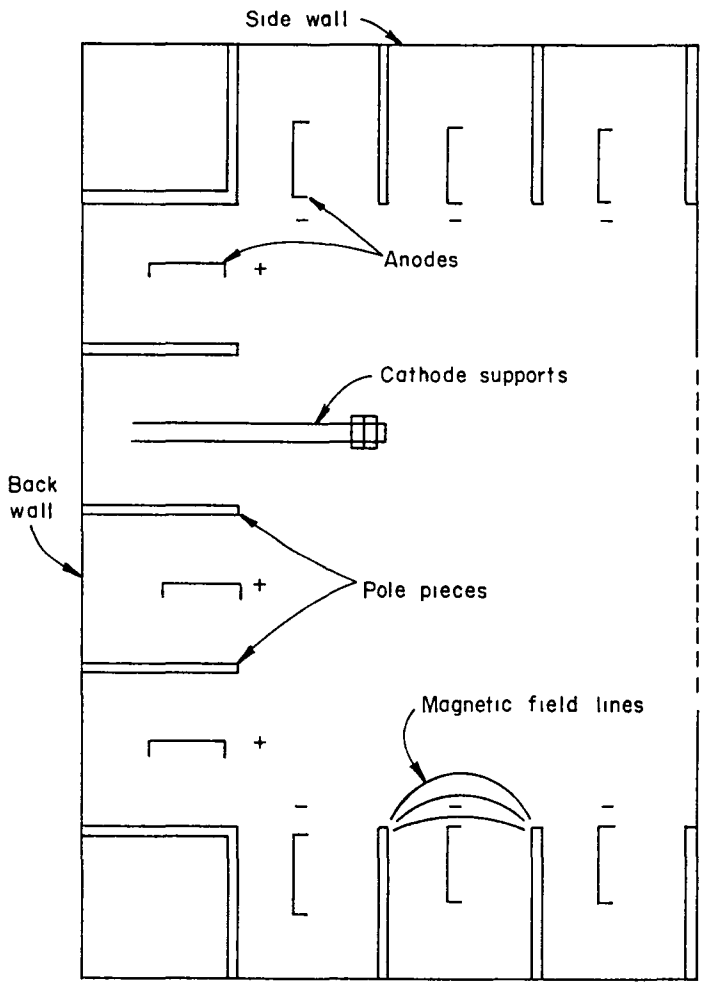

Fig. 1. Discharge chamber cross section.

probe provided a direct measurement of Bohm ion current density, it was felt to be more reliable than the ∿30% higher value indirectly calculated from the electron temperature and plasma density obtained from Langmuir probe data for similar but not identical operating conditions. Conformal probes, insulated with layers of polyimide, were used to measure ion arrival rates to various surfaces.

The discharge voltage was held constant at 40 V. The propellant was argon, with the flow maintained at 472 mA-equiv. Due to the back-flow from the $\sim 4 \times 10^{-4}$ Torr facility environment, the effective flow was higher. The discharge currents of 1-9 A corresponded to low utilizations up to approximately the "knee" of the discharge loss curve.

Experimental Results

Typical results of anode bias tests are shown in Fig. 2 for a back anode magnetic integral of 118×10^{-6} T-m. Measurements of the plasma potential during these tests showed that it was substantially independent of the back anode potential. Thus, for biases greater than 2-5 V, the back anodes were more positive than the plasma potential. Despite the positive potential of the back anodes, no evidence of "ion reflection" was found. Instead, the discharge loss increased monotonically with bias potential.

Increasing the magnetic integral for the back anodes to 241×10^{-6} T-m effectively eliminated the spread due to back anode bias, as indicated in Fig. 3. Although the adverse effects of anode bias were eliminated by the higher magnetic integral, there were still no beneficial effects to be observed from such a bias.

It is also evident from a comparison of Figs. 2 and 3, that the discharge loss at zero bias (all anodes at the same potential) was significantly reduced by the higher magnetic integral. This improvement was probably due in part to the better containment of energetic electrons by the stronger field. It was probably also due to the stronger field extending farther from the pole pieces, thus confining ion generation to a volume closer to the ion optics.

The discharge power during biased operation could be separated into what might be termed "productive" and "biased-anode" portions. The productive power was defined as the discharge current times the discharge voltage. The biased-anode power was the current to the back (biased) anodes times the bias voltage. Because the plasma potential did not change significantly with bias voltage, this biased-anode power must have been dissipated in the magnetic fields near the back anodes. Further, studies of the diffusion processes involved indicate that most of the bias potential difference appears close to the anodes involved.[7] The power for biasing the back anodes is therefore believed to contribute little to the generation of ions that reach the ion optics.

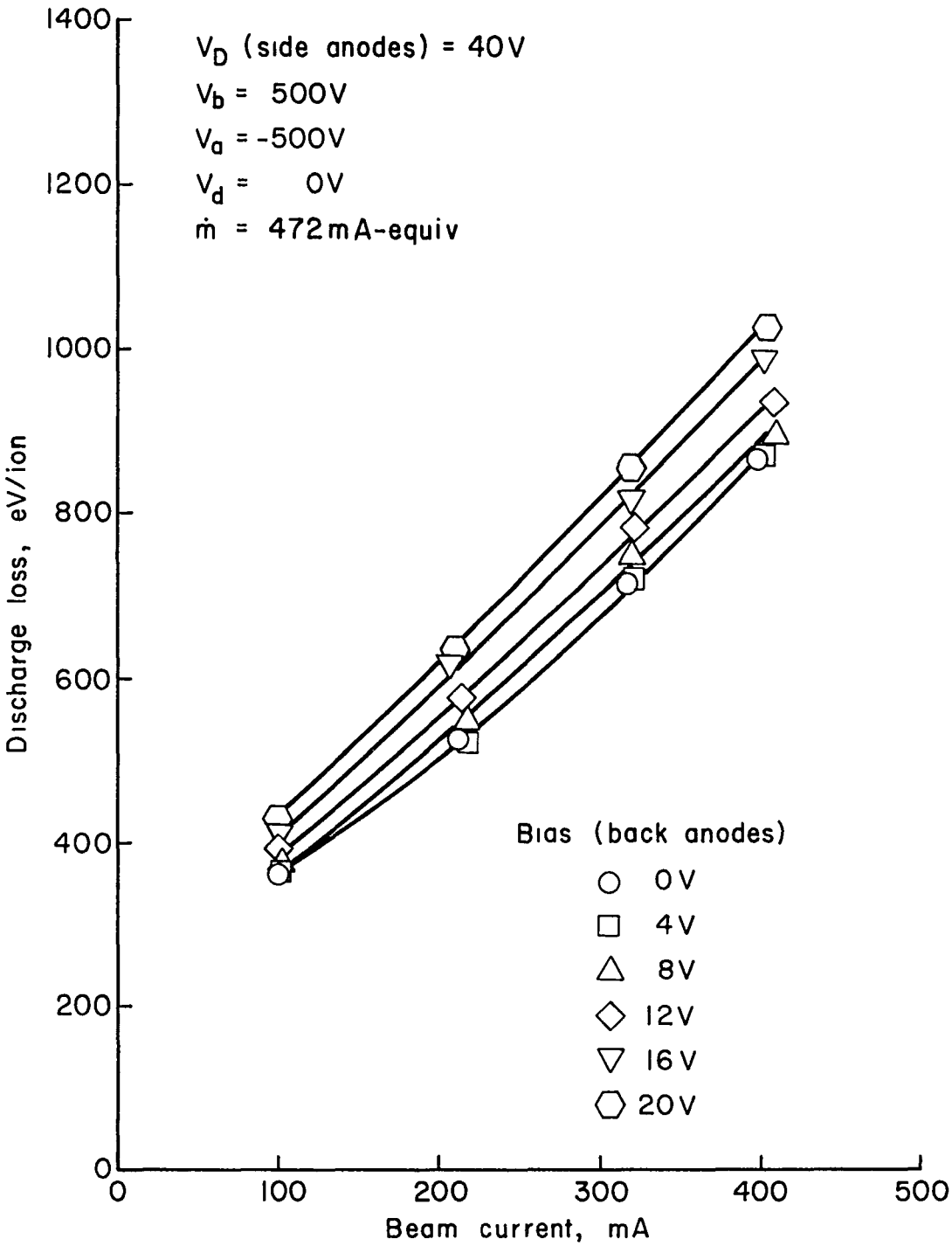

Fig. 2. Discharge loss versus beam current for a back anode magnetic integral of 118 × 10^{-6} T-m.

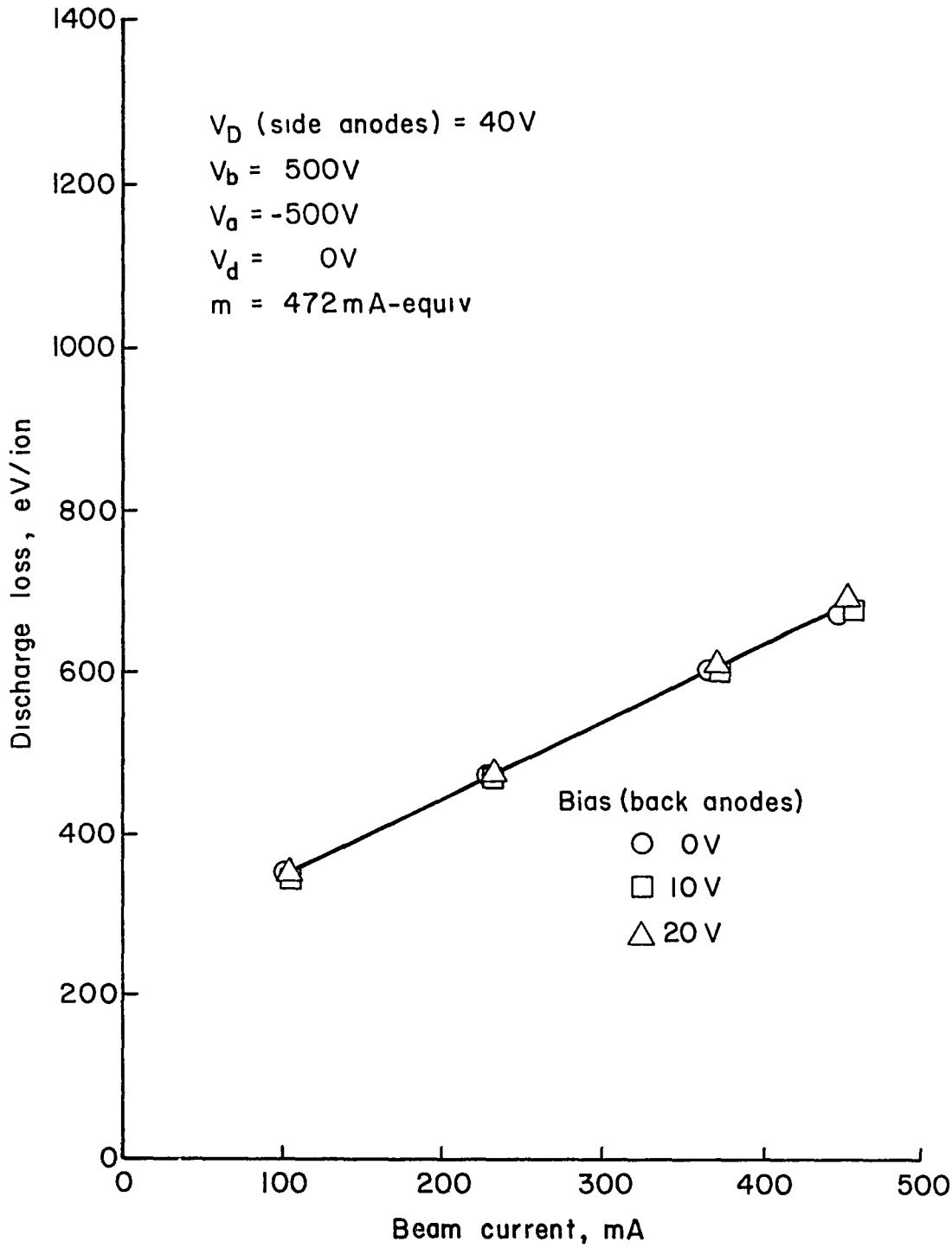

Fig. 3. Discharge loss versus beam current for a back anode magnetic integral of 241 × 10^{-6} T-m.

When the biased-anode power is subtracted from the total discharge power, the data of Fig. 2 are reduced to a single line for all bias voltages. This indicates that the major effect of biasing is to dissipate additional power near the anodes being biased.

The same calculation for the large magnetic integral of Fig. 3 does not result in any noticeable change. That is, the larger magnetic integral resulted in much smaller power being associated with the anode biasing, so that the subtraction of this power did not significantly affect the appearance of the data.

From the data of Figs. 2 and 3, together with the above calculation concerning biased-anode power, it was concluded that biasing anodes positive relative to the discharge plasma was not effective in lowering the discharge power requirement for production of a given current of beam ions. Other bias experiments were also conducted with this rectangular thruster, and are reported in detail elsewhere.[8]

The wide range of magnetic integrals and biases used for the back anodes also provided a systematic investigation of electron diffusion through a multipole magnetic field. A previous study indicated that small electron currents through the magnetic field are accommodated by density-gradient diffusion, and larger currents results in the establishment of a potential difference to the low-density end of the density-gradient region near the anode.[7] From this previous study, an effective magnetic integral was defined as

$$(\int Bdx)_{eff.} = \int Bdx - (\int Bdx)_{therm.} - (\int Bdx)_{\Delta V} . \qquad (1)$$

In this definition, $\int Bdx$ is the total magnetic integral between the anode and the plasma discharge; $(\int Bdx)_{therm.}$ is the field integral to which an electron at the most probable thermal velocity can penetrate (corresponding to two cyclotron radii); and $(\int Bdx)_{\Delta V}$ is the magnetic integral that can be crossed by an initially motionless electron due to a potential difference of ΔV, in this case assumed to be the bias potential. This definition of net magnetic integral is consistent with the assumptions found previously to agree best with experimental measurements of electron diffusion.[7] That is, the electron current should be determined by density-gradient diffusion over the net magnetic integral.

The electron diffusion data were correlated by using this net magnetic integral, as indicated in Fig. 4. The fraction of the discharge current conducted by the back anodes, J_b/J_d, clearly varied in an inverse manner with the value of the magnetic integral. Another result was the initial rapid increase in anode current with bias voltage, followed by a leveling off, or saturation, at higher values of bias voltage. This saturation would be expected from the diffusion model used. The slow approach to saturation in Fig. 4, however, indicates

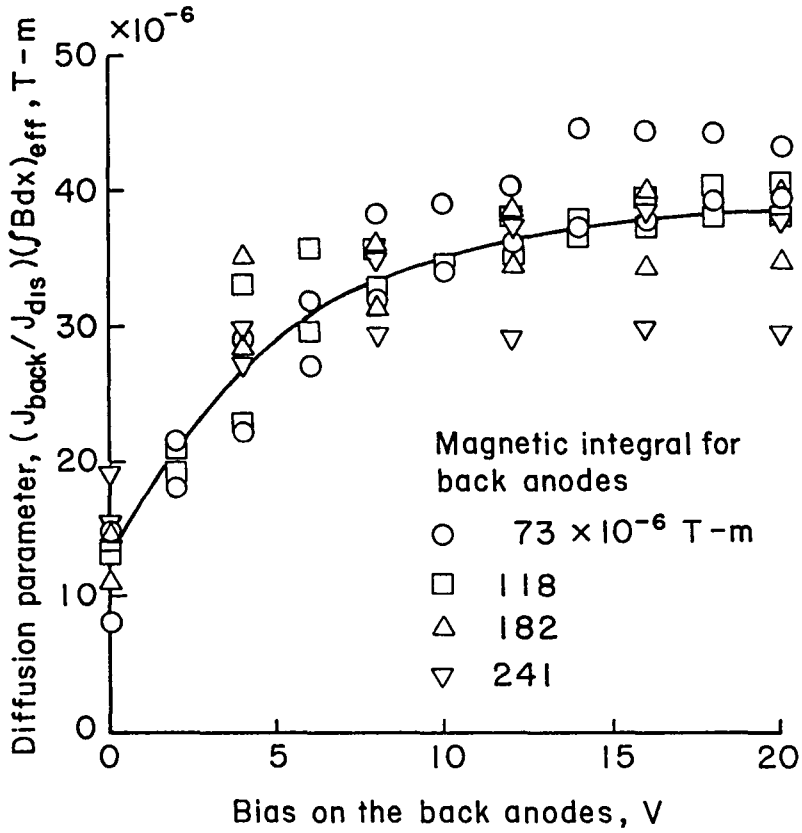

Fig. 4. Correlation of back anode current ratio as a function of bias voltage using the effective magnetic field integral

that there is some blending of the density-gradient and potential-difference diffusion processes.

To better understand what was happening in the discharge chamber, surface probes were used to evaluate ion flows to various discharge chamber surfaces. A detailed evaluation at pole piece surfaces gave the results indicated in Fig. 5. The peak ion current density was found on the exposed edges of the pole pieces, with a current density value at this location close to the Bohm value in the bulk of the discharge plasma. When averaged over the equivalent boundary, indicated by the dashed line in Fig. 5, the ion arrival rate corresponded to only about one-fourth of the Bohm value. This arrival rate was nearly constant ($\sim$0.21-0.26) regardless of discharge current or positive anode bias.

The ion arrival at the anode surface was also investigated. To obtain an ion current, the anode probe required a negative bias to near cathode potential. Because the probe covered a section of the anode about 0.5 cm long, this large negative potential may have been a significant disturbance on local ion flow. The measured ion flow, about one-third of that to a pole piece, should therefore be considered the upper limit of the possible ion flow during normal operation.

Using ion flow measurements from a number of probes on different discharge chamber surfaces, it was possible to estimate the total ion production. Within experimental accuracy, the total ion production was a function only of discharge current. As mentioned earlier, the propellant flow and discharge voltage were held constant, so that the range of discharge current corresonded to a utilization range up to approximately the "knee" of the discharge loss curve. The volume production cost increased monotonically from about 53 eV/ion at a 1 A discharge to about 77 eV/ion at 9 A.

The extraction efficiency of the ion optics also varied, so that energy per extracted ion varied over a larger ratio. Based on the Bohm current density and the screen open area, the extraction efficiency decreased from about 86% at a 1 A discharge to about 65% at 9 A. The 45% increase in volume ion cost over this discharge current range was thus translated into almost a doubling of loss for extracted ions. It should also be noted that the relatively low maximum value of extraction efficiency, 86%, is believed the result of a fairly thick screen grid, 0.51 mm compared to a screen-hole diameter of 2.0 mm.

Tests were also conducted with two back anodes held at cathode potential to determine the effect on ion flow. With an anode switched to cathode potential, the ion losses to that anode and the associated pole pieces were about double the ion losses with an operating anode. Most of this increase was due to increased ion arrival at the anode. This large increase in ion loss with an anode set at cathode potential was also the reason for suspecting that a macroscopic probe at cathode potential on an operating anode would give excessively high ion currents.

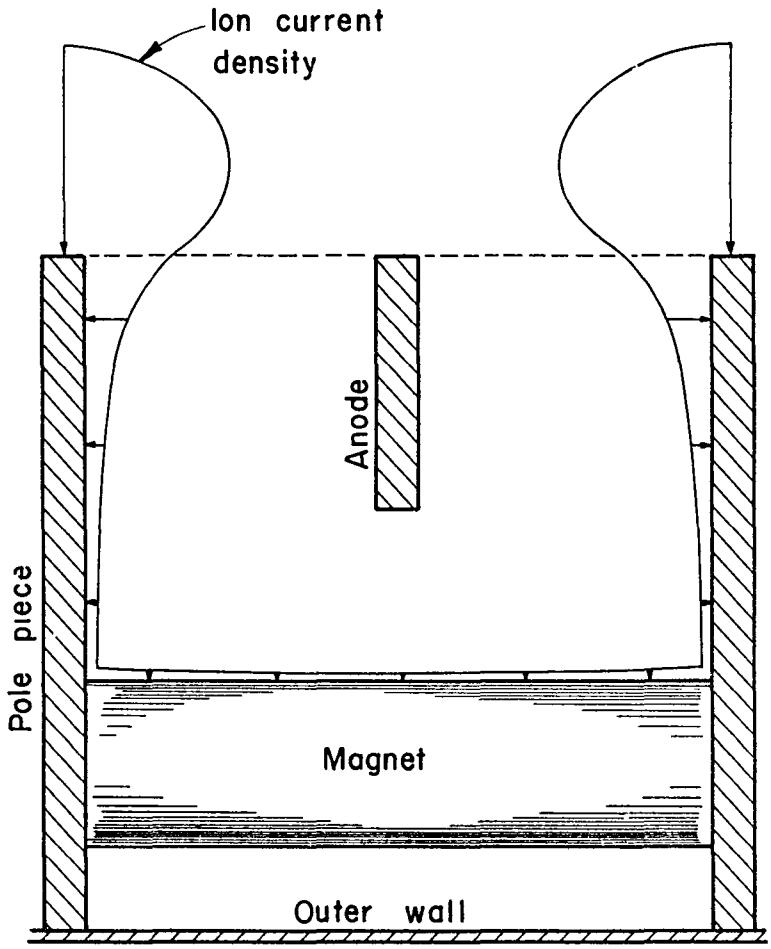

Fig. 5. Ion arrival rate in multipole configuration (length of arrows indicates magnitude of arriving ion current density).

From the ion arrival rates with both operating and cathode-potential anodes, it is clear that an operating anode directs much of the local ion flow away from that anode. From the anode-bias tests, the exact level of electron current to an operating anode appears to be unimportant in determining this preferential ion flow. But effectively stopping the electron current by reducing the anode to cathode potential stopped much of the preferential ion flow.

It should be noted that the ion losses for an anode at cathode potential did not rise to Bohm value when averaged over the local boundary area, but, instead to only about half of that value. Only two anodes were switched at a time because the discharge could not be maintained with a greater number of anodes not conducting discharge current. It might therefore be hypothesized that the ion flow to an inoperative anode represented a compromise solution with adjacent operating anodes.

Proposed Ion Flow Model

From the preceding experimental results, it should be clear that the preferential flow of ions toward the ion optics can exist as a part of normal operation in a multipole discharge chamber. It is important that the cause of this preferential flow be understood.

The flow outward from a region of ion production in an otherwise field-free plasma is a well understood phenomenon. Some review of this process will be useful for the subsequent discussion of how the ion flow can be altered.

The potential distribution in the discharge plasma is determined by Poission's equation,

$$\nabla^2 V = -\rho/\varepsilon_o \ , \tag{2}$$

where ρ is the local charge density and ε_o is the permittivity of free space. Although three dimensions are involved in real problems, the important concepts can be demonstrated with variations in only one dimension. In one dimension, Poisson's equation is

$$d^2V/dx^2 = -\rho/\varepsilon_o \ . \tag{3}$$

Assuming free access of electrons to all parts of the plasma, the electron density will be of the form

$$n_e \propto \exp(eV_p/T_e) \ , \tag{4}$$

where e is the absolute electronic charge, V_p is the local plasma potential, and T_e is the electron temperature in eV. The mean free paths of the ions are normally large compared to discharge chamber dimensions. The ions therefore follow conservative paths with local velocity determined by the local plasma potential. Assuming negligible initial velocity when an ion is created from a neutral, which is reasonable for typical neutral temperatures, and defining plasma potential, V_p, so that zero is the effective origin potential of the ions, the ion density for flow in one dimension is of the form

$$n_i \propto j_i/(-V_p)^{1/2} \ , \tag{5}$$

where j_i is the local ion current density. In practice, the ions do not originate at a single potential. There is, however, a narrow enough spread in origin potential that the density expression given above is a reasonable approximation outside of the ion production region.

Now consider a region of ion production, with drift spaces and negative-potential surfaces to reflect electrons on both sides of this production region, as indicated in Fig. 6. Within the ion production region, the newly created ions with negligible initial velocity will result in a positive net charge density. From Eq. (3), a positive net charge density will result in a negative value for d^2V/dx^2, hence a concave-downward potential variation in the ion production region. This potential variation serves to direct ions outward toward the bounding negative-potential surfaces. The negative surfaces will attract the ions and potential disturbances will propagate back toward the ion generation region, thereby establishing the ion velocity in the drift region. The equilibrium condition is one in which the ions are moving at the propagation velocity for a potential disturbance, so that disturbances can no longer propagate back toward the ion production region. This velocity can be found by equating the electron and ion densities. The resulting equation is differentiated with respect to plasma potential, then solved for the value of plasma potential that will permit plasma neutrality to be observed for small variations of potential about this value. This value of plasma potential is

$$V_p = -T_e/2e \ , \tag{6}$$

which is, of course, both the energy per unit charge associated with ion acoustic velocity and the minimum ion approach velocity for a stable sheath solution.

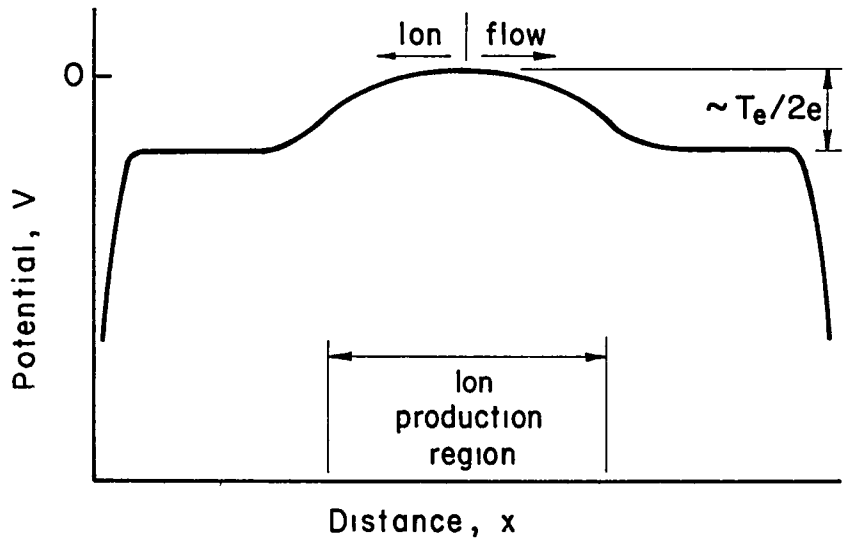

Fig. 6. Schematic variation of plasma potential with localized ion production region.

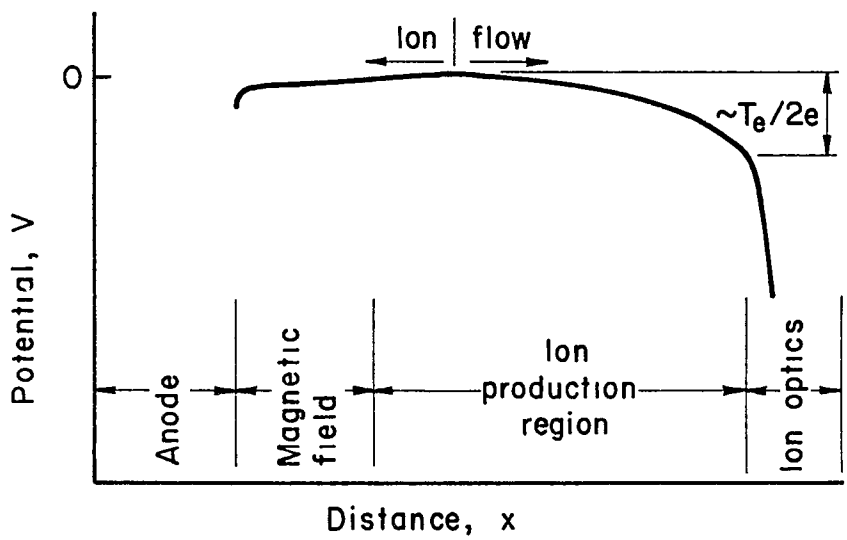

Fig. 7. Approximate variation of plasma potential through multipole discharge chamber.

The plasma potential in the drift regions is therefore established as $-T_e/2e$. With plasma neutrality at this potential, examination of Eqs. (4) and (5) will show that the net charge density of the plasma will be positive for $V_p < -T_e/2e$. Hence, the potential variation will be concave-downward for $V_p < -T_e/2e$. For $V_p > -T_e/2e$, one might also expect a positive net charge density and a concave-downward curvature. But as the ion-production region is entered, J_1 in Eq. (5) is reduced and a net negative charge density and a concave-upward curvature are both permitted. These shapes are shown for the potential variation in Fig. 6, and have been described by Dunn and Self.[9]

Although large drift regions are indicated in Fig. 6, the same approach velocity will be established at a plasma sheath, as long as the sheath thickness is small compared to the dimensions of the ion production region. In other words, as long as the ion production is negligible within the sheath.

Consider next the one-dimensional representation of a multipole discharge chamber in Fig. 7. The anode is on the left. The magnetic field near the anode comes next, followed by the ion production region. On the right the potential drops sharply for the plasma sheath at the ion optics. From the discussion in connection with Fig. 6, it should be evident that the ion velocity at the edge of the ion-optics sheath is the ion acoustic velocity.

The conditions near the anode differ sharply from those near the ion optics. There is a magnetic field region, with an electron current to the anode through this field. Consider first the consequences of assuming that the approach velocity of ions to the magnetic field is the ion acoustic velocity. With the magnetic integrals used in most multipole designs, the ions will pass through the magnetic field, essentially unimpeded. Equation (5) may therefore be used for ion density. The electron flow, however, is impeded by the magnetic field. Within the magnetic field, then, the electron density will always be less than that given by Eq. (4). The appropriate constants for Eqs. (4) and (5) can be determined outside of the magnetic field region from the requirement for neutrality in the plasma approaching the ion optics at ion acoustic velocity. Given these constants, it can be shown that no plasma potential will permit plasma neutrality if: (1) the current density of ions, j_1, is the same as at the ion optics, and (2) the electron density is reduced from that given by Eq. (4). Having assumed ion acoustic velocity for the approach to the magnetic field, (1) must be true. However, the extent of the magnetic field is sufficient that neutrality must be observed within this region. If electron and ion densities cannot be equal, then the assumption of ion acoustic velocity for the approach to the magnetic field cannot be valid.

The velocity of ions approaching the magnetic field cannot be greater than ion acoustic velocity, because the required plasma neutrality could not be obtained with a net charge density always greater than zero. Thus only an approach velocity less than ion acoustic velocity can be considered for a steady-state solution.

Experimentally, it is known that there are no large potential variations in the magnetic field region, with the possible exception of the sheath close to the anode. It is also known that the electron density must vary by a large amount in this region to account for the observed diffusion of electrons.[7] From quasi-neutrality, the ion density must vary in a similar manner. For the ion density to drop sharply as the anode is approached, the ion velocity must be greatly increased (see Eq. (5)). At the same time, after being increased, it must still be below the ion acoustic value. These conditions can only be met if the ion approach velocity to the magnetic field is small compared to the ion acoustic velocity.

Returning to Fig. 7, if the ion approach velocity to the magnetic field is small compared to ion acoustic velocity, then the potential maximum in the ion production region must be located close to the magnetic field. As a consequence, most of the ions generated in the bulk plasma must be directed away from the magnetic field and the anode.

If the particular anode portrayed in Fig. 7 is assumed to be made inoperative by reducing it to cathode potential, the process will be drastically changed. Because there would be no significant flow of electrons through the magnetic field, the electron density would again agree with Eq. (4). The mechanisms for establishing ion acoustic velocity would then be operative and the potential maximum would shift to divide more equally the flow of the ions that are generated. We can now return to the requirement for plasma neutrality within the magnetic-field region. With fewer ions directed toward the magnetic field, the value of j_i in Eq. (5) must be reduced near the magnetic field, in comparison with the value near the ion optics. This reduction in ion current density makes possible the matching of ion density with the reduced value of electron density within the magnetic field.

The preceding is a qualitative model, in that explicit solutions have not been obtained. The concepts described were also expressed in a more mathematical form to provide further confirmation of the proposed model. (See Appendix A.)

The important plasma property changes with the presence of both a magnetic field and an electron current through this field are in the electron energies and densities. In passing from the bulk plasma in the direction of the electron current, the electron density will fall increasingly below the value given by the barometric equation. Also, due to the preferential diffusion of lower energy electrons, the electron temperature will fall increasingly below the bulk-temperature value. Both of these effects were approximated by the inclusion in the barometric equation of a linear decrease in electron temperature with plasma potential using a constant of proportionality, R.

$$n_e \propto \exp[eV_p/(T_e - RV_p)] \tag{7}$$

Without such a variation in temperature, the result is well known. The ion approach velocity to a sheath region must be equal or greater than the ion acoustic velocity, for a stable sheath solution to be obtained. With the inclusion of the temperature variation described in the barometric equation the permissible solutions to the one-dimensional plasma sheath equation extend downward from a maximum value, which is the ion acoustic value. While the one-dimensional solutions obtained are valid only locally over a small range near the sheath boundary, it is felt that a full treatment taking charge conservation into account for the entire plasma will show that the ion velocities obtained may represent upper limits and that lower velocities are physically possible when all boundary conditions are met.

The initial portions of these solutions, close to the bulk plasma, should be realistic. This is because some value of the linear-decrease constant should approximate the real process, and the range of permissible ion approach velocities changed little with changes of this constant. Farther into the magnetic field, the significance appears to be more in the nature of an existence proof for a class of boundary solutions with low ion approach velocities.

Expressed in the most general terms, then, the ion flow to the boundary of an ion production region can be altered by the combined effects of a magnetic field and an electron current through that field. With electron diffusion constrained by the magnetic field, the ion approach velocity to the magnetic field can be reduced to a value that is small compared to ion acoustic velocity. Removing either the magnetic field or the electron current through it will result in a tendency to re-establish ion acoustic velocity.

Relation of Model to Previous Observations

In the past, it has been a convenient assumption that ions will flow equally in all directions away from a region of production within a discharge chamber. This assumption was justified first by an experimental study by Masek,[10] which showed that the ion arrival rate at the boundaries of a particular discharge chamber were in approximate agreement with ion acoustic velocity for all boundaries. Later, the ion production was identified with the primary-electron region, and maximum utilization calculations were found to be consistent with the assumption of uniform ion current density everywhere on the boundary of the primary-electron region.[11] This assumption of constant ion current density at the boundary of the primary-electron region has been used more recently to estimate discharge losses.[1]

In point of fact, there have been few actual measurements of ion current densities at the boundaries of a discharge chamber. At the same time, there were a number of clues that the ion arrival rate might be quite nonuniform.

It is well known that the discharge losses of a simple axial-field thruster continue to decrease with increasing magnetic field strength, above the field strength necessary for primary-electron containment.[12]

This result is consistent with the increased radial impedance resulting in a reduced radial electric field, hence preferential ion direction to the ends of the discharge chamber.

More recently, with a multipole discharge chamber, a reduction in active anode length was directly correlated with increased discharge losses.[13] This result was particularly puzzling, inasmuch as the magnetic field above the inactive anodes was not altered. The ability to contain primary electrons was therefore not impaired, and the ion generation should have been unaffected.

Even the comparison of discharge losses for different chamber length-to-diameter ratios was probably skewed by the wide use of propellant introduction at the chamber end opposite the ion optics. This introduction mode almost certainly led to a shift of ion generation toward the rear of the chamber, resulting in increased ion losses to the walls, thereby giving performance more consistent with the assumed equal distribution of losses. Actually, it has been known for a long time that propellant introduction closer to the ion optics can often signficicantly improve performance.[12]

In retrospect, then, it is clear that the general assumption of uniform ion losses in all directions was not justified. Instead, significant departures from uniformity have probably existed for a wide range of discharge chamber designs. These nonuniformities would have been noted if the results of previous experiments had been examined closely enough, or if proper instrumentation had been used to measure the actual ion-loss distributions.

Design Considerations

For design of a multipole discharge chamber, a volume ion-production loss of 70-80 eV/ion is suggested for argon and operation near the discharge-loss "knee". Use of multipole structures at all boundaries except the ion optics should result in ion-loss current densities at these structures of roughly 1/4 that at the plane of the ion optics, assuming either a small length-to-diameter ratio for the chamber, or propellant introduction close to the ion optics.

Note that this volume loss of 70-80 eV/ion is greater than that proposed earlier,[1] but the earlier work assumed higher ion flows to the multipole boundaries than can now be justified. It should also be apparent that interruptions of the pole-piece structure should be avoided, if at all possible.

Most of the investigation described herein applies directly to a multipole discharge chamber. There are some obvious applications, though, to other types of chambers. If one examines line-cusp discharge chambers, of the type introduced by Limpaecher and MacKenzie,[15,16] one finds that a similar ion flow model should apply. In the line-cusp source, in which the entire discharge chamber wall (except for the ion optics) becomes the anode, the magnetic fields must be considerably

stronger than those used in the present investigation. This is because electron flow must be constrained parallel to the magnetic field, as well as normal to it. At these high field strengths, electron current densities should be small everywhere except near the cusps. As shown by the factor of several ranges for magnetic integral investigated herein, the transverse field regions should still be effective in directing ion flow away from the anode as long as an anode-potential surface is located beyond the transverse field. This viewpoint is supported by experiment (Fig. 4) for very small conducted currents.

Most of the electron current for the discharge in a high field strength cusp design will be conducted near the cusps. To properly contain primary electrons, the field strength near the cusp should constrain electron flow, through both magnetic-mirror effects and limited conduction area. With the use of a high enough magnetic field strength, then, a density gradient should also be introduced near the cusps. This density gradient should thus serve to direct ion flow away from cusp regions, as well as the other regions.

The cusps in line-cusp chambers are, of course, analogous to pole pieces in the multipole chamber studied herein. Inasmuch as the pole pieces are the locations of most ion loss in a multipole chamber, the line-cusp chamber may well offer lower total ion losses.

There are some other factors that should also be considered in discharge chamber design. From a general viewpoint, an ion production region localized near the ion optics and away from the side walls will permit a lower discharge loss per extracted ion, because of the greater probability of an ion being extracted into the ion beam from such a region. An ion production region of this shape can be obtained either with a line-cusp design with few cusps, or with a multipole design with large spacings between pole pieces. With less exposed pole piece length, large spacings should also result in reduced ion losses for the multipole design.

Conversely, if the maximum propellant utilization or maximum beam uniformity is desired, an ion production region that extends farther upstream and closer to the side walls will be preferred. Such an extended ion production region will also increase the wall losses for either the line-cusp or multipole design.

In addition to the general considerations of the shape for the ion production region, there is probably a scaling effect. The volume loss of 70-80 eV/ion is high relative to the 30-40 eV/ion observed in most volume production processes. It appears likely that some of this 70-80 eV/ion loss is due to electron conduction of energy to the walls of the discharge chamber. If this is true, ion production should be more efficient in larger chambers, where electrons have a higher probability of expending their energy before reaching a wall.

Concluding Remarks

Preferential ion flow has apparently existed in many discharge chamber configurations. The conditions necessary for preferential ion flow away from a discharge chamber surface are an electron current toward that surface and a magnetic field strong enough to affect the electron density, and hence the ion density, through interaction with the electron current. These conditions are met for most of the discharge chamber wall (except for pole pieces) in a multipole design. For a strong enough field strength, these conditions can be established over the entire anode surface of a line-cusp design.

In addition to the general principles involved in directing the ion flow in a discharge chamber, design details can also be important. Interruptions of wall protection, through interruptions of either the magnetic field or the electron current, can greatly increase losses. Propellant introduction in a manner that minimizes concentrations of neutral density away from the ion optics can also be important. From the high levels of volume production losses observed in this investigation, improved efficiency may be expected with larger discharge chamber sizes.

Acknowledgement

This work was supported by NASA Grant NSG-3011.

References

1. H. R. Kaufman and R. S. Robinson, "Ion Source Design for Industrial Applications," AIAA J., Vol. 20, pp. 745-760, June 1982.
2. R. D. Moore, "Magneto-Electrostatically Contained Plasma Ion Thruster," AIAA Paper No. 69-260, Mar. 1969.
3. W. D. Ramsey, "12-cm Magneto-Electrostatic Containment Mercury Ion Thruster Development," J. Space. Rockets, Vol. 9, pp. 318-321, May 1972.
4. H. R. Kaufman, R. S. Robinson, and D. C. Trock, "Inert-Gas Thruster Technology," AIAA Paper No. 81-0721, Apr. 1981.
5. R. S. Robinson, H. R. Kaufman, and C. M. Haynes, "A 5 × 40 cm Rectangular-Beam Multipole Ion Source," AIAA Paper No. 81-0667, Apr. 1981.
6. C. M. Haynes, "Rectangular Beam (5 × 40 cm) Multipole Ion Source," NASA Contr. Rep. CR-165239, Dec. 1980.
7. H. R. Kaufman and R. S. Robinson, "Plasma Processes in Inert-Gas Thrusters," J. Spacecr. Roc., Vol. 18, No. 5, 470-476, Sept./Oct., 1981.
8. L. E. Frisa, "Ion Containment," in Electric Thruster Research (H. R. Kaufman and R. S. Robinson, eds.), NASA Contr. Rep. CR-165603, Dec. 1981.
9. D. A. Dunn and S. A. Self, "Static Theory of Density and Potential Distribution in a Beam-Generated Plasma, J.A.P., Vol. 35, pp. 113-122, Jan. 1964.
10. T. D. Masek, "Plasma Properties and Performance of Mercury Ion Thrusters," AIAA J., Vol. 9, pp. 205-212, Feb. 1971.
11. H. R. Kaufman, "Ion-Thruster Propellant Utilization," J. Space. Rock., Vol. 9, pp. 511-517, July 1972.
12. H. R. Kaufman, "Technology of Electron-Bombardment Ion Thrusters," in Advances in Electronics and Electron Physics, Vol. 36 (L. Marton, ed.) Academic Press, New York, pp. 265-373, 1974.
13. R. S. Robinson, "Thirty Cm Ion Source," in Industrial Ion Source Technology (H. R. Kaufman, ed.), NASA Contr. Rep. CR-135149, Nov. 1976.
14. R. Limpaecher and K. R. MacKenzie, "Magnetic Multipole Containment of Large Uniform Collisionless Quiescent Plasmas," Rev. Sci. Instrum., Vol. 44, pp. 726-731, June 1973.
15. J. T. Crow, A. T. Forrester, and D. M. Goebel, "High Performance, Low Energy Ion Source," IEEE Trans. Plasma Science, Vol. PS-6, pp. 535-538, Dec. 1978.

HOLLOW CATHODE

Introduction

Hollow cathodes are a critical component of inert-gas ion thrusters. As such, understanding their operation is important. The hollow cathode investigated employed oxide-free components, mechanically assembled (no welding). This approach has advantages from the research viewpoint in that fabrication of such cathodes is straightforward and the work functions of the surfaces are well known. Further, the assembled construction should avoid the thermal stress problems of welded joints with dissimilar materials and section thicknesses.

In earlier work,[1] a rolled Ta insert was found to be an efficient oxide-free emission surface. Texturing the insert was found to improve the operating characteristics.[2] This present investigation continues the study of a textured, rolled Ta foil insert. Graphite and tungsten tips were both used.

The main objective of the study during this support period was to evaluate the magnitude and distribution of thermal losses.

Apparatus and Procedure

The typical test arrangement for a hollow cathode is indicated in Fig. 1. The body of the hollow cathode was a 6.4 mm outside diameter Ta tube, 6.3 cm long. The tube thickness was 0.51 mm. The Ta tube was attached to an Al block, which was a support structure for most of the components. The rolled foil inserts used in the tests were fabricated from 0.013 mm thick Ta. The inserts were 4 × 8.6 cm and were textured by pressing the foil against 50-grit abrasive paper using an elastomer to apply pressure. The inserts were then rolled into an approximately five-turn insert configuration with a length of 4 cm.

A stainless steel perforated cylinder, 5.8 cm in diameter and 10.2 cm long, was used as the anode. The position of the anode in Fig. 1 is shown displaced for clarity. The tip of the cathode was actually flush with the near end of the anode during these tests.

The only gas introduced into the 45 cm diameter vacuum chamber was the Ar flow through the hollow cathode.

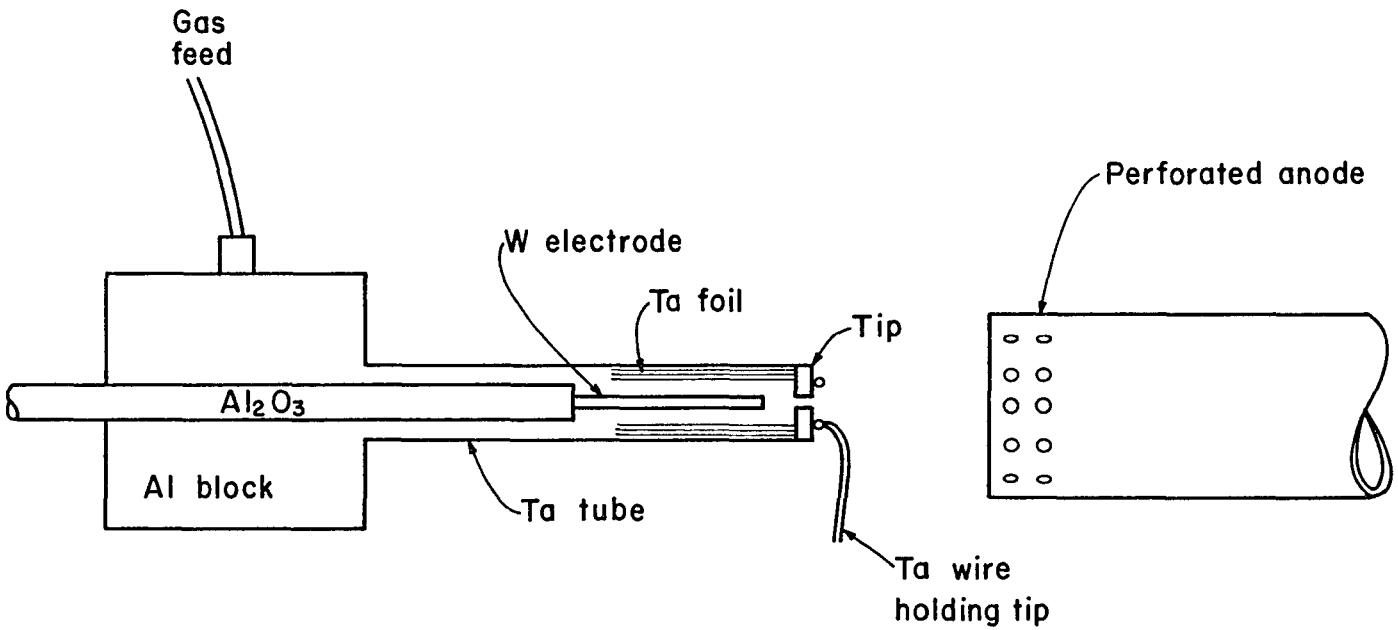

Fig. 1. Hollow cathode assembly.

An internal starting electrode described previously[1] was used throughout this investigation. After operation was initiated, the starting discharge was turned off. Because there was no external source of heat without the starting discharge, a minimum emission was required to maintain operation. This minimum depended on Ar flow, but was typically 3-4 A.

The tip was a 6.4 mm diameter disk, 1 mm thick, with a centered 1.0 mm diameter hole. Because this design is a simple disk without provision for centering in the Ta tube, a surrounding piece of 0.013-mm-thick Ta was spot-welded to the Ta tube to perform this centering function.

The testing procedure included obtaining current-voltage characteristics, with the current varied from the minimum required to maintain operation up to either the power supply limit (25 A) or the emission limit.[3] Tests designed to determine thermal power losses also involved temperature measurements. These temperature measurements were taken with either a thermocouple or an optical pyrometer (see Appendix B), depending on the temperature range. Tests were typically conducted at Ar flows of 0.6, 0.7, 0.8, 0.9, and 1.0 A-equiv.

Thermal Power Losses

Tip Radiation Losses. Two tip materials were tested, W and grade HPD-1 graphite (Union Poco). In a previous study,[2] it was found that the cathode operating characteristics improved with the use of a W tip over that obtained with a graphite tip. Figure 2 indicates the difference in cathode performance.

Tip temperature profiles were taken at several Ar flows (0.6 to 1.0 A-equiv). The tip temperatures were measured with an optical pyrometer. Figure 3 shows the difference in temperature for the two tip materials for a representative Ar flow at various emission levels. It was found that the graphite tip had a higher temperature than the W tip at the same emission level. The tip temperatures also appear to be essentially independent of flow rates.

From the tip temperatures, it was possible to calculate the power radiated from the tips. For these calculations, the total emissivities of graphite and tungsten were needed. For tungsten, the total emissivity was found by a linear least-squares fit to experimental data,[4] which yielded

$$\varepsilon_W = 0.0651 + 9.495 \times 10^{-5} T \ , \qquad (1)$$

where T is in °K. This fit had a correlation coefficient of 0.91. The value of total emissivity used for the graphite was 0.90. This value was chosen because HPD-1 grade graphite typically has a total emissivity between 0.88 and 0.92.

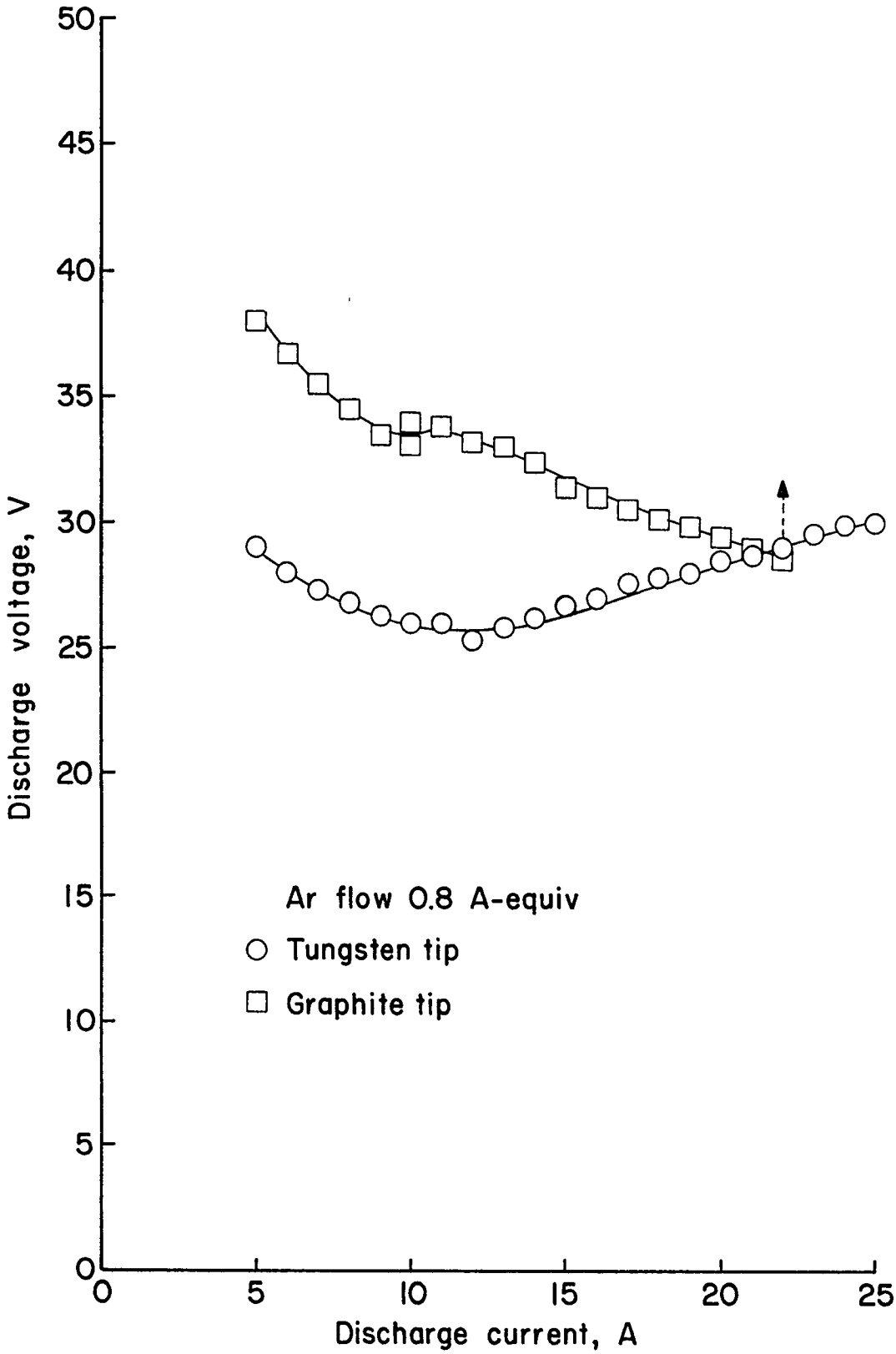

Fig. 2. Comparison of cathode performance for two different tip materials.

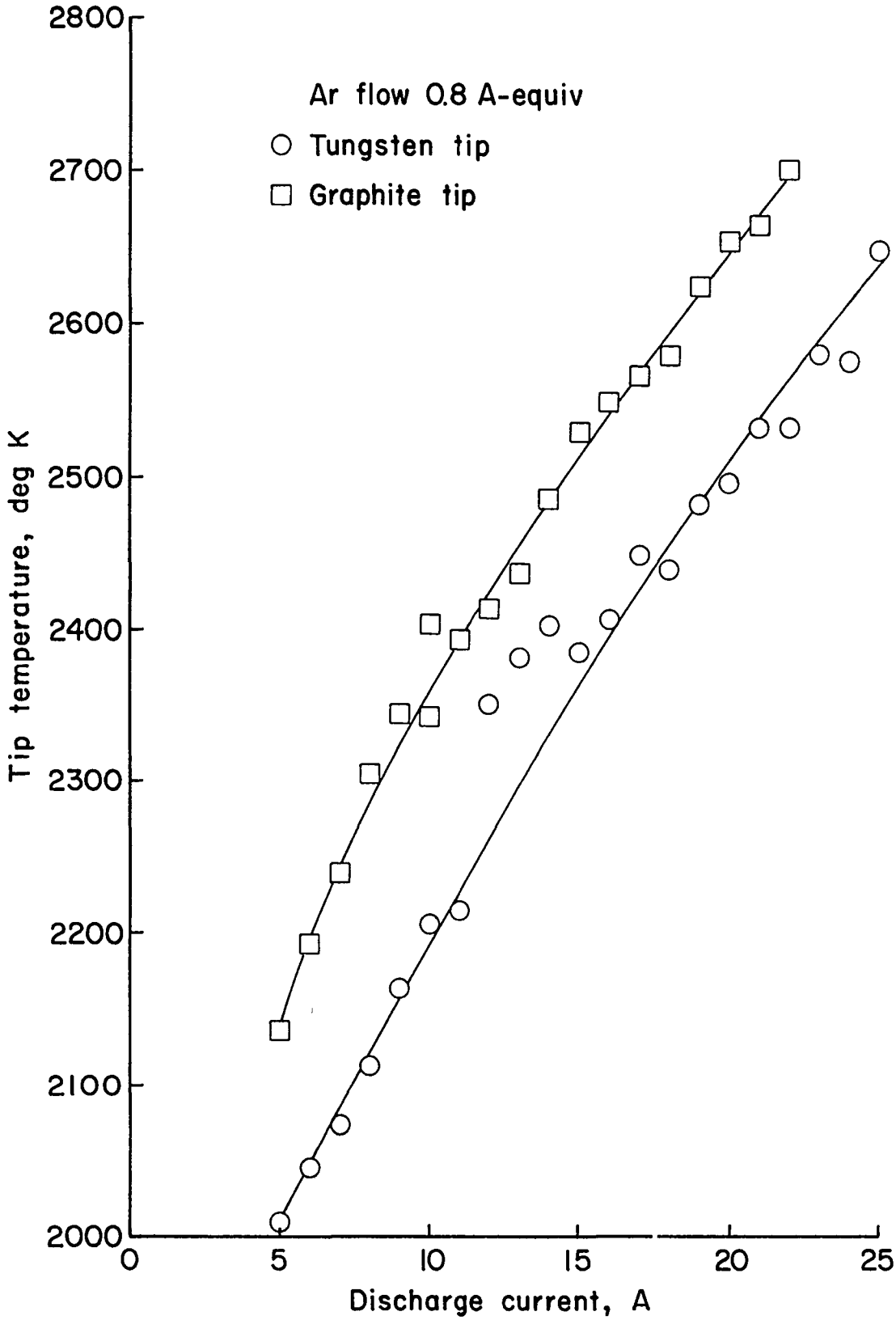

Fig. 3. Temperature profiles of W and graphite tips for different emission levels.

The radiated tip power was calculated from

$$P_{rad} = \varepsilon A_{tip} \sigma T^4 , \qquad (2)$$

where ε is the total emissivity, A_{tip} is the surface area of one face of the tip (6.35 mm diameter), and σ is the Stafan-Boltzmann constant (5.67×10^{-8} watts $m^{-2}°K^{-4}$). Using the calculated radiated powers from the two tips, the difference in radiated tip power was calculated and compared to the difference in discharge power (Fig. 4). For the five Ar flow rates tested, it was found that the radiated tip power difference accounted for roughly 44% of the discharge power difference of the two tip materials. The discharge power difference is thus not completely accounted for by the difference in radiated tip power. This result is consistent with the tip material affecting the heat balance between the foil insert and the tip. It further implies that the difference is primarily due to the difference in tip radiation characteristics, rather than a more direct involvement in the discharge.

Comparing the thermal power loss of the tip to the total discharge power, the graphite tip radiated roughly 14% of the discharge power, while the W tip radiated roughly 5% of the total discharge power. The percentage of the discharge power that was lost by tip radiation decreased slightly with increasing current emission.

Cathode Tube Radiation Losses. Temperature profiles of the cathode (Ta) tube were taken. The tests were conducted using both W and graphite tips at an Ar flow rate of 0.8 A-equiv. The temperature measurements were made with an optical pyrometer. To ensure that successive temperature measurements were carried out at the same locations along the cathode tube, an Al grating with slots every 2.54 mm was placed parallel to the cathode axis approximately 0.5 cm from the tube. Temperature profiles of the cathode tube were taken over a full range of emission currents (see Apparatus and Procedure) in steps of 1 A. A problem that was encountered in the temperature measurements was the small range of temperature found along a vertical segment of the tube at a few of the axial locations. These ranges in temperature were probably caused by varying degrees of contact between the Ta tube and the Ta foil used to position the tip, which was spot-welded to the outside of the tube (see Apparatus and Procedure). An attempt was made to measure the same spot on the cathode tube each time, but a small amount of scatter in the data did result from this effect.

Figure 5 shows a temperature profile of the cathode tube for an emission level of 11 amps. The profile was measured along the axial dimension of the tube, where the origin was defined as the end of the tube in contact with the tip. The results indicate that the temperature of the cathode tube is essentially independent of the tip material.

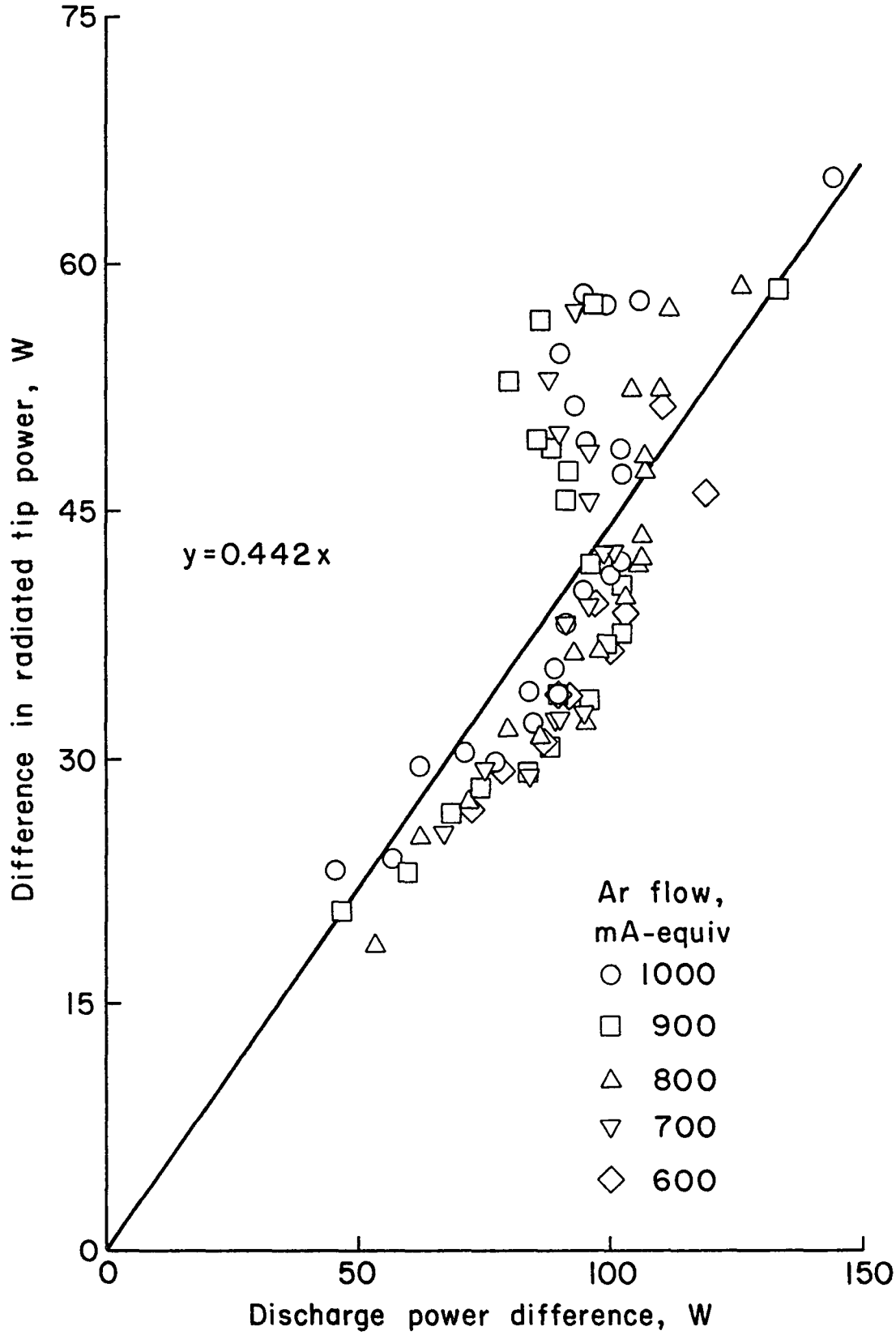

Fig. 4. Difference in radiated tip power versus difference in discharge power for W and graphite tips at various gas flow rates.

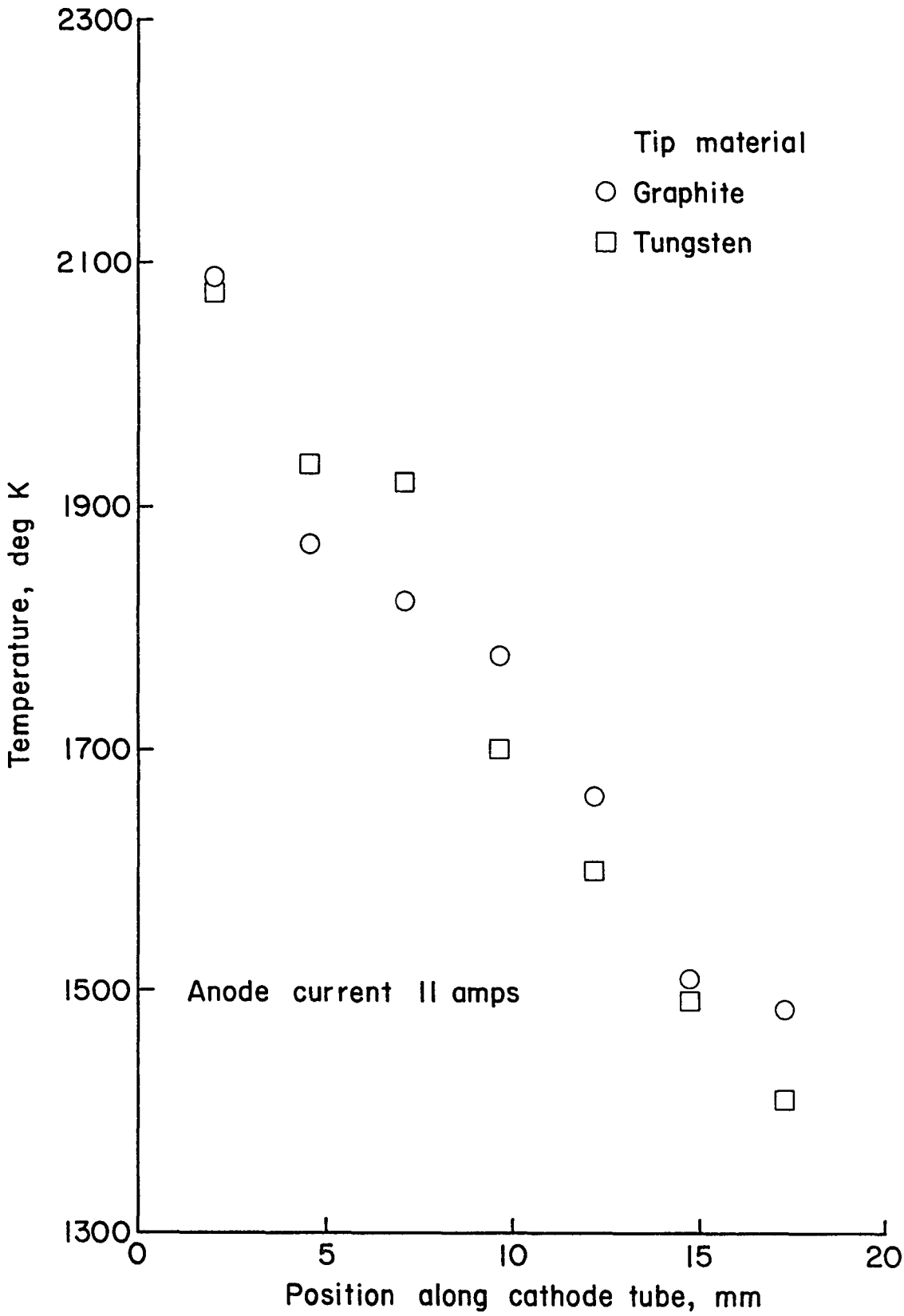

Fig. 5. Temperature profile for cathodes with graphite and W tips.

Figure 6 shows a comparison of the temperature increases for the different locations along the cathode tube as a function of emission level. The mean curves shown in Fig. 6 were determined from linear least-squares fits of the data (both W and graphite tips). The correlation coefficients varied from 0.46 to 0.91. Figure 6 clearly indicates that the rate of increase of temperature with respect to emission level is highest closest to the tip (20°K/amp) and lowest at the position furthest from the tip (5.7°K/amp). This trend indicates that the heat generation, and hence probably the emission, is concentrated close to the tip.

To calculate the radiated power loss from the cathode tube, it was necessary to integrate the temperature profile along the cathode tube. The power loss was calculated using

$$(P_{rad})_{tube} = \sigma\pi d\int\varepsilon_{Ta}T^4 d\ell \ , \qquad (3)$$

where d is the outside diameter of the tube (6.5 mm), ℓ is the position along the cathode tube axis and ε_{Ta} is the total emissivity of tantalum. The expression used for ε_{Ta},

$$\varepsilon_{Ta} = -4.48 \times 10^{-3} + 1.182 \times 10^{-4}\ T \ , \qquad (4)$$

was found by a linear least-squares fit to published experimental data.[5] The correlation coefficient for this fit was 0.99. The temperature of the cathode tube was a function of position along the tube. For a constant emission level, a linear least-squares fit was made of the temperature variation with length. The correlation coefficient was greater than 0.95 for all fits. Although the temperature profile was only taken over a third of the cathode tube length, because of the linearity of the data it was felt that extrapolating the profile would give reasonable results. The total radiated power from the cathode tube can be divided into three regions, ℓ = 0 to 2.03 mm, ℓ = 2.03 to 17.18 mm, and ℓ = 17.18 to 50.5 mm (50.5 mm is where the cathode tube enters the Al block). The central region, ℓ = 2.03 to 17.18 mm is the region in which the data were obtained. The radiated power over this area comprises approximately 60% of the total radiated power of the cathode tube. The region closest to the tip, ℓ = 0 to 2.03 mm, comprises approximately 20-25% of the power loss. There is probably little error in extending the temperature profile through this region, since the profile is very linear and is extrapolated over only a short length. The third region, ℓ = 17.18 to 50.5 mm, probably contains the most error since the temperature profile is extended over a region twice the length over which the temperature profile was measured.

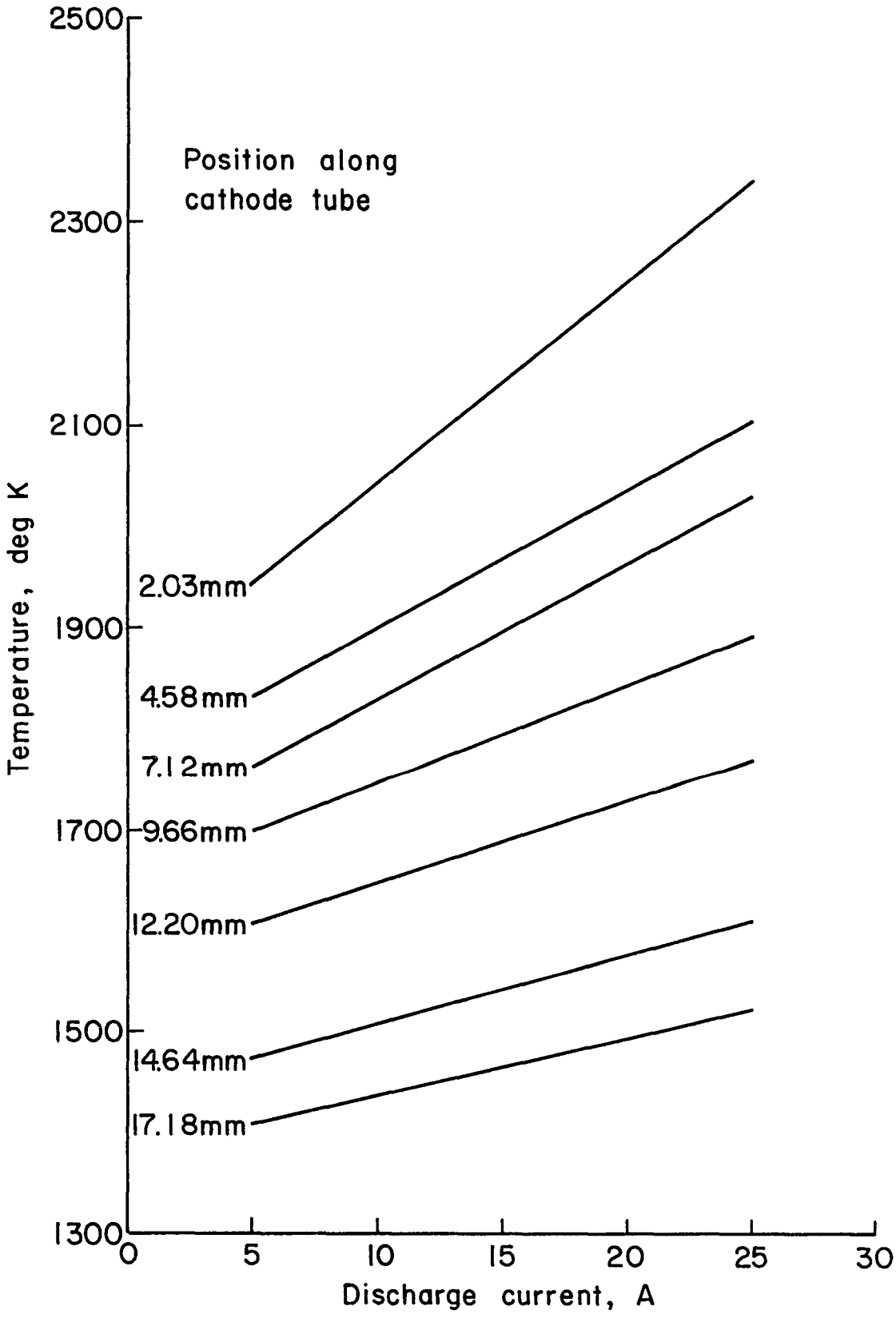

Fig. 6. Temperature profile of cathode as a function of discharge current. (Values calculated from least-squares fit data)

However, since the temperature drops linearly and the radiated power is proportional to T^4, most of the radiated power would be concentrated in the length of the tube immediately adjacent to the measured region. This third region contributes approximately 15-25% of the total power radiated from the cathode tube. The radiated power from the cathode tube is thus felt to be determined within perhaps ±20%. The power radiated from the tube accounts for 28 to 10% of the total discharge power, decreasing with increasing emission. The uncertainty in radiated power from the cathode tube should thus be a small part of the total power loss.

Cathode Tube Conduction Losses. Temperature measurements were taken using thermocouples spot-welded to the cathode tube at positions 4.1 and 4.55 cm upstream of the tip. These measurements were taken in order to calculate the power loss due to conduction of heat in the cathode tube. The positions for measurement, 4.1 and 4.55 cm, were chosen to be upstream of the insert so that the heat sources would be minimized in the region measured. These positions were also upstream of the region where radiation was found to be important. The temperature measurements were taken at emission steps of 1 A. Operation was sustained at each condition for 5-10 minutes to permit the temperature to reach a steady-state value before recording data. Figure 7 shows the temperature profile of the two positions measured as a function of emission level.

The power loss due to conduction is given by

$$P_{cond} = kA_{ct} \frac{dT}{d\ell} , \tag{5}$$

where k is the thermal conductivity and A_{ct} is the cross-sectional area of the cathode tube (0.195 cm^2). In calculating the conduction loss, an average value of thermal conductivity of 0.59 $Wcm^{-1}{}^{\circ}K^{-1}$ was used.[6] The conduction power loss varied from 65 to 85 watts, increasing with emission level. This level accounted for 50 to 10% of the total discharge power, decreasing with increasing emission level.

Anode Radiation Losses. The anode radiation power loss is given by

$$(P_{rad})_{anode} = \varepsilon_{ss}\sigma A_a (T^4 - 300^4) , \tag{6}$$

where ε_{ss} is the total emissivity of stainless steel and A_a is the area of the anode contributing to the radiation. The term A_a includes the view factors associated with the interior surface of the anode, including the effects of the holes. The view factor for the interior surface of the anode, F_{12}, is given by

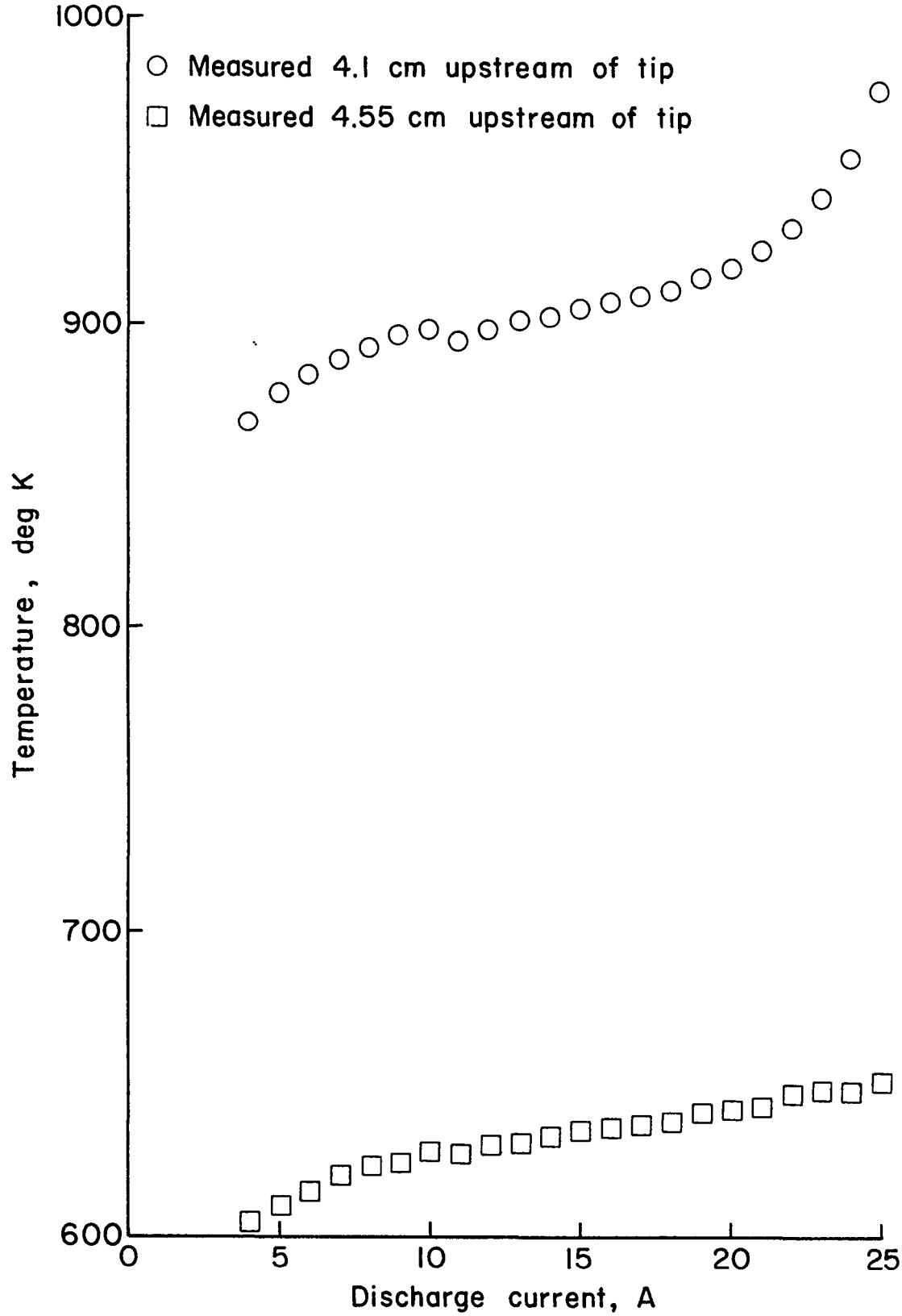

Fig. 7. Temperature of cathode body as a function of discharge current for two positions on the cathode.

$$F_{12} = \frac{1}{A_1} \int_{A_1} \int_{A_2} \frac{dA_1 \cos\phi_1 dA_2 \cos\phi_2}{\pi r'^2} \quad , \tag{7}$$

where dA_1 is a surface element on the interior surface of the anode, dA_2 is a surface element on an open end of the cylinder and r' is a straight line connecting the two area elements. The angles ϕ_1 and ϕ_2 are measured from the surface normal to the line r', as shown in Fig. 8(b).

The view factor, F_{12}, was approximated by the expression

$$F_{12} \simeq \frac{A_2}{A_1} \int_{A_1} \frac{dA_1 \cos\phi_1 \cos\phi_2}{\pi r'^2} \quad . \tag{8}$$

Equation (8) represents the view factor as seen by an observer on the centerline of the cylinder at an open end. The dimensions are shown in Fig. 8(b) and given in the following expressions:

$$dA_1 = 2\pi f R d\ell \tag{9}$$

$$A_2 = \pi R^2 \tag{10}$$

$$\phi_1 = -\tan^{-1}(\ell/R) \tag{11}$$

$$\phi_2 = 90° - \phi_1 \quad , \tag{12}$$

where ℓ is the position along the length of the cylinder, R is the inner radius of the cylinder, and f is the closed area factor (0.76). Equation (8) was numerically integrated to yield a view factor of 0.13. A similar treatment was used to calculate a view factor of 0.22 for the inside of each hole. There were 894 holes in the cylinder, 3.0 mm in diameter and 0.94 mm deep. Using these values, the total anode area contributing to radiation, A_a, was found to be 176.5 cm^2.

A value of $\varepsilon_{ss} = 0.5$ was used, from experimental data for a piece of stainless steel that was heated and cooled repeatedly,[7] which is believed consistent with the observed discolored appearance of the anode.

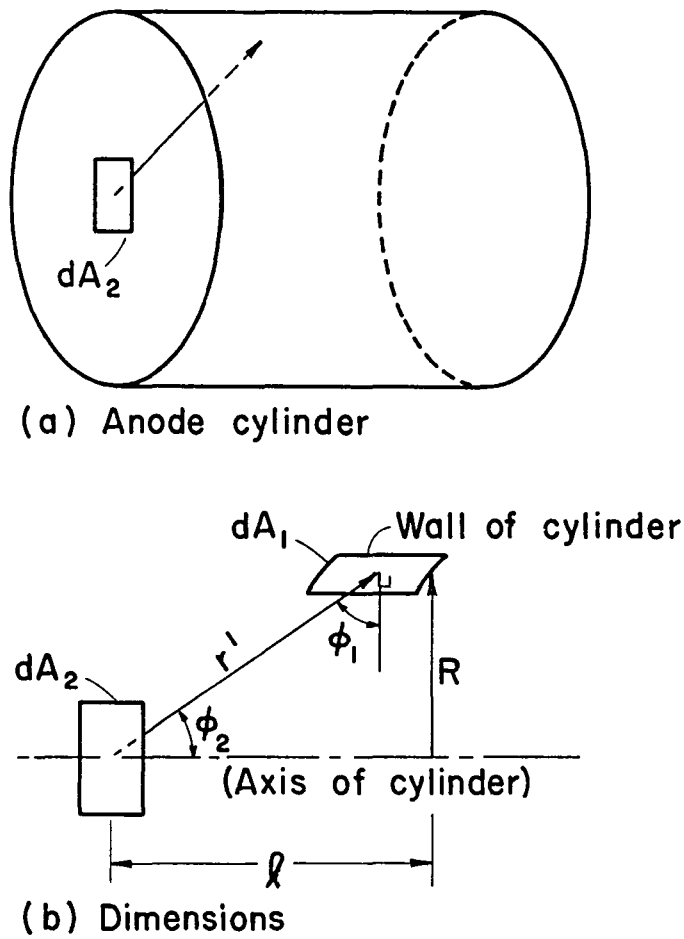

Fig. 8. Geometry for calculating anode radiation losses.

The temperature of the anode was measured by a thermocouple spot-welded to the anode. The anode temperature measurements were taken at an Ar flow rate of 0.8 A-equiv with a W tip. The temperature of the anode was found to vary from 530 to 670°K during operation, increasing with increasing emission. The radiated power from the anode varied from 36 to 100 watts, accounting for 33 to 11% of the total discharge power. The percentage of discharge power decreased with increasing emission level.

Total Thermal Losses. The temperature measurements and thermal losses for the cathode tube, tip and anode have been analyzed separately. In this section they will be compared and the total thermal losses discussed.

Figure 9 shows the temperature profile of the cathode tube, together with tip and anode temperatures, for three emission levels. From Fig. 9, it is evident that the temperature is highest at the tip and decreases upstream along the cathode tube. Figure 9 also indicates that, as emission increases, the temperatures of all the cathode components (tip, anode, and cathode tube) increase.

Figure 10 shows the thermal power losses, as a fraction of discharge power, and a function of emission level. From the results shown, it is evident that the conduction of heat along the cathode tube, radiation from the cathode tube, and radiation from the anode are roughly equal in magnitude. As such, these loss mechanisms are of most interest.

It should be noted from Fig. 10 that the total thermal losses are 107% of the discharge power at an emission level of 5 amps. This value is probably an indication of the error caused by the various approximations made in calculating the power losses. The thermal losses thus account for almost all of the discharge power at low emission levels.

Figure 10 also shows that, as the emission level increases, less of the discharge power is accounted for. Visual observations showed that, as the emission level increases, the glow near the tip orifice also increases. This glow is an indication of discharge power being lost directly through increased radiation from atoms and ions. One would also expect an increase in energy transport to the vacuum facility walls with energetic species to accompany an increase of observed glow.

Insert Emission

The emission in a hollow cathode is believed to be by field-enhanced thermonic emission process.[8] With thermonic emission as a major contribution to the emission process, temperature profiles of the insert are of interest.

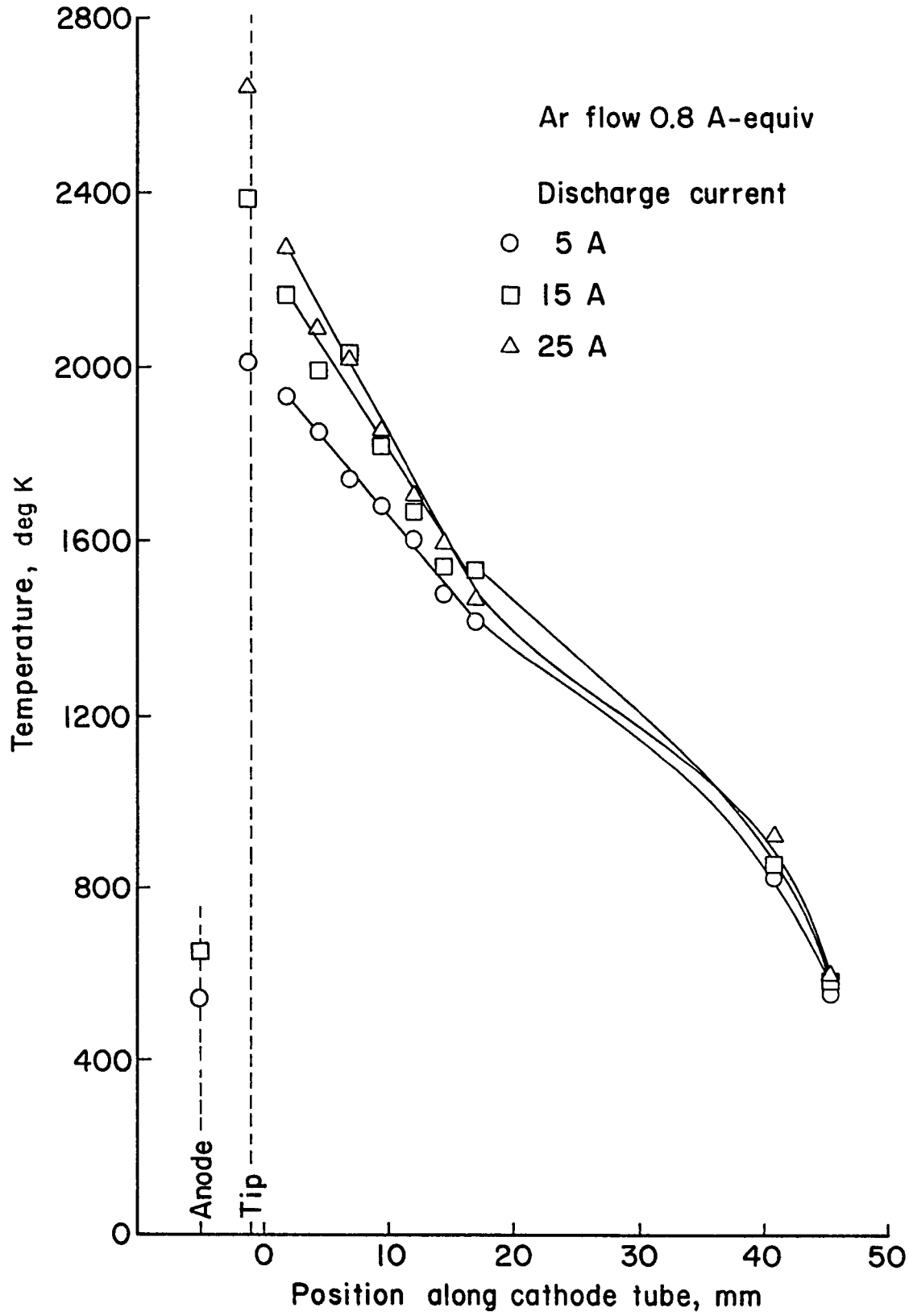

Fig. 9. Temperature profile of cathode components for three emission levels.

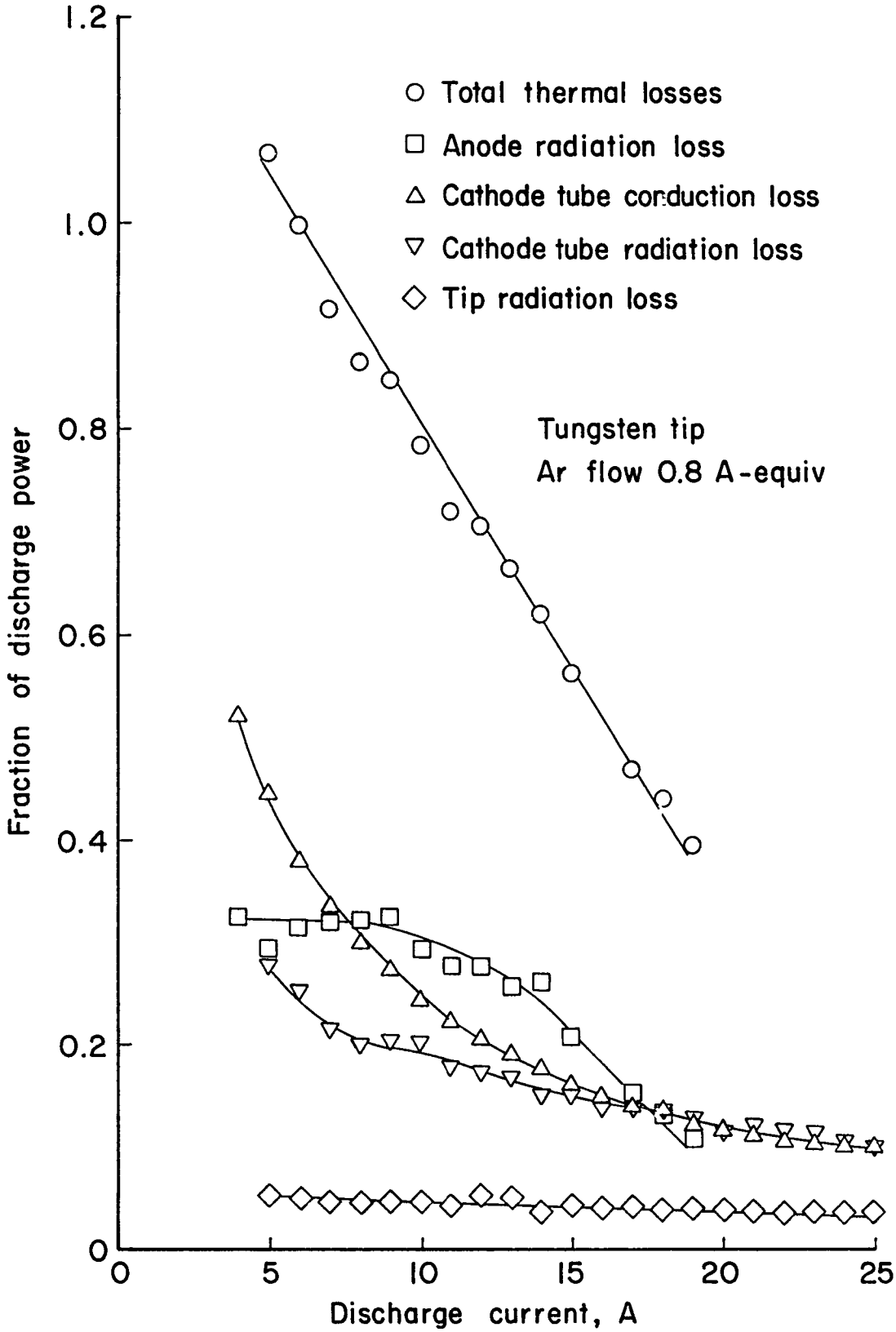

Fig. 10. Thermal power losses of cathode components.

To measure the temperature of the insert, ten holes, each 1 mm in diameter, were drilled through the Ta tube and four outer layers of the textured insert over a tube length of 25 mm. A fifth untextured turn was inserted and pressed against the textured turns after the holes had been drilled. In this way the temperature of the innermost turn could be measured with an optical pyrometer. The Ar flow rate was 1.0 A-equiv, although this value should be considered to be only qualitative, inasmuch as there was considerable gas leakage through the holes. The results of these measurements are shown in Fig. 11 for three emission levels.

From the results shown in Fig. 11, there is a substantial temperature drop at about 6 mm (from the upstream side of the tip) indicating that most of the emission occurs from the first 6 mm of the insert. This is in agreement with the observations of Siegfried[8] in that the majority of emission occurs from a small portion of the insert closest to the tip. While Siegfried found that the emission occurred from the first 2 mm of the insert, his model[8] predicts that the portion of the insert contributing the majority of emission depends on various cross-sections of the propellant gas. Thus, since Siegfried used Hg, one would expect the insert length contributing to emission from an Ar hollow cathode to differ somewhat from that of a Hg hollow cathode.

Figure 11 also shows that, as the emission level is increased, the insert temperature at all positions increases. This increase with emission level, however, is small.

Concluding Remarks

A previous investigation showed that a hollow cathode with a W tip exhibited a wider range of emission and lower anode voltages than one with a graphite tip. The present investigation demonstrated that the improved performance of the W tip was not only due to higher power radiation from the graphite tip, but that the internal heat balance with the insert is also important.

The thermal losses for the entire cathode were calculated. This calculation indicated that, as emission increases, plasma collisions external to the cathode, and eventually appearing as increased vacuum-facility wall losses, constituted an increasingly greater fraction of the discharge power.

Insert temperature profiles were measured, indicating that the majority of emission occurs within the first 6 mm of the insert, which is in qualitative agreement with other workers.

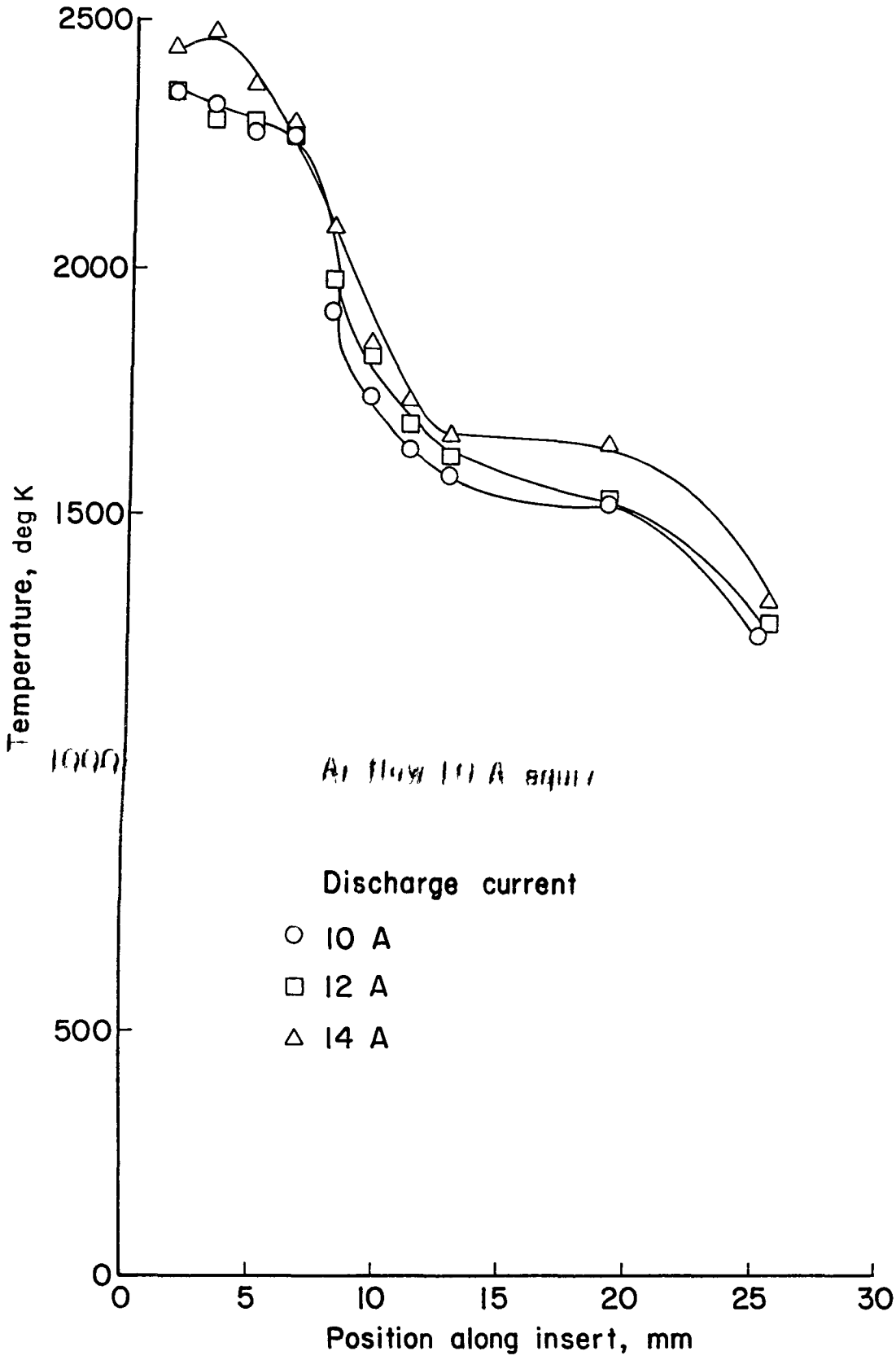

Fig. 11. Temperature profile of insert.

References

1. H. R. Kaufman and R. S. Robinson, "Inert Gas Thrusters," NASA Contr. Rep. CR-165332, pp. 3-17, December 1980.
2. R. P. Stillwell, "Hollow Cathodes," in Electric Thruster Research, NASA Contr. Rep. CR-165603, pp. 50-75, December 1981.
3. D. C. Trock, "Hollow Cathode Research," in Inert Gas Thrusters, NASA Contr. Rep. CR-159813, pp. 43-70, November 1979.
4. W. J. King, "Emissivity and Absorption," in CRC Handbook of Chemistry and Physics, 56th edition, R. C. West, editor, CRC Press, Cleveland, Ohio, pp. E229-E230 (1975).
5. R. E. Taylor, F. E. Davis, R. W. Powell and W. D. Kimbrough, "Determination of Thermal and Electrical Conductivity, Emittance and Thomson Coefficient at High Temperatures by Direct Heating Methods," AFML-TR-62-277, October 1969.
6. C. Y. Ho, R. W. Powell and P. E. Liley, "Thermal Conductivity of Selected Materials - Part 2," NSRDS-NBS 16, February 1968.
7. E. M. Sparrow and R. D. Cess, Radiation Heat Transfer, McGraw-Hill, New York, 1978.
8. D. E. Siegfried, "A Phenomenological Model for Orificed Hollow Cathodes," NASA Contr. Rep. CR-168026, December 1982.

EXPERIMENTAL INVESTIGATION OF A HALL-CURRENT ACCELERATOR

Abstract

The Hall-current accelerator is being investigated experimentally for use in the 1000-2000 sec range. Two models of this thruster have been tested. The first model has three permanent magnets to supply the magnetic field and the second model has six magnets to supply the field. The second model thus has approximately twice the magnetic field of the first. All other factors remain the same for both models except for the anode-cathode distance which is changed to allow for the two thrusters to have the same magnetic field integral between the anode and the cathode. Tests have been conducted on the Hall thrusters to determine the plasma properties, the beam characteristics, and the thruster characteristics. The thruster operates in three modes: (1) main cathode only, (2) main cathode with a neutralizer cathode, and (3) neutralizer cathode only. The plasma properties were measured along an axial line, 1 mm inside the cathode radius, 0.2 to 6.2 cm from the anode. Results obtained from these tests show that the current to heat the cathode produces non-uniformities in the magnetic field, hence also in the plasma properties. A Hall thruster of this general design appears to provide the most thrust when operated at a magnetic field less than the maximum value studied.

Introduction

Electric propulsion research in the United States has recently been restricted to electrostatic, MPD, and Teflon pulsed plasma thrusters. The electrostatic thruster, with ion acceleration provided by electric fields between closely spaced grids, in particular, appears to meet the needs of interplanetary missions, in which mission times are long.[1-2]

For geocentric missions, a lower range of specific impulse is of more interest, typically 1000-2000 sec. The need for lower specific impulses in geocentric applications results from consideration of mission lifetime. In interplanetary missions, the added mission time due to the use of electric propulsion is a small fraction of the total mission time. In geocentric missions, however, a mission time of hundreds of days is usually unacceptable when the equivalent chemically propelled mission takes only a few hours.

The most serious obstacle to the use of electrostatic thrusters at low specific impulses (<3000 sec) is the ion-current limitations of electrostatic acceleration. Hall-current acceleration is, however, an alternative to electrostatic acceleration between grids.

Hall-current accelerators have been studied as electric thrusters in the past in the U.S., but were dropped because of low efficiency.[3-4] It was, for example, difficult to accelerate more than about one ion downstream for each electron that travelled upstream. This limitation put an upper limit on thruster efficiency of about 50% due to the acceleration process alone. In comparison, the electrostatic thruster has an overall efficiency of about 70% at 3000 sec, and is capable of higher efficiencies at higher specific impulses. This relatively poor performance of the Hall-current accelerator, at the high specific impulses that were then being considered, resulted in its demise in the U.S. about 1970.

If we consider low specific impulses, though, the relative performance of the Hall-current accelerator is at much less of a disadvantage. As indicated above, the electrostatic thruster becomes increasingly limited in ion current capacity as specific impulse is reduced. The Hall-current accelerator has no such limitation. The electron backflow results in a serious loss at high specific impulses. But at low specific impulses this backflow is more easily recovered by using it to generate ions.

The investigation of the Hall-current accelerator reported herein was undertaken as a part of a preliminary attempt to re-evaluate this type of thruster for electric propulsion. The preliminary nature of this investigation should be emphasized. It has been over a decade since the Hall-current accelerator was last seriously considered for electric propulsion in the U.S.

Design Considerations

The design of the Hall-current accelerator is based on the force equation for a charged particle moving in a magnetic field $\vec{F} = q(\vec{E}+\vec{v}\times\vec{B})$. This equation indicates that if an electron has a velocity in a direction perpendicular to a magnetic field then a force will be applied to the electron at a right angle to the perpendicular component of the velocity and the direction of the magnetic field. Thus, if an electron has a velocity directed along the axis in a cylindrical radial magnetic field, the electron will acquire a circumferential velocity about the axis.

The simplest geometry for a Hall-current accelerator is an acceleration channel in the shape of an annular ring with one of the pole pieces in the center and the other the outer wall. This approximate arrangement is indicated in Fig. 1. If the anode is placed at one end, upstream end, then an electric field will be established with the electric field vector directed downstream from the anode. Positive ions will be accelerated in the direction of the electric-field vector, while electrons will experience a force in the opposite direction. The force on the electrons will, of course, result in their precession about the axis. Diffusion toward the anode will take place as the result of

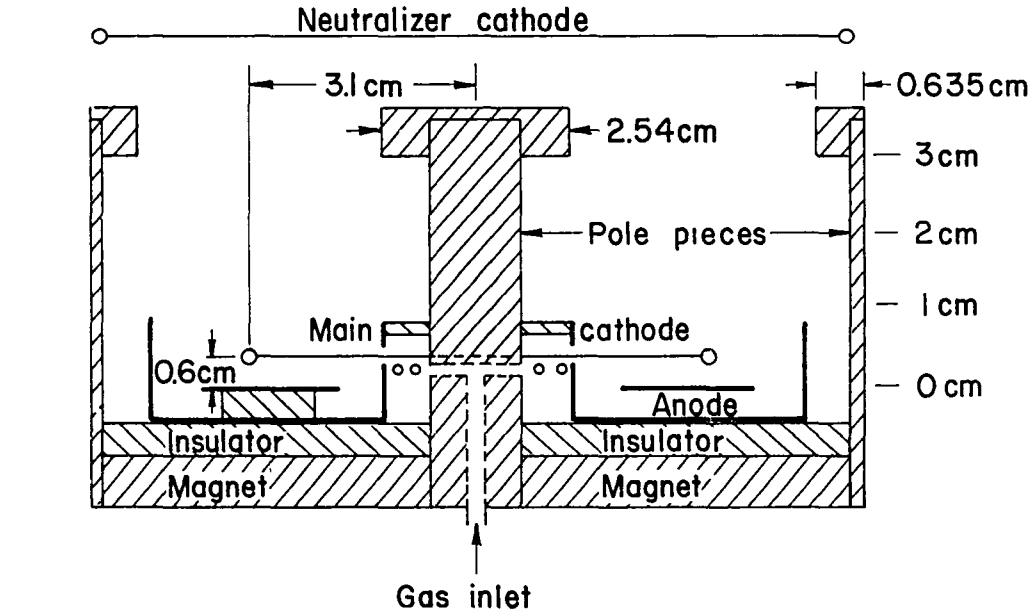

(a) Side view.

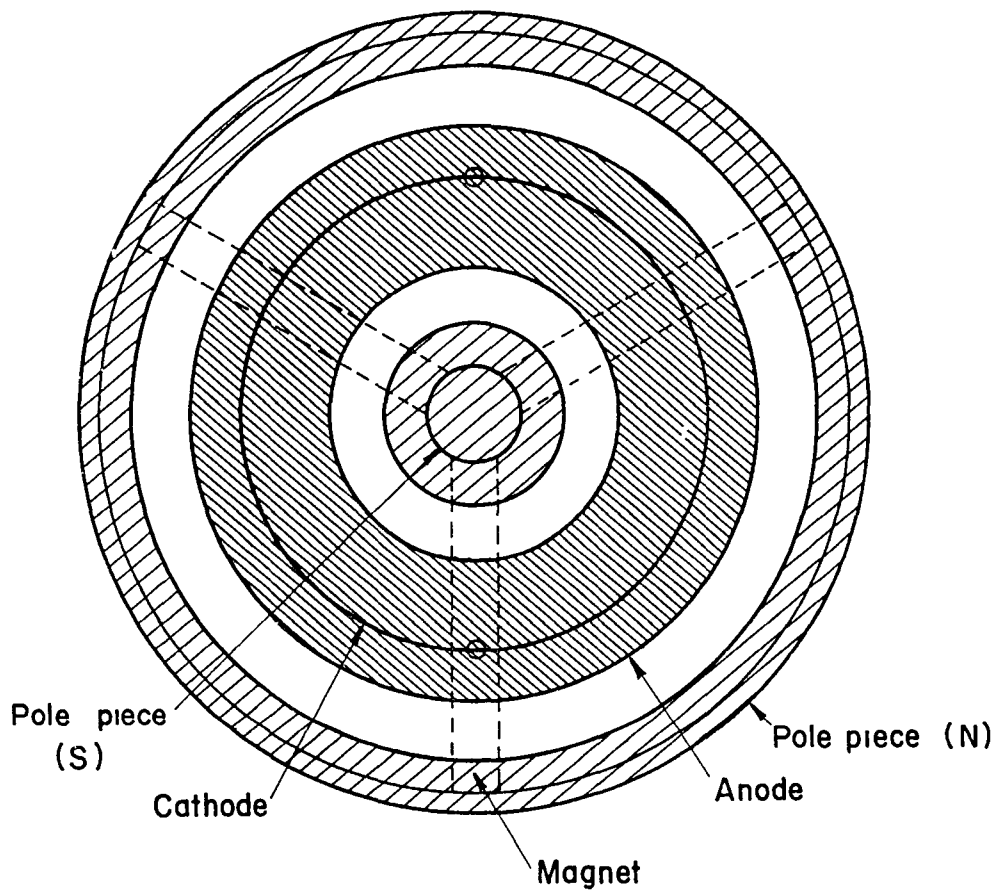

(b) End view.

Fig. 1. Drawings of Hall-current thruster, three and six magnets with modified pole pieces.

collisions during this precession. As indicated in a concurrent paper,[5] most of these collisions are believed to be due to "turbulence" in the plasma. As the anode is approached, the electron energy will tend to increase, resulting in an increased probability that an ionizing collision will take place.

From the viewpoint of obtaining a high acceleration efficiency (a high ratio of accelerated ion current to electron current flowing in the opposite direction), a high magnetic field strength is desired in the acceleration channel. At the same time, efficient use of the electron energy to produce ions, as the electrons approach the anode, requires a low magnetic field strength near the anode. This variation of field strength is obtained by having the pole pieces farther apart near the anode, and closer together at the downstream end of the acceleration channel, as indicated in Fig. 1a. With an upstream "discharge chamber" cathode this design also offers a low magnetic field integral between the anode and this cathode for ease in starting. The shape of the magnetic field in a Hall-current thruster is equivalent in importance to the design of the grids in an electrostatic thruster.

Construction

The Hall-current thruster investigated herein, indicated in Figs. 1a and 1b, used two cylindrical magnetic pole pieces to generate an essentially radial magnetic field. As indicated in Figs. 1a and 1b, a non-magnetic annular anode was located at the upstream end of the acceleration channel. A non-magnetic annular cup, to contain the discharge, surrounded the anode. Two refractory metal cathodes were used, one located near the anode (main or discharge cathode), the other approximately one centimeter beyond the exit plane of the acceleration channel (neutralizer cathode), as indicated in Fig. 1a. The main cathode near the anode was fabricated of 0.51 mm diameter W, with an emission of 1 A for a nominal 17.5 A heater current. (The two semicircular segments of this cathode were effectively in parallel, resulting in a heater power supply current of 35 A.) The neutralizer cathode was two strands of 0.25 mm diameter W, wire with an emission of 1 A for a nominal 6 A heater current. The propellant (Ar) was introduced through the central pole piece and a propellant distributor geometry to achieve a circumferentially uniform gas flow into the ion-production region. To assure uniformity, rings of insulator (mica) were used to force the gas to flow through evenly distributed small holes in the inner cylinder of the annular cup, Fig. 1a.

For the work described herein, two models of the thruster were tested, the first with the thruster as described above using three evenly spaced magnets, Fig. 1b, and the second the same basic thruster but with six evenly spaced magnets. The magnets were made of Alnico V and are 0.6 cm in diameter by 4.6 cm in length. (These magnets were remagnetized in a 1 T field before use.)

Magnetic Field

The magnetic integral in a radial-field configuration varies with the radius at which the integration is performed. Still, the concept of the magnetic integral is a useful one for general design considerations. For this work the magnetic integral between the anode and cathode, at the cathode radius, is set to be 20×10^{-6} T-m (20 Gauss-cm) for all tests on both models (a 6 mm anode-cathode spacing for the three magnet thruster and a 3 mm spacing for the six magnet thruster). This value is low compared to the typical $50\text{-}60 \times 10^{-6}$ T-m between the anode and cathode in an electron-bombardment discharge chamber. The low integral value used was selected after a magnetic integral of 60×10^{-6} T-m was tried, but proved impossible to operate in the <100 V range that was felt to be of interest.

The magnetic field of the operating Hall-current thruster, however, has two major components to the local field strength. First there is the radial magnetic field produced by the magnets and the cylindrical pole pieces. The strength of this component is indicated in Figs. 2 and 3 for the three and six magnet thrusters, respectively. These figures show contours of constant magnetic field strength at the axial locations between the anode and cathode. Figure 4 shows the mean axial variation of the magnetic field strength of the three and six magnet thrusters.

The second component is the contribution due to the main cathode heater current. To avoid the problem of measuring the magnetic field close to a current carrying element, the main cathode field component was calculated. The mean axial variation at the cathode radius of the cathode-current field is indicated in Fig. 5.

The main cathode heater current clearly has a significant effect on the magnetic field distribution. On one side of the thruster the 17.5 A heater current reduces the anode-cathode magnetic integral from 20×10^{-6} T-m to approximately 10×10^{-6} T-m and on the other side increases it to approximately 30×10^{-6} T-m. (20×10^{-6} T-m is the magnetic field integral with no cathode heater current.)

This significance of the heater current appears to be a sharp distinction from electron-bombardment thruster experience. In the latter, the background field near a refractory cathode is normally quite small. Inasmuch as the cathode heater current is not enough to result in localized containment of the emitted electrons, the effect of the heater current on discharge-chamber performance is usually insignificant.

Experimental Results

Operation

The Hall-current thruster design was tested for three operating modes; main cathode only, main cathode and neutralizer cathode, and

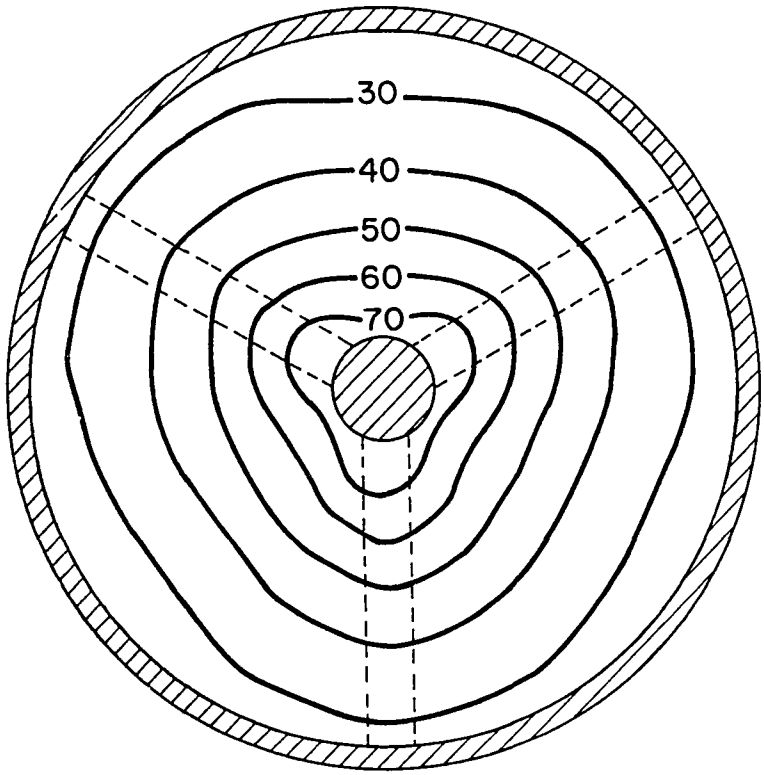

Fig. 2. Contours of constant magnetic field strength, axial location 2 mm. (Field strength indicated in Gauss. Cathode not operating.) Three magnets with modified poles.

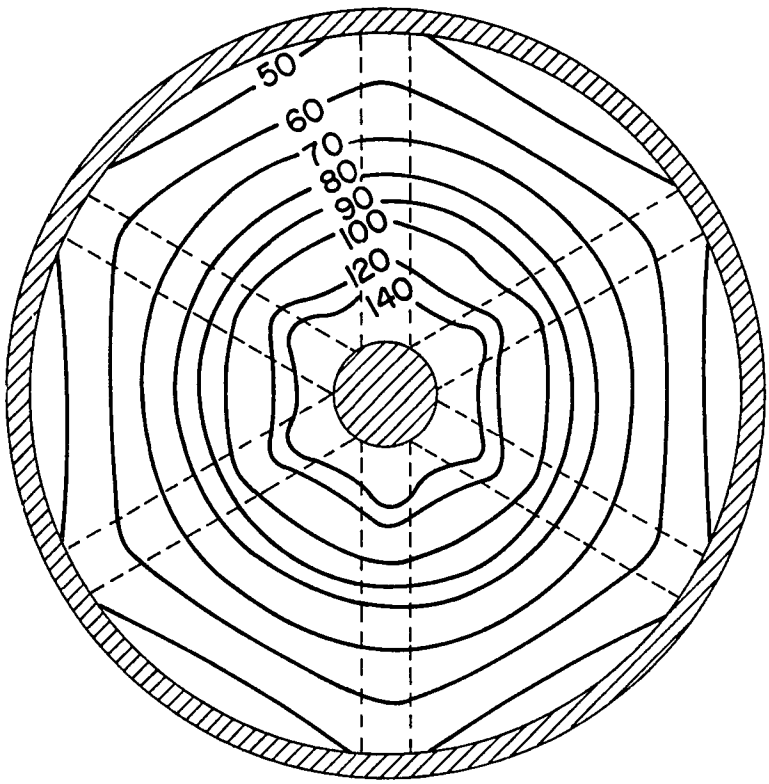

Fig. 3. Contours of constant magnetic field strength, axial location 2 mm. (Field strength indicated in Gauss. Cathode not operating.) Six magnets with modified poles.

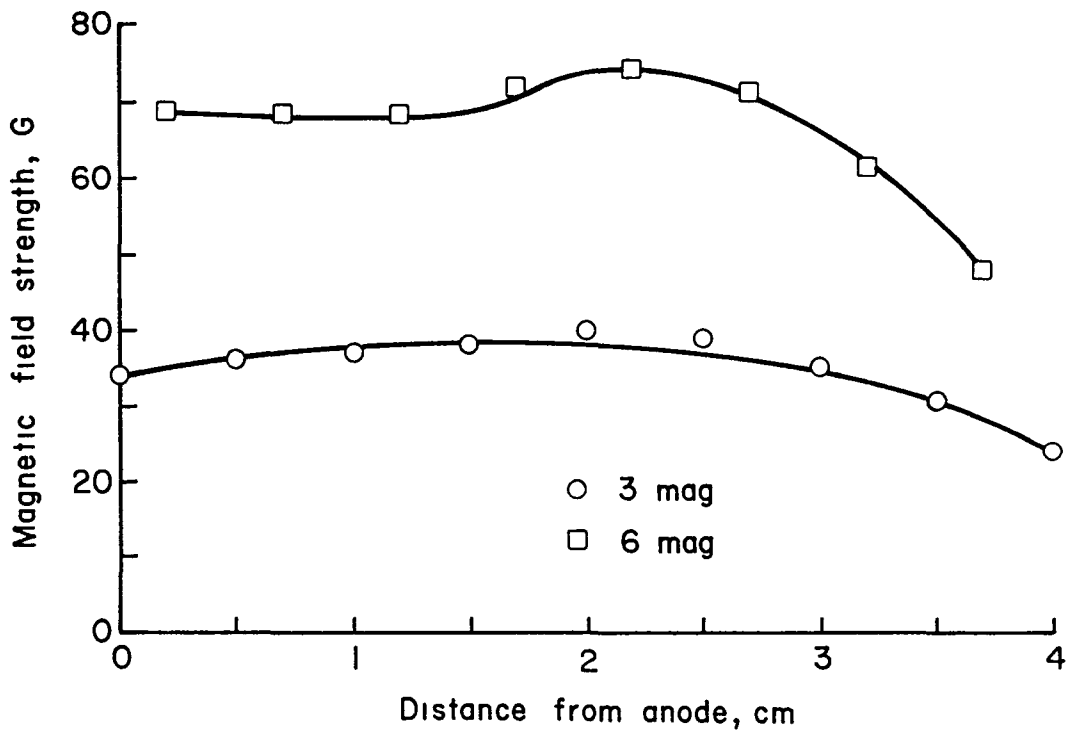

Fig. 4. Mean axial variation of magnetic field strength for the two thrusters at the cathode radius. (Cathode not operating.)

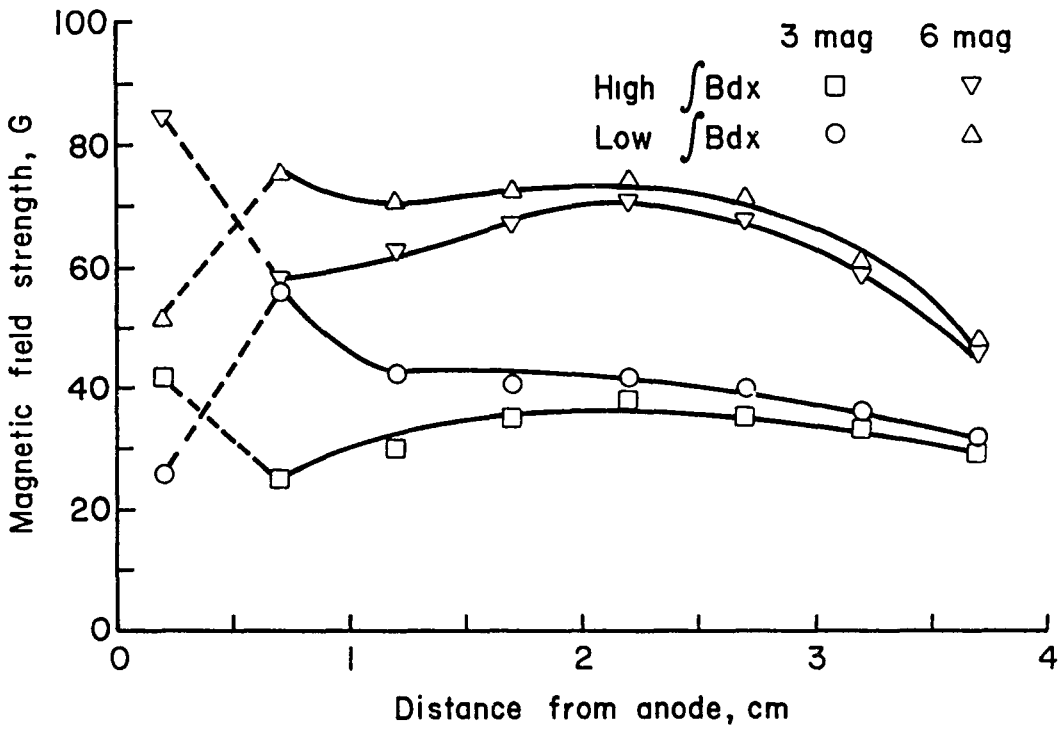

Fig. 5. Mean axial variation of magnetic field strength for the two thrusters at 1 mm inside the cathode radius. Constant field plus effect of ±17.5 A cathode current.

neutralizer cathode only. Operation was achieved with Ar flows of about 300-1000 mA-equiv and system pressures in the range of $3\text{-}10 \times 10^{-4}$ Torr. (The relation between flow and pressure was close to linear.)

The operating ranges for the three magnet thruster, Figs. 6-8, indicate at what discharge voltages the discharge initiated and extinguished over a range of system pressures. The main cathode only mode was seen to initiate a discharge at a voltage of

$$V = 103\text{-}6.5 \times 10^{4} P \quad (1)$$

and extinguish the discharge at a voltage of

$$V = 44\text{-}1.6 \times 10^{4} P \quad (2)$$

where P is the system pressure in Torr, over the range $3\text{-}9 \times 10^{-4}$ Torr. (The data from which Eqs. (1) and (2) were obtained is shown in Fig. 6.) When the neutralizer cathode was also used, at a temperature sufficient to emit 1 A, the discharge was initiated at approximately the voltage of Eq. (1). The voltage at which the discharge was extinguished, however, had two distinctly different slopes at high and low pressures. At low pressures, $3\text{-}5 \times 10^{-4}$ Torr, the discharge was extinguished at a voltage of

$$V = 93\text{-}10.2 \times 10^{4} P \quad (3)$$

while at high pressures, $5\text{-}9 \times 10^{-4}$ Torr, it extinguished at a voltage approximately the same as Eq. (2). (The data from which these relationships were obtained are shown in Fig. 7.) While operating in neutralizer cathode only mode (where the discharge was initiated using the main cathode, which was then turned off) with a neutralizer emission of 2.0 A the discharge extinguised at a voltage of

$$V = 147\text{-}9.2 \times 10^{4} P \quad (4)$$

(The data from which Eq. (4) was obtained is shown in Fig. 8.)

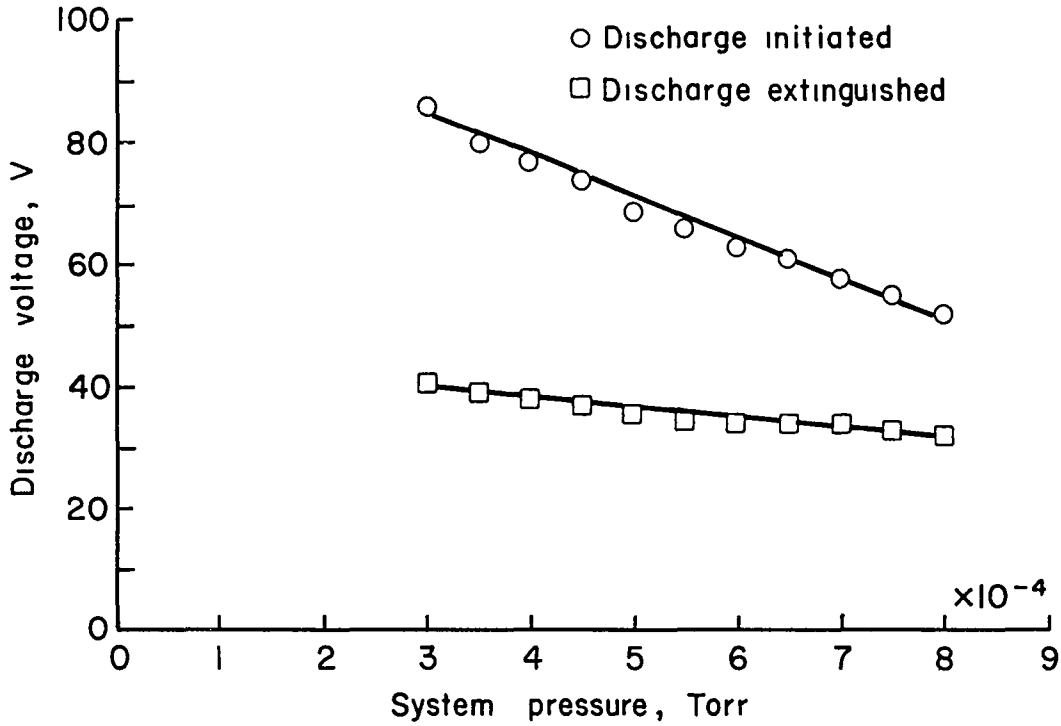

Fig. 6. Anode voltage required to initiate and extinguish the discharge. (No neutralizer cathode emission. Discharge current 2.5 A.)

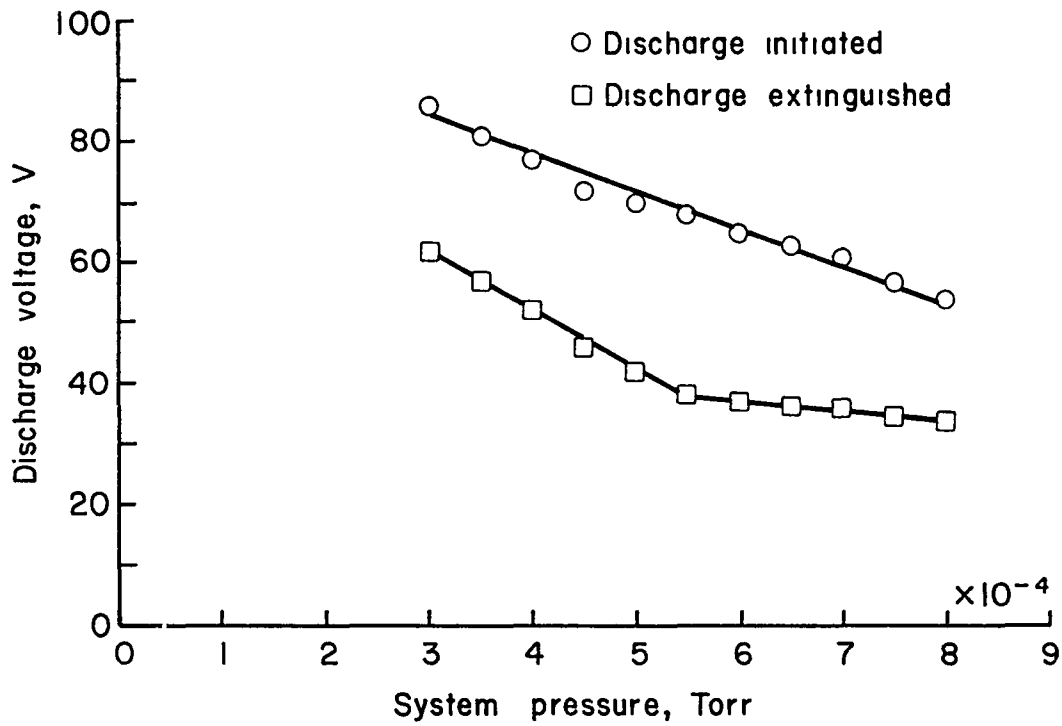

Fig. 7. Anode voltage required to initiate and extinguish the discharge. (Neutralizer emission 1 A. Discharge current 3.5 A.)

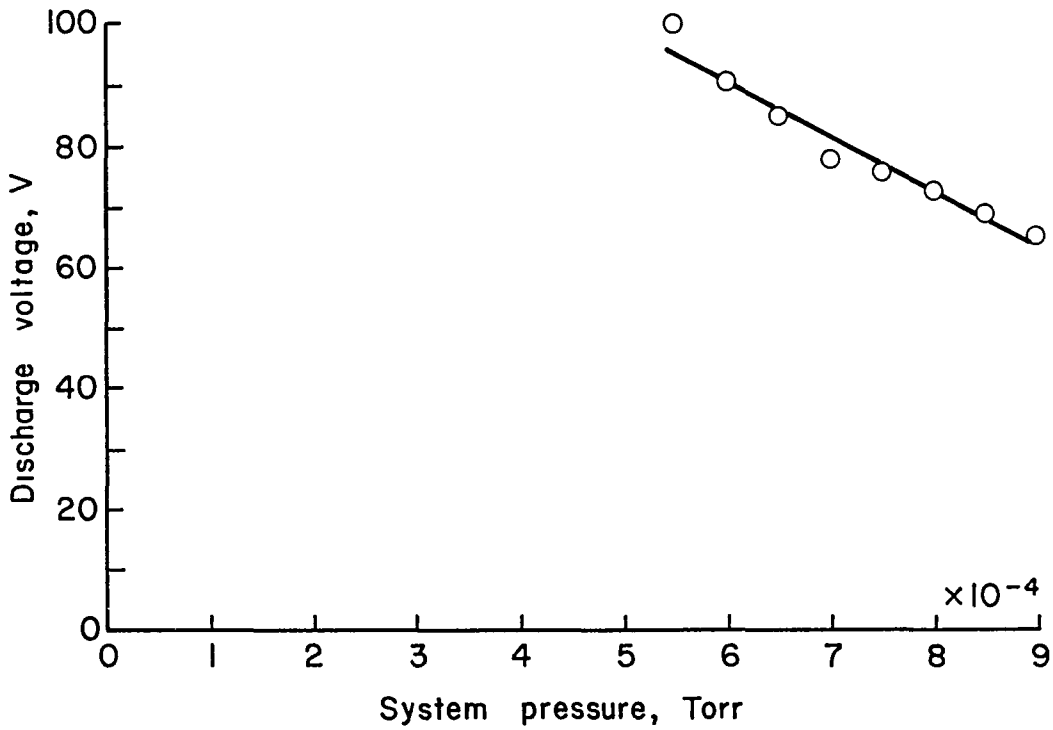

Fig. 8. Anode voltage required to maintain the discharge. No main cathode emission, neutralizer emission 2.0 A. Discharge current 2.5 A.

The interaction between the two cathodes indicated in Fig. 7 is typical of this investigation. Also, simply increasing the neutralizer emission at a fixed main cathode emission usually resulted in the discharge being extinguised. On the other hand, if the main cathode emission was reduced as the neutralizer emission was increased, it was occasionally possible to operate at higher neutralizer emissions than otherwise, if the change was made slowly.

Plasma Properties

The plasma properties were profiled by taking Langmuir probe measurements on an axial line at a radius of 3.2 cm, which was at a radius 1 mm less than that of the main cathode. The associated operating point was at: discharge voltage (V_d) 80 V, discharge current (J_d) 3.5 A, neutralizer emission (J_N) 0.4 A, system pressure (P) 5×10^{-4} Torr. The power supply circuit for these currents is the same as given in the last annual report for this grant (Fig. 4-9 in CR-165603). The discharge current is the total collected by the anode.

Results obtained from this profiling are shown in Figs. 9 through 11. As indicated in connection with Fig. 5, the high and low $\int Bdx$'s in the legends of Figs. 9 through 11 refer to the effect of the cathode heater current on the magnetic field between the cathode and the anode. Because these two sides of a thruster behaved differently, the data for the two sides are presented separately.

The three magnet thruster had a plasma potential drop of approximately 20 V on leaving the thruster. However, when the number of magnets was doubled, the plasma potential drop increased by approximately 9 V. Figure 11 shows that there was a much higher electron temperature in the chamber than downstream, outside the thruster.

As indicated by Figs. 9 through 11, the effect of the cathode's magnetic field on the plasma properties of the two sides was significant. The different magnetic integrals had a dramatic effect on the electron density with a lesser effect on the plasma potential and electron temperature.

The electron distribution function was also determined. Examining the electron distribution by comparing it to the best fit Maxwellian function it was found that the plasma does not fully thermalize.

Note that the absence of a fully thermalized distribution is consistent with the theoretical approach used for this thruster type.[5] That is, the collisions of the electrons in the enhanced diffusion process were assumed to be primarily with relatively slow moving ion-plasma waves, moving at ion acoustic velocity. Such collisions would tend to randomize the direction of the electron velocity more rapidly and more fully than the electron energy.

Beam Characteristics

The beam can be characterized by three parameters, the beam current (Fig. 12), the average beam energy (Fig. 13), along with the beam

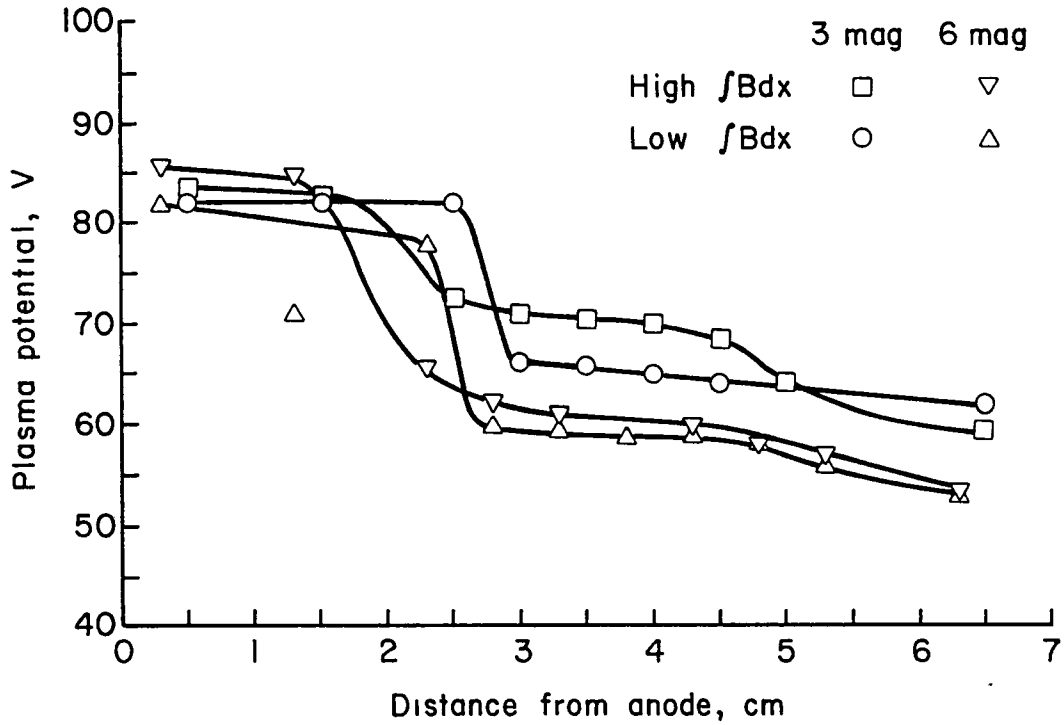

Fig. 9. Plasma potential, three and six magnet thrusters with modified poles. (Op. V_d = 80 V, J_d = 3.5 A, J_N = 0.4 A, P = 0.5 mTorr.)

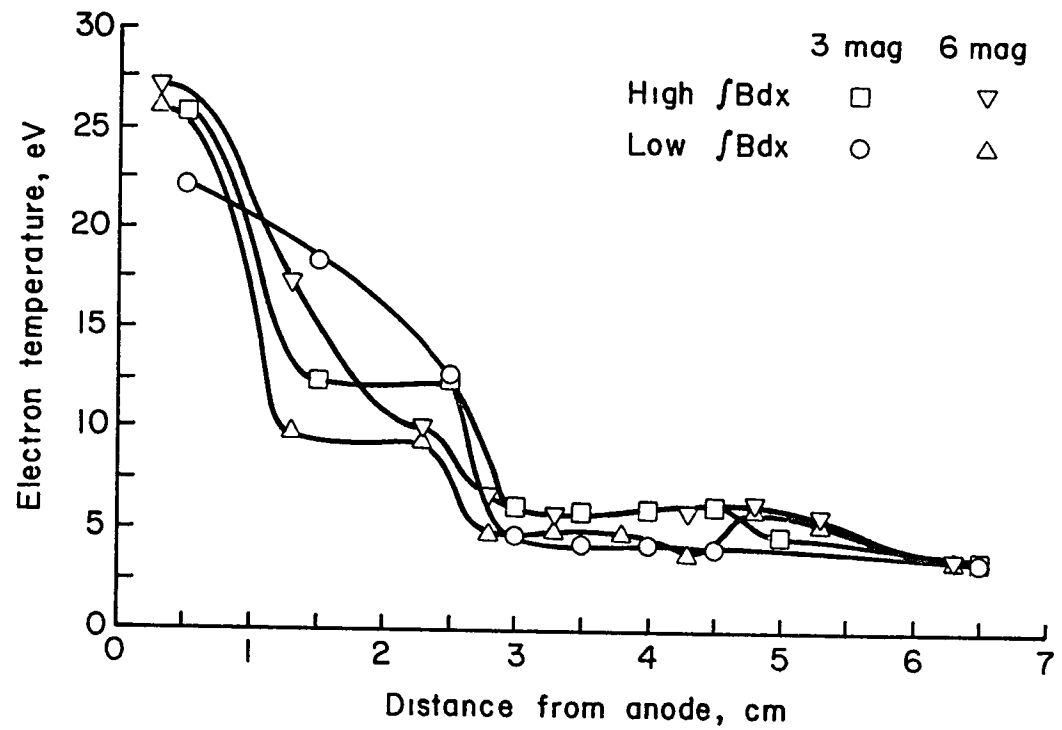

Fig. 10. Electron temperature, three and six magnet thrusters with modified poles. (Op. V_d = 80 V, J_d = 3.5 A, J_N = 0.4 A, p = 0.5 mTorr.)

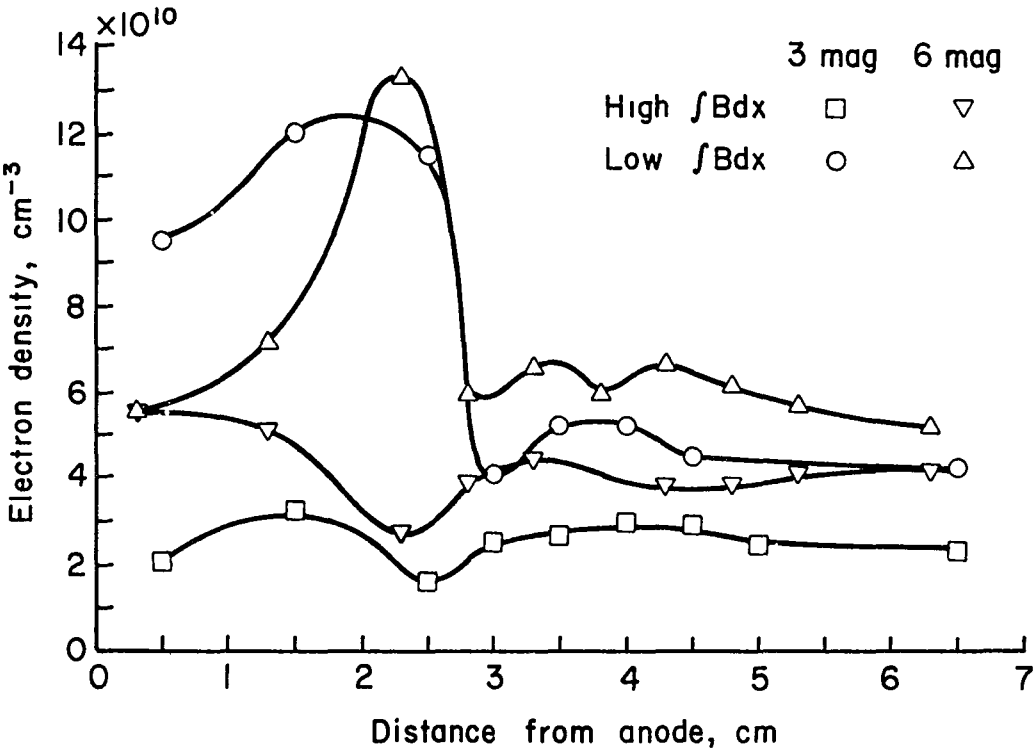

Fig. 11. Electron density, three and six magnet thrusters with modified poles. (Op. V_d = 80 V, J_d = 3.5 A, J_N = 0.4 A, P = 0.5 mTorr.)

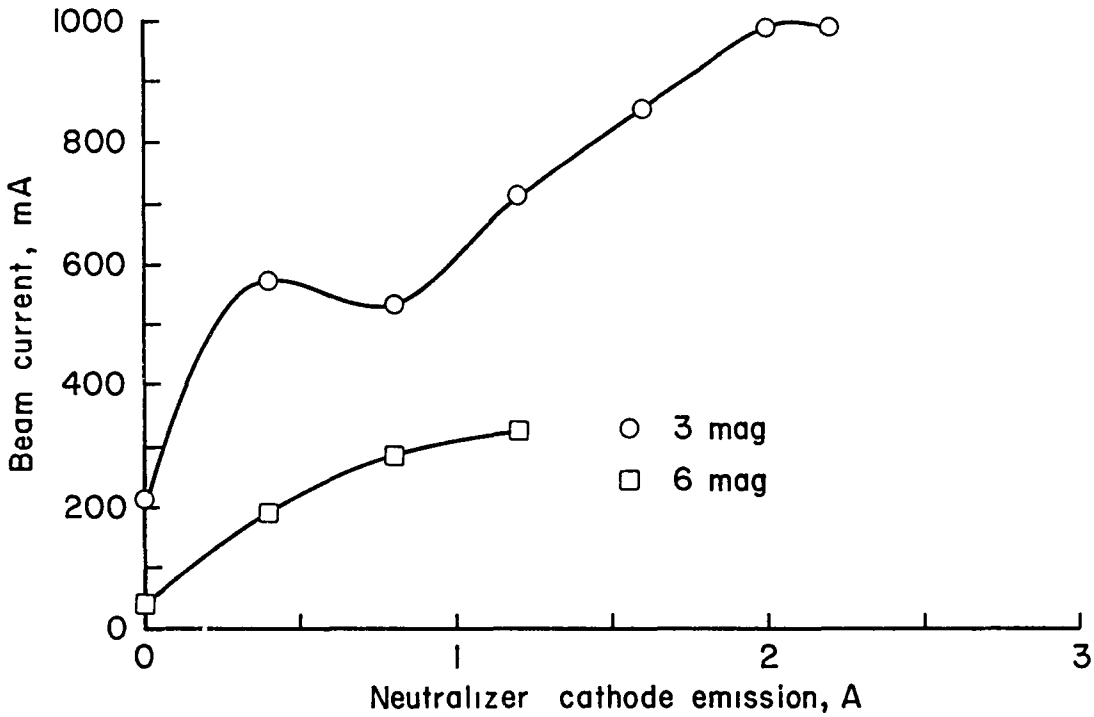

Fig. 12. Total beam current at exit plane of thrusters. (Op. V_d = 80 V, J_d = 3.5 A, P = 0.5 mTorr.)

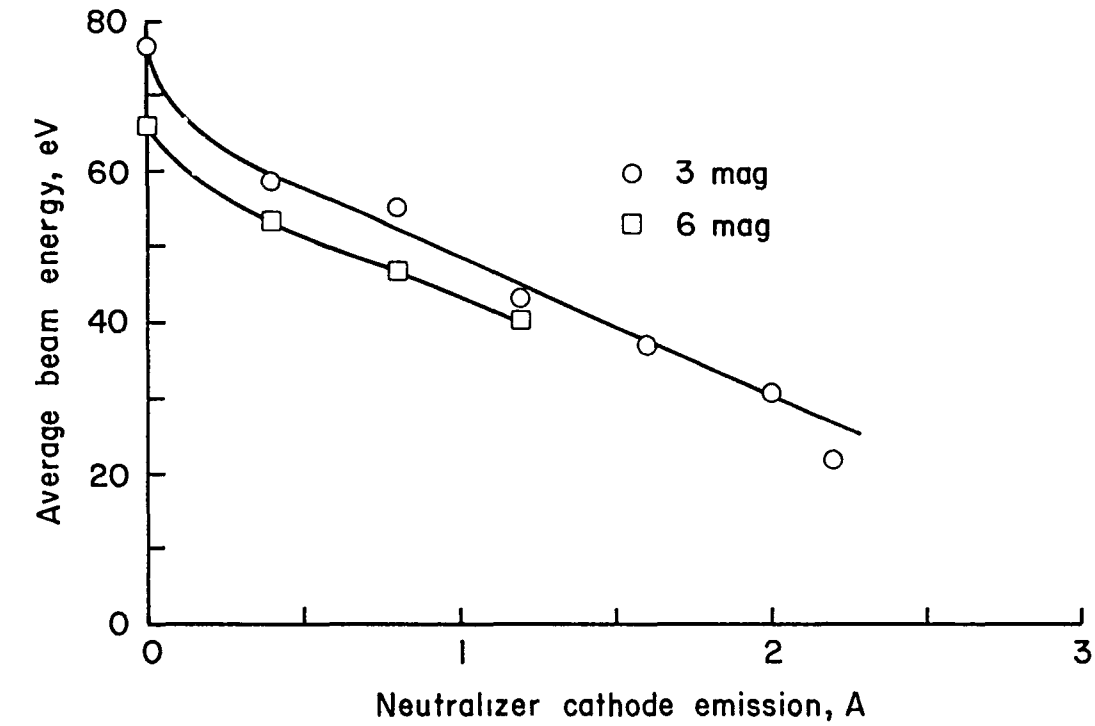

Fig. 13. Average discharge energy of the beam ions. (Op. V_d = 80 V, J_d = 3.5 A, P = 0.5 mTorr.)

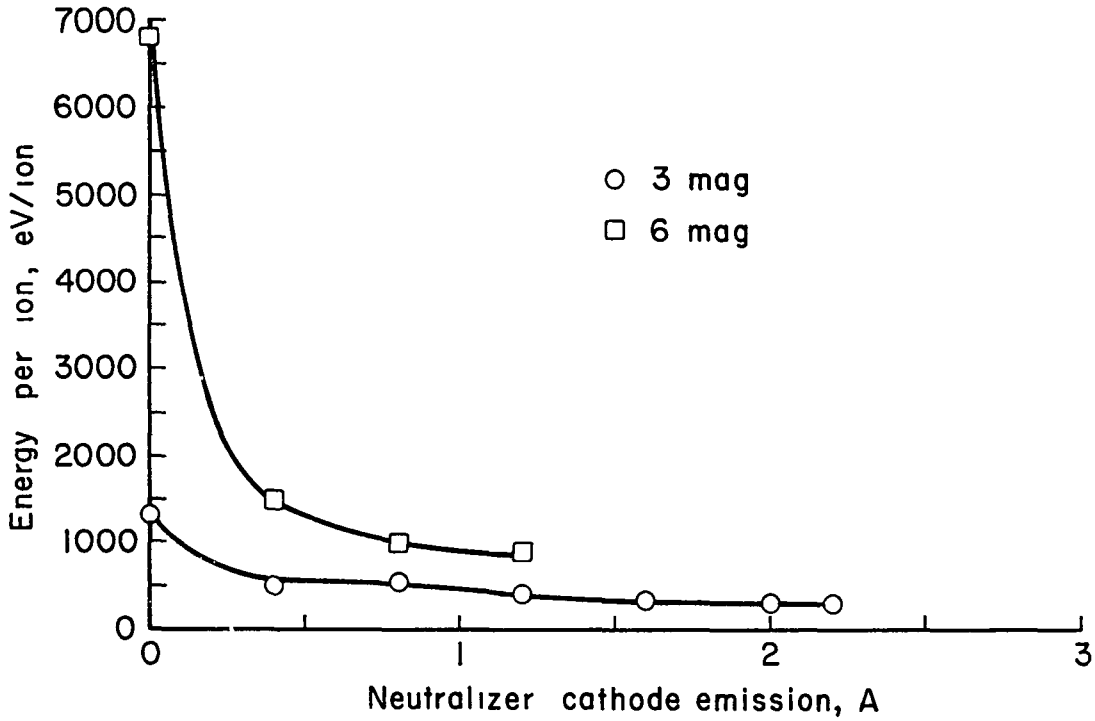

Fig. 14. Average energy cost per beam ion. (Op. V_d = 80 V, J_d = 3.5 A, P = 0.5 mTorr.)

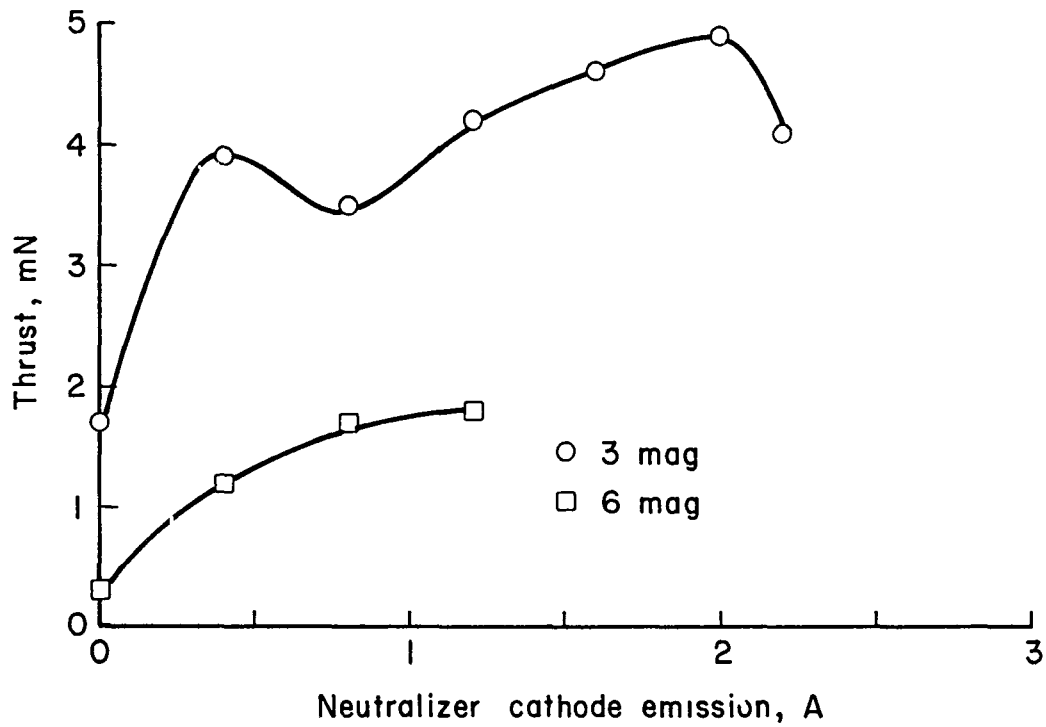

Fig. 15. Total thrust of the Hall-current accelerators. (Op. V_d = 80 V, J_d = 3.5 A, P = 0.5 mTorr.)

divergence angle. These beam parameters were found by using a Faraday cup to obtain an average energy profile over the entire beam. The beam divergence was measured to be approximately 14°, with essentially all of the beam current falling inside this half-angle. As shown in Fig. 12, the three magnet thruster provided approximately three times the beam current as the six magnet thruster. Also the average beam energy at low neutralizer emission is lower for the six magnet thruster than the three magnet thruster.

Thruster Characteristics

The thruster performance can be characterized by the cost per ion (Fig. 14) and the thrust provided (Fig. 15). As shown in Fig. 14 the energy cost per ion for the six magnet thruster was much greater than that of the three magnet thruster. Also from Fig. 15 it can be seen that the three magnet thruster provided more thrust than the six magnet thruster.

Conclusions

Two experimental Hall-current thrusters were tested with refractory metal cathodes where the major difference in the two thrusters was the number of magnets (three in one and six in the other) and hence the strength of the magnetic field. The magnetic field integral between the anode and cathode was reduced from an initial value of 50-60 $\times 10^{-6}$ T-m to 20 $\times 10^{-6}$ T-m to facilitate starting and operating at low voltages (<100 V). This change in integral was accomplished by moving the cathode closer to the anode.

The use of refractory metal cathodes resulted in serious circumferential variations in the magnetic field, which resulted in corresponding variations in plasma properties. Some of the limited voltage isolation capability (the potential difference from inside to outside the thruster) observed was probably due to the adverse affects of the refractory cathode on circumferential uniformity.

The higher magnetic field offered by the six magnet thruster while increasing the voltage isolation capabilities beyond that of the three magnet thruster also severely reduced the total beam current that the thruster would deliver. The higher magnetic field also reduced the average energy of the beam. Both the reduced beam current and the lower average energy contribute to the six magnet thruster having less thrust and a higher energy cost per ion than the three magnet thruster.

Various operating modes were possible with the main and neutralizer cathodes. Operation with the neutralizer cathode only, however, was severely hampered by the high Ar system pressures necessary to maintain a discharge. Operating at these high pressures, there was a tendency for a plasma arc to become established with surrounding hardware, causing the thruster to fail. It was found that the thruster generally produced a higher beam current at higher neutralizer emissions. But as

the neutralizer emission increased, the average ion energy in the beam also decreased. Since the increase in beam current with increasing neutralizer cathode emission was much greater than the decrease of average energy, there was a net increase in thrust when the neutralizer cathode supplied most of the discharge current.

The optimum Hall-current accelerator should probably have a total magnetic field equivalent to some number of magnets between zero and six. The optimum operating condition with both cathodes operating would probably be achieved when the thruster operates with the neutralizer cathode supplying approximately 70% of the emission current and with the main cathode supplying the remainder. This recommendation should be tempered with two considerations. First, the optimum magnetic field could shift when the circumferential nonuniformity due to cathode heating current is corrected. Second, the tests described herein were carried out in a small vacuum facility that was not well suited to the high beam-current capacity of a Hall-current thruster. The optimum magnetic field could also shift when the thruster is operated in a more suitable vacuum facility.

References

1. Staff of NASA Lewis Research Center, "30-cm Ion Thrust Subsystem Design Manual," NASA Tech. Mem. TM-79191, June 1979.
2. H. R. Kaufman, "Performance of Large Inert-Gas Thrusters," AIAA Paper No. 81-0720, April 1981. (A closely related paper is H. R. Kaufman and R. S. Robinson, "Large Inert-Gas Thrusters," AIAA Paper No. 81-1540, July 1981.)
3. M. C. Ellis, Jr., "Survey of Plasma Accelerator Research," in Proc. NASA - University Conference on the Science and Technology of Space Exploration - Vol. 2, NASA, Washington, D.C., pp. 361-381, Nov. 1962.
4. G. S. Janes and R. S. Lowder, "Anomalous Electron Diffusion and Ion Acceleration in a Low-Density Plasma," Phys. Fluids, Vol. 9, pp. 1115-1123, June 1966.
5. H. R. Kaufman, "Theory of Ion Acceleration with Closed Electron Drift," AIAA Paper No. 82-1919, Nov. 1982.

TECHNOLOGY OF CLOSED-DRIFT THRUSTERS

Abstract

The technology of closed-drift thrusters was reviewed. The experimental electron diffusion in the acceleration channel was found to be within about a factor of 3 of the Bohm value for the better thruster designs at most operating conditions. Sharply higher experimental diffusion was found at magnetic integrals above about 50 times the minimum value required to prevent direct trajectories to the anode. A calculation procedure was also presented for thruster performance, and compared with available experimental data. Thruster efficiencies of about 0.5 appear practical for the 1000 to 2000 s range of specific impulse. Lifetime information is limited, but values of several thousands of hours should be possible with anode-layer thrusters operated $\leq$2000 s.

Introduction

A closed-drift thruster is defined herein as a thruster in which ions are electrostatically accelerated in essentially the thrust direction, with the accelerating electric field established by an electron current interacting with a transverse magnetic field. One component of the electron motion is counter to the ion flow. Another component is normal to that direction. The current associated with this normal component is called the Hall current. In a closed-drift accelerator, there is a complete, or closed, path for the Hall current. In addition, for the ions to be accelerated in essentially a single thrust direction, the ion cyclotron radius must be much larger than the total acceleration length.

Closed-drift thrusters usually employ axially symmetric electrodes and pole pieces, with the magnetic field in the radial direction and the electric field in the axial direction. The Hall current flows in a circular closed path in such a configuration. A few closed-drift thrusters without axial symmetry have also been investigated.

The closed drift thruster is particularly well suited for operation in the 1000 to 2000 s range of specific impulse. It is difficult to operate above about 1000 s with an electrothermal thruster due to excessive excitation and ionization losses. On the other hand, the space-charge-flow limitations of gridded electrostatic thrusters will not permit practical ion current densities below about 2000 s.

Within the 1000 to 2000 s range, the electron backflow required to establish ion acceleration can, for the most part, be used to generate ions. The generation of ions constitutes the major closed-drift thruster loss in this range of specific impulse, and this loss can be under 100 eV per beam ion.

The power processing requirements are also moderate. In a properly designed closed-drift thruster, only one power circuit is required for steady-state operation, with the voltage of this circuit typically in the 50 to 500 V range.

Historical Development

Most of the early closed-drift thrusters had dielectric channel walls and a channel length at least equal to the channel width, as indicated in Fig. 1.[1-7] In addition, the electron cyclotron orbit was small compared to the acceleration length. The ion production was by either a contact-ionization process or an electron-bombardment volume-production process. This closed-drift thruster was called a Hall-current type.[1,4-7]

During this early period another variation of closed-drift thruster was also studied, in which the length of the acceleration channel was considerably less than the channel width.[8-9] The acceleration in this type of thruster was believed to take place over a distance of the order of the local electron-cyclotron orbit. This closed-drift thruster was called a space-charge-sheath type.

The initial hope was that the electron current required to establish the accelerating electric field would be governed by classical diffusion. It was soon established that these axial electron currents were orders of magnitude above the classical value, presumably due to the turbulence, or oscillations, involved in the acceleration process.[5]

The range of interest for specific impulse in electric primary propulsion was 5000 to 10,000 s during the 1960-70 period. The electron backflow at these high specific impulses was energetic enough that it was difficult to efficiently use in volume ion production. The large electron backflow therefore constituted a major loss. It is true that this electron backflow could have been used to heat the ionizer of a contact-ionization thruster. But contact ionization had other problems, including excessive heating-power requirements and difficult fabrication problems.

Compared to gridded electrostatic thrusters of the 1960-70 period, the closed-drift thrusters had much lower efficiencies. For a proper historical prospective, it should be kept in mind that the 5000 to 10,000 s range of interest for specific impulse resulted from early projections of very light-weight power sources, and interest in interplanetary missions. As a result of these lower efficiencies, much of this early work on closed-drift thrusters ceased about 1970.

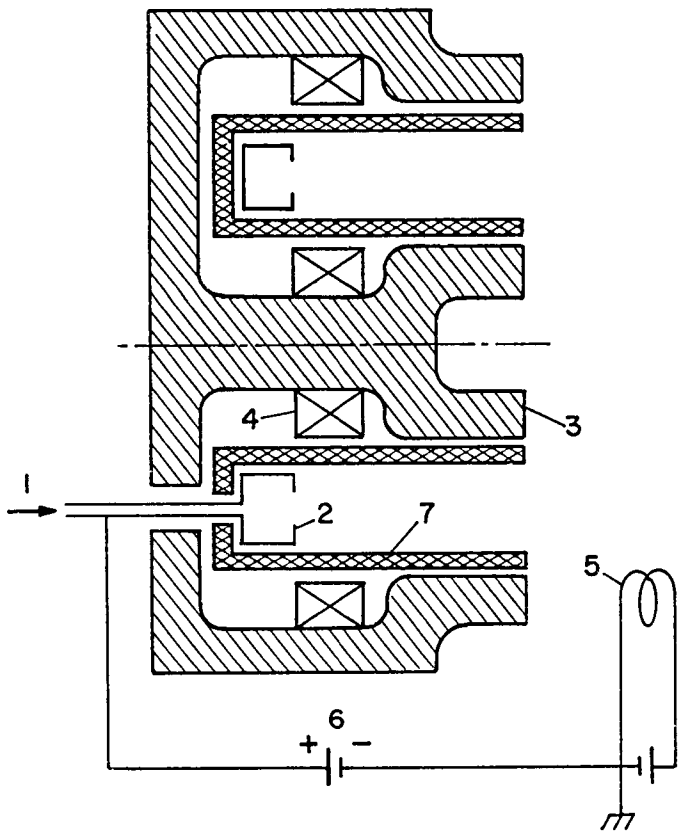

Fig. 1. Hall-current, or closed-drift extended-acceleration (CDEA), thruster (single-stage). (1) Propellant feed; (2) anode-distributor; (3) magnetic circuit, pole pieces; (4) magnet winding; (5) cathode-neutralizer· (6) discharge power supply; (7) insulator.

However, other programs involving closed-drift thrusters continued.[10-34] About the time that the space-charge-sheath type of thruster[8] was operated, an analysis of the closed-drift acceleration process showed that two distinctly different acceleration processes could take place.[12] In one case the electrons in the acceleration region were assumed to be at a negligible temperature (zero). The potential variation throughout the acceleration region was then found to be smooth and continuous, as had been implicitly assumed in the earlier closed-drift thruster work. If, however, the electrons were assumed to heat up as they flowed from the ion exhaust to the ion formation region, then a near-discontinuous potential jump occurred at the positive end of the acceleration channel. The remainder of the acceleration was assumed to take place in an axial length of the order of the local electron cyclotron orbit.

With this acceleration model to serve as a guide, experimental verification of this anode-layer acceleration process was soon found in studies of the Penning discharge.[35-40] Subsequent studies of the Penning discharge gave additional verification and information.[41-49] These and other studies made clear some of the distinctions between the two types of closed-drift thruster.

In the first type of thruster, with a relatively long acceleration channel and dielectric wall (see Fig. 1), collisions of energetic electrons and ions with the dielectric walls served to emit low-energy secondary electrons. The high conductivity along magnetic field lines permitted energetic electrons to reach the walls and be continuously replaced by low-energy secondaries. This process served to limit the electron temperature to a moderate value in the acceleration region. As a result of the continuous and extended acceleration process, this type of thruster has been called a closed-drift extended-acceleration, or CDEA, thruster in recent work.[14,15,16,18,31,34]

In the other type of thruster (see Fig. 2), the short channel walls give less opportunity for ion and electron collisions with the walls. Further, the metallic channel walls in this type are at the potential of the electron emitter, so that (except for the high-energy "tail" of a turbulent electron distribution) electrons will be reflected from the walls. The electrons will therefore tend to conserve total energy as they flow toward the anode, resulting in an increased electron temperature as the anode is approached. At some point, the increase in electron temperature will result in a downstream contribution to electron diffusion that will equal the upstream component due to the potential gradient. This point is the downstream boundary of the potential jump to near anode potential. This type of thruster is called, appropriately enough, an anode-layer thruster in recent work. It should be noted that this thruster type is very similar to the space-charge-sheath thruster studied earlier.[8,9]

Because the majority of both the total work and the recent work on closed-drift thrusters has used the CDEA and anode-layer designations, these designations will be used for the two major types in the remainder of this paper.

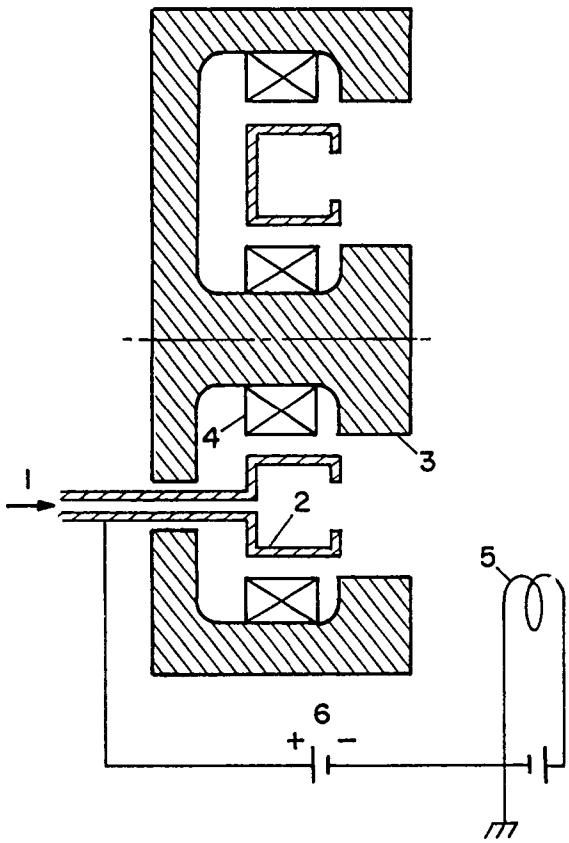

Fig. 2. Anode-layer thruster (single-stage). (1) Propellant feed; (2) anode-distributor; (3) magnetic circuit, pole pieces; (4) magnet winding; (5) cathode-neutralizer; (6) discharge power supply.

Operating Characteristics

The typical single-stage closed-drift thruster requires one major power supply, for the discharge between the electron-emitting cathode and the anode. If permanent magnets are not used, an auxiliary supply will be required for the magnet winding. A heating supply will also be required if a refractory-filament cathode is used. If a hollow cathode is used, a separate power supply will be required for initiation of the cathode discharge. Depending on the hollow-cathode design, no power supply may be required for its operation after it is started and coupled to the main discharge.

The operating characteristics of the main discharge are of particular interest. The characteristics of a single-stage CDEA thruster can be deduced from a large number of publications, but are described in a compact form by Morozov, et al.[14] Information is less complete for the single-stage anode-layer thruster, but most of what is available appears to be similar to that of the CDEA thruster. The following general description therefore applies directly to a CDEA thruster, but should, for the most part, also apply to an anode-layer thruster. Where differences appear to exist for the two closed-drift thruster types, these differences will be pointed out.

Assuming both the mass flow rate and the magnetic field strength are held constant, the current-voltage characteristics for the range of most interest can be approximated as a nearly constant-voltage region below a "knee" and a nearly constant-current region above (see Fig. 3). The current at the knee is roughly related to the current-equivalent of the mass flow rate, calculated with one electronic charge assigned per atom or molecule. To the extent that the propellant utilization is less than unity, the current at the knee will be reduced. The electron backflow to establish the accelerating electric field and double ionization will both tend to increase the knee value of current. The actual current value will include all of these effects, with some approximate overall relationship with the mass flow rate.

The sharpness of the discharge-characteristic knee is most evident with easily ionized materials, such as cesium and xenon. Figure 3 is characteristic of such an easily ionized material. With a less easily ionized material, such as argon, the curve shape can become much more rounded than is indicated in Fig. 3, so that a "knee" is only vaguely defined.

To a first approximation, the accelerated ion current will be a constant fraction of the discharge current in Fig. 3. The operation in the nearly constant-voltage region therefore corresponds to a range of propellant utilizations, with the highest utilization obtained at the highest current. The nearly constant-current region is also called the current saturation region.

Because charged particles with both signs are present in the acceleration region, there is no space-charge limit for the current density of the accelerated ions. Ion current densities in the A/cm^2 range are therefore practical.[6,13]

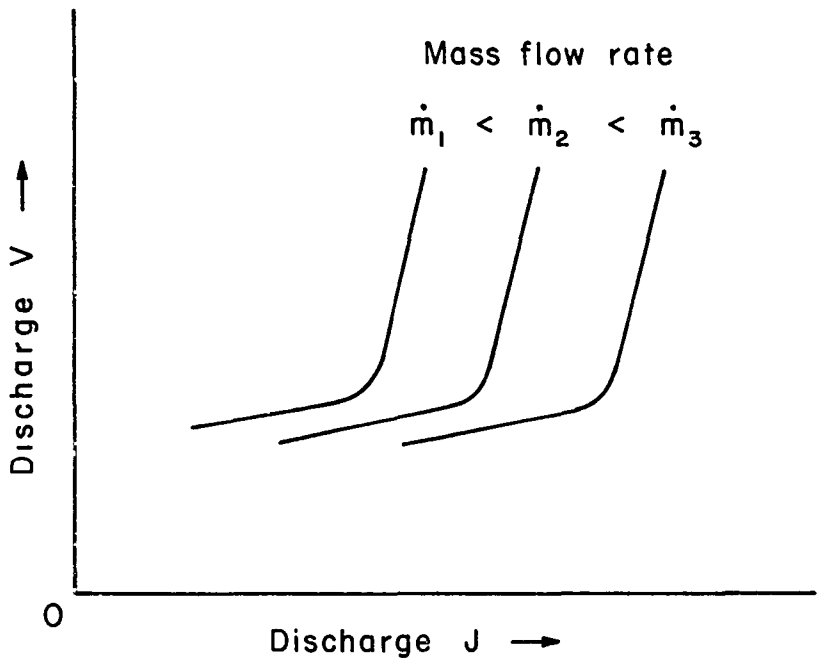

Fig. 3. Discharge characteristics for single-stage closed-drift thruster. (Magnetic field strength held constant.)

Oscillations and fluctuations are generally observed in the operating regions of interest for a closed-drift thruster.[16] A typical disturbance in the nearly constant-voltage region is an ionization, or drift, wave. The fundamental mode of an ionization wave has a wavelength equal to the mean circumference of the annular channel. The wave velocity is lower than the electron drift velocity, E/B, typically by a factor of several. The frequencies observed for ionization waves are normally in the tens of kHz range, with a discrete frequency for the fundamental the usual dominant mode.[16] Because an ionization wave is driven by variations in the ion production rate, its amplitude decreases as the discharge current is increased and the utilization increased.

A typical disturbance in the nearly constant-current region is the transit-time oscillation.[16] This type of oscillation has a broad band of high frequencies. The center of this broad band roughly corresponds to the ion transit time through the acceleration channel. The amplitude of this oscillation increases with discharge voltage and can reach 20-30% of the mean applied voltage.

The amplitudes of these two types of oscillations tend to decrease as the knee is approached. Although there are varying degrees of overlap of the two oscillations near the knee, this region is one of comparative stability. This stability, together with high utilization, makes the general vicinity of the knee the preferred region for thruster operation. If the ion beam current is to be varied, the mass flow rate should also be varied so as to maintain the operation near the knee (see Fig. 3).

In the above discussion, two main types of oscillations have been emphasized. Other types of oscillations are also possible, including system oscillations, which depend on power-supply characteristics. Even with these other oscillations present, the knee region is still, in general, the preferred operating region.

The effect of varying the magnetic field strength is indicated in Fig. 4 for a fixed discharge current.[14] The mass flow rate is also assumed constant, at a value sufficient to avoid operation above the discharge-characteristic knee. The discharge voltage under these conditions (Fig. 4(a)) tends to increase with increasing magnetic field strength, then level-off above some critical magnetic field. The fraction of the current through the main power supply (termed discharge current herein) that results from accelerated ions (Fig. 4(b)) follows a similar trend. Useful values of the ion current typically range from 50-70% of the total discharge current.

The critical magnetic field is believed to be an artifact of the walls of the acceleration channel, inasmuch as bulk diffusion considerations alone would indicate a monotonic increase of voltage with an increasing magnetic field.

From the limited data available[14,28] and physical considerations, it is believed that the relative trends of Figs. 4(a) and (b) differ for CDEA and anode-layer thrusters. As will be discussed in the next

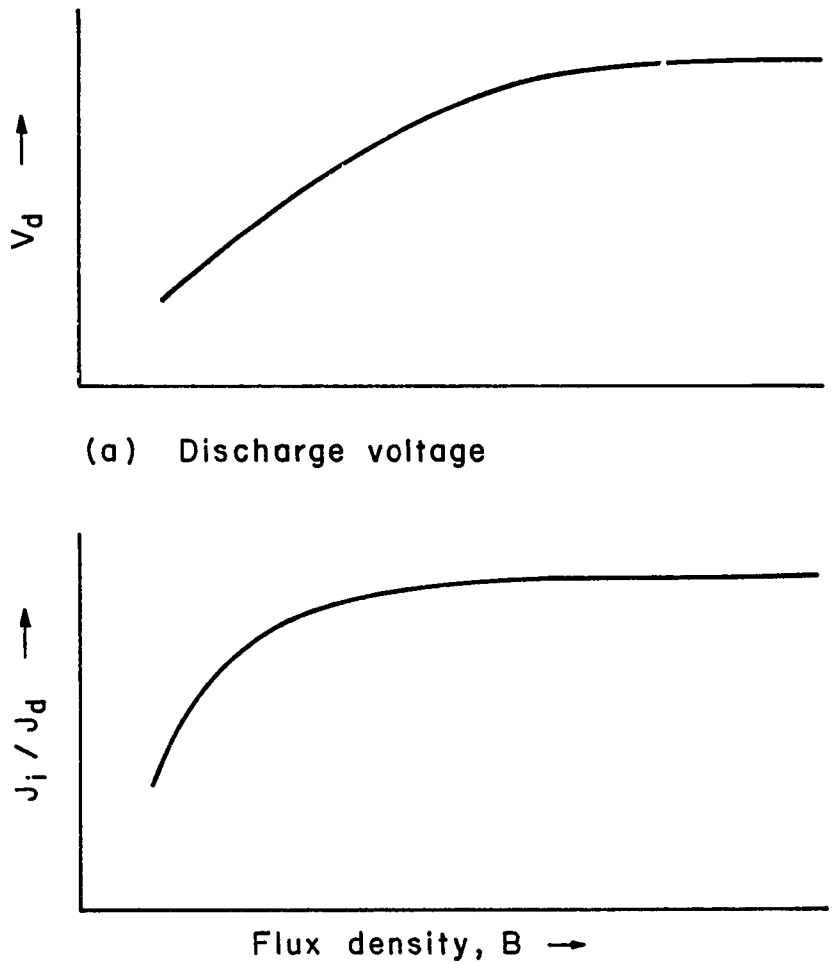

Fig. 4. Effect of magnetic field strength on operation of single-stage closed-drift thruster.

section, the temperature of the backstreaming electrons in a CDEA thruster tends to be limited by wall processes. The production of ions will thus tend to be linearly related to the backstreaming electron current in such a thruster. The matching condition for the ion production and acceleration portions of a CDEA thruster will therefore result in a nearly constant current ratio, J_i/J_d, over a broad range of operating conditions. For a CDEA thruster, then, the nearly constant region of J_i/J_d in Fig. 4(b) should extend over most of the range of voltage shown in Fig. 4(a).

For an anode-layer thruster, though, the temperature of the backstreaming electrons, as they reach the ion production region, should vary nearly linearly with total applied voltage. A given ion current should therefore be produced with less backstreaming electron current at higher applied voltages. For moderate voltages, up to several hundred volts, the matching condition for ion production and acceleration would be expected to shift with voltage, giving a monotonically increasing value of J_i/J_d with increasing voltage.

Multistage closed-drift thrusters (see Fig. 5) have also been investigated. An additional cathode, at the potential of the intermediate electrode, has been optional.[29-31] The advantage of a multistage design is that the ion production process can be made more independent of the acceleration process. For example, a high-current, low-voltage stage can be used to form the ions. Then the electron backflow can be minimized through the high-voltage accelerating stage, thereby maximizing acceleration efficiency. It appears that any efficiency advantage for a multistage thruster should be greatest at high acceleration voltage. For low-voltage thrusters, particularly of the anode-layer type, the energy of the backstreaming electrons can be effectively used for ion production. The multistage approach may therefore be less efficient at low voltages.

There are also some specific details of closed-drift thruster designs that are important. Departures from circumferential uniformity by 5-15% for various parameters can cause large adverse effects on performance.[27,29] For neutral flow, though, the uniformity requirement refers to the general circumferential variation. The use of twenty uniformly spaced holes apparently had no adverse effect relative to a circumferentially uniform annular opening.[20,21]

The foregoing discussion also implicitly assumes passive pole-piece surfaces. If electron-emissive coatings are possible, a wide range of adverse effects can be obtained.[27] When using propellants such as cesium, it is preferable to have the thruster hot enough to avoid any significant condensation on internal surfaces.

Lifetime information is quite limited. Values of up to 1000 hours are given for CDEA thrusters.[33,34] It is suspected that the ion bombardment of the insulating channel walls causes degradation of the insulator surface, eventually causing substantial surface conductivity.

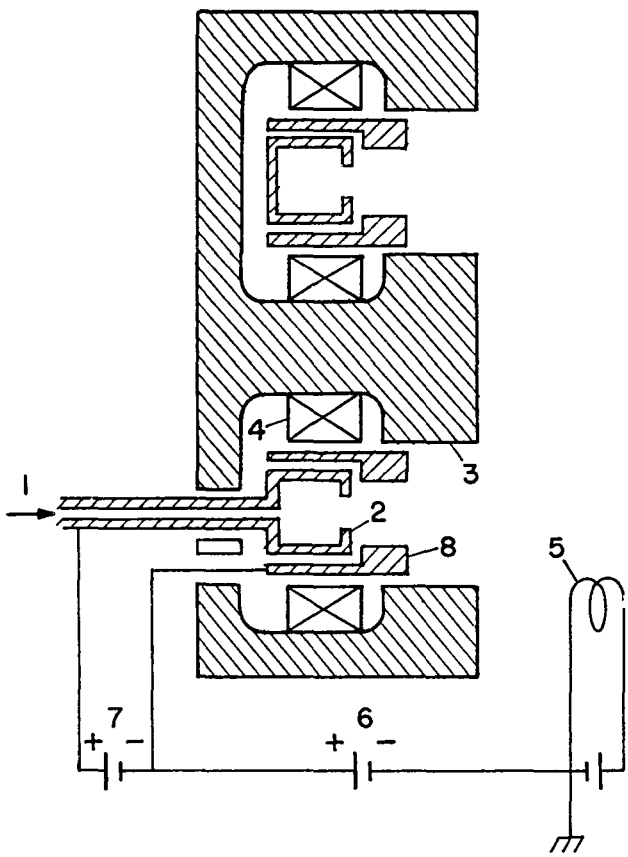

Fig. 5. Two-stage anode-layer thruster. (1) Propellant feed; (2) anode-distributor; (3) magnetic circuit, pole pieces· (4) magnet winding; (5) cathode-neutralizer; (6) acceleration-stage power supply; (7) ionization-stage power supply, (8) intermediate electrode.

This process would be voltage and propellant dependent, so that more inert propellants and lower voltages would tend to give longer lifetimes. With this mode of failure, it is possible that large increases in lifetime, above the 500-1000 hour range, may not be practical.

In the anode-layer thruster, only conducting surfaces are exposed to energetic ions. Greater lifetimes should therefore be possible with an anode-layer thruster than a CDEA thruster, with other operating aspects assumed to be similar. The electrode erosion in an anode-layer thruster appears to be caused primarily by off-axis trajectories of energetic ions near the edges of the ion beam.[19,34] The scaling law for this erosion process is not clear at present, but, using moderate extrapolations from CDEA tests, lifetimes of up to several thousands of hours should be readily possible. Required thrust durations for various missions tend to vary roughly with specific impulse, so that a few thousands of hours may be adequate for many missions in the 1000-2000 s range of specific impulse.

Electron Diffusion

It should be apparent that electron diffusion across a magnetic field is an important aspect of closed-drift thruster operation. As mentioned above, an early and important analysis of electron diffusion indicated the qualitative difference between CDEA and anode-layer acceleration.[12] This analysis was carried out assuming $1/B^2$ classical diffusion, which was experimentally found to be orders of magnitude too low. The use of classical diffusion in this critical analysis has apparently led to some confusion as to whether classical diffusion is required for anode-layer thruster operation.[14]

The early diffusion analysis[12] has since been repeated with the assumption of 1/B anomalous diffusion,[50] which is more consistent with experimental observations. The assumption of uniform and constant electron-current density (in the direction counter to ion acceleration), together with 1/B diffusion results in the integral $\int B dx$ being the significant magnetic parameter. This mathematical approach was apparently used first in the diffusion calculations for the discharge chamber of a gridded electrostatic thruster.[51]*

---

*The integral $\int B dx$ (or $\int \vec{B} \times d\vec{x}$) has significance from several viewpoints. It is the proper magnetic parameter for the deflection of an isolated charged particle passing through a region of uniform potential, but varying magnetic field strength.[52] It was later shown to be the proper parameter for a charged particle passing through a region in which both the plasma potential and the magnetic field strength varied.[53] It is also an empirical parameter for closed-drift acceleration, based on the observation that the local time-averaged electric field varied approximately as the local magnetic field strength.[14]

The two general forms of analytical results obtained for the acceleration region of a closed-drift thruster are indicated in Fig. 6. The plasma potential is defined as zero at the accelerator exhaust plane and V_o at the source potential for the ions. The potential parameter V/V_o thus increases from zero to unity when moving from the accelerator exhaust to the source of the ions. In the electron diffusion parameter, j_e is the axial electron current density (assumed to be a constant), B is the transverse flux density, x is the axial distance measured from the exhaust plane, e is the electronic charge, and n_o is the electron (or ion) density at the exhaust plane. For a given thruster configuration and operating condition, only the integral $\int Bdx$ is a variable, which increases from zero to a maximum when going from the exhaust plane to the upstream end of the closed-drift acceleration region.

In one form of solution, the potential ratio, V/V_o, increases smoothly and continuously from 0 to 1, when passing through the acceleration region. This solution is obtained only for a zero electron temperature throughout the acceleration region. The other form of solution is obtained when the electron temperature is greater than zero. In this form the electron diffusion downstream due to a finite electron temperature becomes, at some point, equal to the upstream diffusion due to the potential gradient. At this point, indicated by an arrow in Fig. 6, the slope of the potential variation becomes infinite. The mathematical solutions can be continued beyond this point, as shown by the dashed line, but they become physically meaningless.

In terms of physical application, the two types of solutions indicated in Fig. 6 can be organized into two other categories. In the first category, the electron temperature is assumed constant throughout the acceleration region. This category also includes the unique zero-temperature solution of Fig. 6. The diffusion-parameter values for the entire closed-drift acceleration region are then given by[50]

$$j_e \int Bdx/en_o V_o = \frac{1}{8}\left[1 + \frac{T}{2V_o} - (1-V/V_o)^{1/2} - \frac{T/V_o}{2(1-V/V_o)^{1/2}}\right] . \qquad (1)$$

The corresponding maximum values for V/V_o are given by

$$V/V_o = 1 - T/2V_o . \qquad (2)$$

Note that the value of V/V_o goes to unity as T/V_o goes to zero. The general form of the solutions indicated by Eqs. (1) and (2) depends on 1/B electron diffusion. The numerical constants result from the assumption of the Bohm value for this 1/B diffusion.

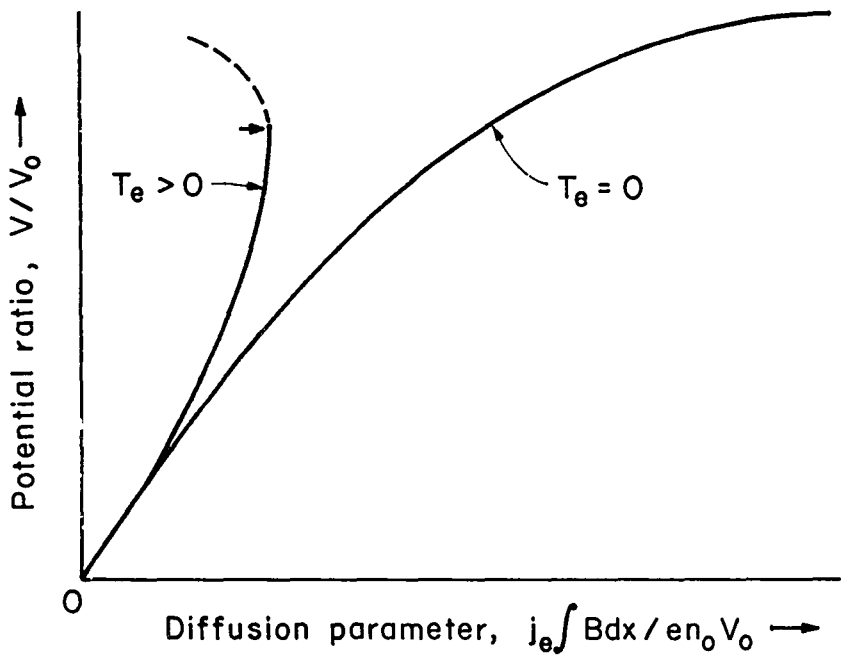

Fig. 6. Forms of solutions for 1/B electron diffusion in closed-drift acceleration.

Because the maximum value of V/V_o is <1 for $T/V_o>0$, there will, in general, be an infinite slope of potential at the upstream end of the acceleration region. If the ions are assumed to come from a plasma located at the upstream end of the acceleration region, it is reasonable to assume that they are accelerated to ion acoustic velocity before leaving the ion production region (the Bohm condition for a stable sheath). If the background electrons in the production and acceleration regions are at the same temperature, the acceleration will be just sufficient to reduce the plasma potential at the boundary of the ion production region to the value given by Eq. (2).

For ion production in a plasma, then, constant electron temperature in the acceleration region implies an absence of a potential discontinuity between the production and acceleration regions. Note that this conclusion is dependent on the production of ions in a plasma. If contact ionization is used, for example, a potential jump of T/2 will be found close to the ionizer.

In the second category of solutions the electron energy is assumed to be conserved as the electrons flow upstream. This results in a temperature rise, in eV, equal to 2/3 of the potential difference, in V, through which the electron passes. The diffusion parameter values for the entire closed-drift acceleration region are then given by[50]

$$j_e \int B dx / e n_o V_o = \frac{1}{24} \left[5 + \frac{3T_o}{2V_o} - 4(1-V/V_o)^{1/2} - \frac{2+3T_o/V_o}{2(1-V/V_o)^{1/2}} \right] . \quad (3)$$

The corresponding maximum values for V/V_o are given by

$$V/V_o = \frac{3}{4} (1-T_o/2V_o) . \quad (4)$$

Because the electron temperature varies throughout the acceleration region, T_o is the electron temperature in the exhaust plane.

For the production of ions in a plasma, T_o should also approximate the temperature of background electrons in this plasma. The normal acceleration of ions by a potential difference of $T_o/2$ will not be sufficient to avoid a potential discontinuity at the junction of the production and acceleration regions. This discontinuity, which exists from the viewpoint of continuum equations, should be accommodated by a single, collision-free electron orbit.[50]

Experimentally, the constant electron-temperature solutions should be approximated with CDEA thrusters, where collisions of ions and energetic electrons with the insulating walls will result in the continual replacement of energetic electrons by lower energy secondary electrons.[32]

In the anode-layer type, this exchange process is generally prevented and the acceleration process should approximate the conserved energy solutions.

Experimental electron backflows were compared with the theoretical predictions of Eqs. (1) through (4) for several closed-drift thrusters, and presented in Fig. 7. All of these data were analyzed with the constant-temperature solutions of Eqs. (1) and (2), except for the data of Ref. 9. These last data were obtained with a channel length-to-width ratio of $\sim$0.2. Even though an insulating coating was used on the channel walls, there was little opportunity for many wall collisions in such a short channel, and the conserved-energy solutions of Eqs. (3) and (4) were used instead. The data were generally incomplete, so that assumptions were necessary for such parameters as electron initial, or constant, temperature. These assumptions were felt to contribute an uncertainty in the final values of Fig. 7 of less than ±20%.

The experimental-to-Bohm electron current ratios in Fig. 7 range over two decades, with no readily apparent dependence on the magnitude of the magnetic integral. The data presented in Fig. 7 include a wide range of designs, some of which are known to be poor. Eliminating the data from poor designs should therefore result in a reduction of the range of electron current ratio.

The data of Morozov et al.[15] included a magnetic-field configuration that was strongest at the upstream end of the channel, another that was uniform, and still another that was strongest at the downstream end of the channel. The highest ratios of J_{exp}/J_{Bohm} were for the former, while the lowest were for the latter (see the three groups of data in Fig. 7). One way of interpreting these results is to recognize that the channel length-to-width ratio (axial channel length divided by the difference of the inside and outside channel radii) was about 4 for these data, and it has been observed that only the downstream portion of a long channel is effective.[26] The efficiency of a long acceleration channel is thus improved by concentrating more of the total magnetic field near the exhaust plane, in effect making the channel shorter. Another interpretation, perhaps equivalent, is that ions produced in the upstream portion of a long channel have little chance of escape without striking the channel walls. Concentration of magnetic field at the upstream end of the channel should therefore be expected to concentrate ion production further upstream, thereby decreasing the electrical efficiency. Only the data for lowest group in Fig. 7, for which the magnetic field was concentrated at the downstream end, are included from this reference in Fig. 8. The data from Plank, et al.[56] were also excluded from Fig. 8 due to known large circumferential variations in magnetic field.

The remaining data were replotted against the normalized magnetic-field integral in Fig. 8. The normalized integral is defined as the experimental integral at the mean radius, divided by the integral required to barely prevent an initially stationary electron from directly

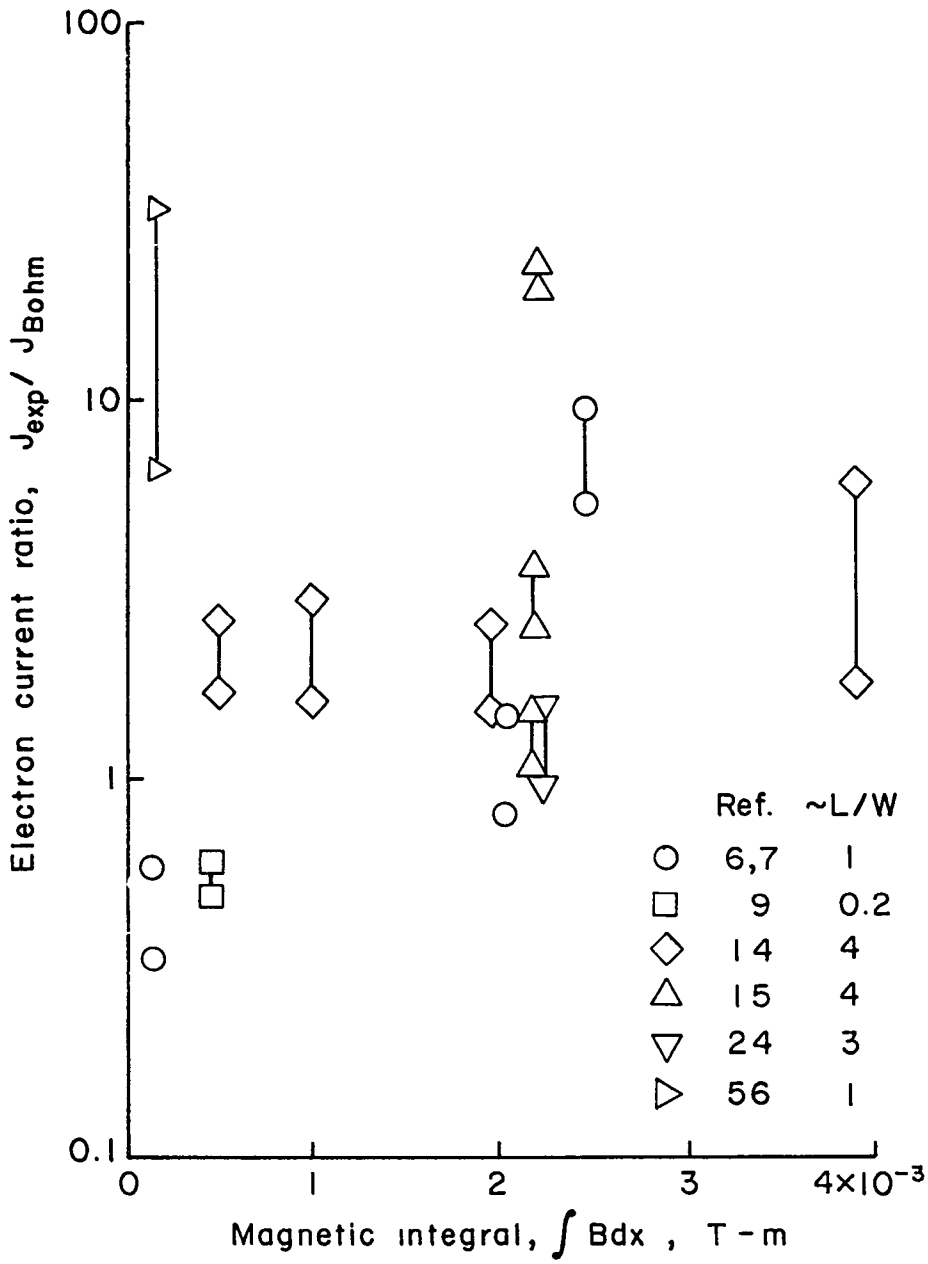

Fig. 7. Ratio of experimental-to-theoretical electron currents, with Bohm diffusion used for the theoretical value. Two symbols connected by a line represent a range of operation, or a group of data points.

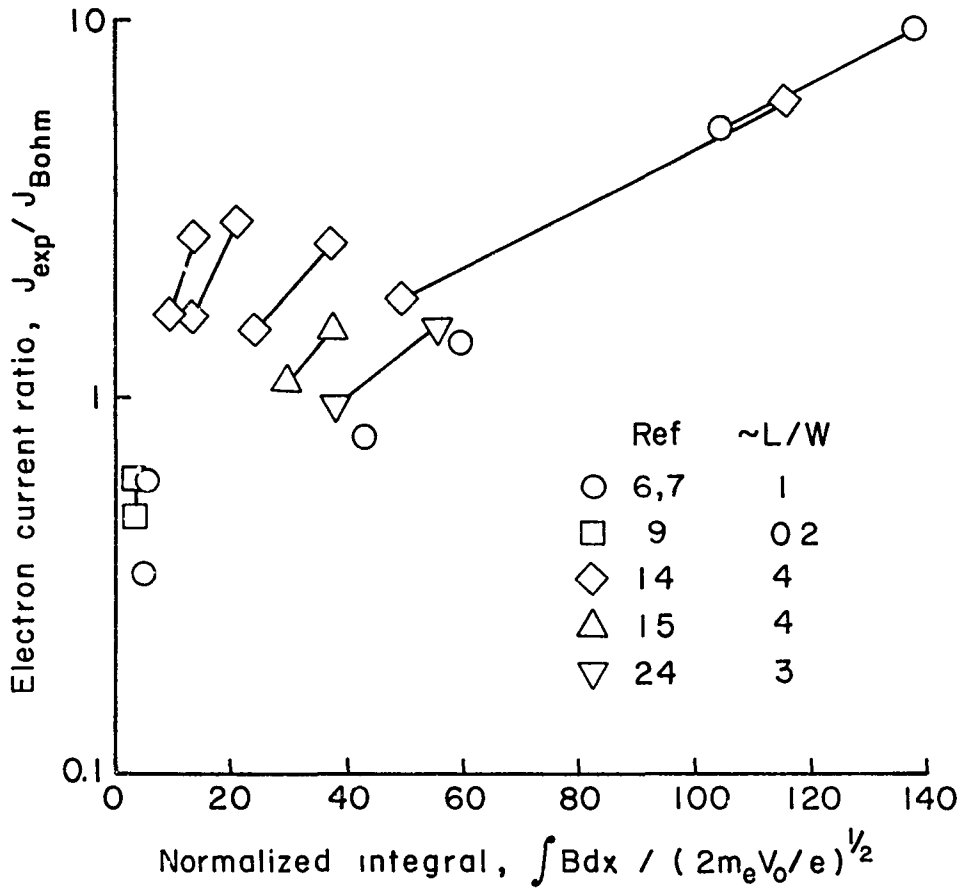

Fig. 8. Ratio of experimental-to-theoretical electron currents, as a function of the normalized magnetic integral.

(without a collision) reaching the anode. This miminum integral required to prevent a direct trajectory is $(2m_eV/e)^{1/2}$. For the normalized integral range from about 3 to 50, the experimental electron current is within about a factor of 3 of the value predicted using Bohm diffusion. At higher values of normalized integral, the experimental current from two investigations rises higher, up to about 10 times the Bohm value, even though there is no apparent flaw in the thruster designs used.

The increase of anomalous electron diffusion above the classical value is most often attributed to potential fluctuations within the bulk of the plasma.* Morozov, et al.[14] have pointed out that wall effects could also cause anomalous diffusion. The rough agreement with Bohm diffusion over a large range of normalized magnetic-field integral suggests a single anomalous-diffusion mechanism. The rise in experimental currents at high values of normalized integral suggests a second mechanism. It is common in a wide range of experimental investigations to observe a shift from one mode of operation to another as an operating parameter is indefinitely increased. It would not be surprising if anomalous diffusion in closed-drift thrusters shifted from being caused by bulk fluctuations to being caused by wall effects, or vice versa, as the magnetic field is increased.

Summarizing the conclusions drawn from Fig. 8, the electron diffusion in closed-drift thrusters appears to be within about a factor of 3 of Bohm diffusion for a wide range of normalized magnetic-field integrals, but rises sharply at the highest normalized integrals. Detailed considerations of ion losses at channel walls suggest that the agreement with Bohm diffusion would be further improved by restricting channel length-to-width ratios to ≤ 1. The drop in the maximum values of J_{exp}/J_{Bohm} might be as much as 30-40% for such a channel-length restriction in the 3 to 50 range for normalized integral. Although operation at higher normalized integrals than 50 is possible, the data of Fig. 8 indicate that the electron backflow will simply increase continuously above the Bohm value for these higher integrals.

It should be noted that the approximate limit of 50 for normalized magnetic integral is not understood from a theoretical viewpoint. New designs or operating regimes might therefore drastically alter this limit. If, however, a normalized integral of 50 is used, together with Bohm diffusion, the minimum ratio of electron backflow to xenon ion acceleration, J_e/J_i is about 0.5. This value is in reasonable agreement with experimental values for this minimum ratio. Diffusion theory also indicates that this minimum ratio should vary as the square-root of

---

*A recent analytical study of diffusion indicates that roughly the Bohm level of diffusion would be expected from thermal fluctuations alone.[57]

propellant atomic mass, but the limited data do not support this conclusion.[6,9,14,15,28] Instead, a constant minimum ratio of about 0.5 appears to be a reasonable value for all propellants. Because of the limited data, however, this conclusion can be considered only tentative.

Ion Production

The other important aspect of closed-drift thruster operation, besides electron diffusion in the acceleration region, is the production of ions. The losses in this production process consist of both the electron energy required for ion production and the escape of neutrals.

The anode-layer thruster should have an inherent advantage over the CDEA thruster in terms of efficiency, by more effectively using energy from backstreaming electrons to generate ions. For that reason, the anode-layer thruster is emphasized in the discussion of this section. Because of the basic similarity of all closed-drift thrusters, the conclusions reached will also have considerable validity for CDEA thrusters.

Most of the ion generation in an anode-layer thruster occurs in a thin layer at the upstream end of the acceleration region.[29] This region has a thickness of the order of the dimensions of an electron cyclotron orbit. The ion production process in this thin layer can be approximated from existing knowledge of gridded thruster operation.

Considering first the discharge energy required for ion production, a recent gridded thruster investigation using argon indicated 70-80 eV/ion on a total volume production basis.[58] There have been many such studies in the past, but this recent study was selected because of the new developments in this field. On the basis of limited data, the general assumption was made previously that ions generated in the discharge chamber of a gridded thruster flow nearly equally to all discharge-chamber boundaries. This assumption was satisfying, in that it was also consistent with ion flow at ion acoustic velocity in all directions from the region of production.

It was experimentally determined in this recent study, however, that the ions were directed preferentially away from any boundary in which: (1) a transverse magnetic field existed, and (2) an outwards flow of electrons took place across this magnetic field.[58] Theoretical considerations were also used to show that the directed ion flow toward such a boundary had to take place at far below ion acoustic velocity. To the first approximation, therefore, all ions should be expected to be directed away from a boundary with both a transverse field and an outward flow of electrons.

These conditions are, of course, precisely the conditions in the ion production region of an anode-layer thruster. With a thin ion production region and common ion beam dimensions, essentially all ions

should be directed away from the anode and therefore into the ion beam. From knowledge of ion production in gridded thrusters, then, the discharge loss for "knee" operation should be 70-80 eV/ion. From previous experience with various inert gases, this discharge loss should be roughly the same for argon, krypton, and xenon.

This discharge-loss value is supported by a detailed study of ion production and energy losses in a CDEA thruster operated on xenon.[26] Based on the ion beam extracted, a production loss of roughly 100 eV/ion was obtained. Correcting for the wall losses, which should be greatly reduced in an anode-layer thruster, the production loss for total ion production was found to be 60-70 eV/ion.

A discharge loss of the order of 70 eV/ion therefore appears reasonable for an anode-layer thruster operating on inert gases from argon through xenon. Depending mostly on the length of acceleration channel, the losses for a CDEA thruster would be expected to be higher. Some variation of discharge loss would be expected with propellants having significantly different ionization potentials. But experience indicates that the discharge loss variation is considerably less than linear with ionization potential.[59]

The other major loss that should be considered is the escape of neutral, or nonionized, propellant. The operation of a low-pressure discharge to generate ions has been found to depend on the maintenance of a minimum neutral density, with the exact value of neutral density dependent on the geometry of the ion production region.[59] For an anode-layer thruster, the pertinent geometry parameter is the depth of the ion production region. This depth as mentioned earlier, is of the order of an electron cyclotron orbit. From existing theory, then, the loss rate of neutrals, expressed as an equivalent current density, is expected to vary as

$$j_o = K_1 B / V_o^{1/2} , \tag{5}$$

where K_1 is some constant that depends on the propellant, B is the magnetic field strength in the ion production region, and V_o is the discharge voltage. Numerical evaluation of the constant K_1 indicates a value of the order of 10^5 for xenon. For a typical operating condition of 2×10^{-2} T and 200 V, the equivalent current density of the neutral loss should be roughly 0.1-0.2 A/cm^2. It should be evident from this neutral loss that an anode-layer thruster must operate in the A/cm^2 range for the extracted ion beam, if an acceptable propellant utilization is to be obtained. A CDEA thruster would be expected to have slightly lower neutral losses due to the extended ionization zone, but not substantially lower

The experimental measurements of propellant utilization in closed-drift thrusters are limited,[14,28] but consistent with the general picture presented above. Experimentally, a magnetic-field configuration which increases in strength in the downstream direction has been found desirable. From Eq. (5), such a variation permits the ion production region to be in a low magnetic field strength region, thereby reducing neutral losses. At the same time, the high field strength in the acceleration region is generally desirable to reduce electron diffusion in the upstream direction. This type of magnetic field variation thus tends to accommodate the conflicting requirements of ion production and acceleration.

If high ion-beam current densities are required to obtain high propellant utilizations, the upper limit on the permissible ion-beam current density is of interest. One limit, of course, is a need to radiate, or otherwise reject, waste energy. From available literature, this has not appeared to be a serious limitation. Another limit can be that of required lifetime, with excessive current densities resulting in unacceptably short lifetimes. Duration tests are clearly required to determine this limit.

Still another limit is that of the ratio of acceleration force relative to the magnetic-field force. That is, if the current density of accelerated ions is sufficiently large, the reaction of this acceleration force will seriously distort the magnetic field. It would be expected that the maximum ion-beam current density from this consideration is of the form

$$j_i = K_2 B^2 / V_o^{1/2} , \qquad (6)$$

with the value of K_2 dependent on the exact configuration used. If the acceleration force per unit beam area is simply set equal to the stress in the magnetic field, $B^2/2\mu_o$, the value of the constant K_2 for xenon is about 2.4×10^8. For the previously used conditions of 2×10^{-2} T and 200 V, the maximum current density is found to be about 0.7 A/cm^2. This limitation will, as mentioned, depend on the exact configuration used. It should be clear, however, that it can be a very real limitation to maximizing propellant utilization.

Scaling

The previous sections have emphasized details of design and operation. General overall performance trends with major dimensional changes are also of interest. The two major dimensions of a closed-drift thruster are the magnetic integral, $\int B dx$, and some characteristic length, L.

The magnetic integral determines the electron backflow through the acceleration region. From Eqs. (1) and (3), this electron backflow is of the form

$$j_e \int B dx / e n_o V_o = K_3 \ , \tag{7}$$

where K_3 depends on the electron temperature variation through the acceleration channel. Inasmuch as the ion current density, j_i, is proportional to $e n_o V_o^{1/2}$, Eq. (7) can be rewritten as

$$j_e / j_i = K_3' V_o^{1/2} / \int B dx \ , \tag{8}$$

or

$$j_e / j_i = K_3'' / (\int B dx)_{norm} \ , \tag{9}$$

where $(\int B dx)_{norm}$ is the normalized magnetic integral, as used in Fig. 8.

At low applied voltages (and low exhaust velocities), the ratio of j_e/j_i is determined by the electron backflow required to ionize the propellant. As the voltage is increased, the required electron current decreases. From Eq. (8), for j_e/j_i to decrease as V_o is increased, $\int B dx$ must increase more rapidly than $V_o^{1/2}$. This decrease in j_e/j_i continues until j_e/j_i reaches a minimum, which is associated with a maximum value of normalized magnetic integral (herein assumed to be about 50). For all higher voltages, $\int B dx$ should increase with $V_o^{1/2}$.

The selection of the proper magnetic integral thus depends primarily on the desired operating voltage. As described in connection with Fig. 3, hard-to-ionize propellants have poorly defined regions of optimum operation. The relation of magnetic integral with applied voltage will be less clearcut with such propellants. On the other hand, propellants with low ionization potentials and large cross sections will tend to have a closer relation between magnetic integral and V_o.

If the operating voltage is assumed to be fixed, the effect of size can be determined by varying the characteristic dimension L. For simplicity, all other spatial dimensions were assumed to vary with L. Because the voltage is fixed, the magnetic integral should also be fixed. If $\int B dx$ is to be fixed while L varies, then B should vary inversely with L.

$$B \sim 1/L \tag{10}$$

From considerations of magnetic field stress, Eq. (6) gives a maximum ion current density of the form

$$j_i \sim B^2 . \tag{11}$$

Combining relations (10) and (11),

$$j_i \sim 1/L^2 . \tag{12}$$

The total ion current, J_i, is the product of beam area and ion current density. Because beam area varies as L^2, the maximum ion current (from magnetic stress considerations) is independent of thruster size.

Note that this result depends, at higher voltages, on the existence of a maximum permissible normalized integral. If higher integrals can be effectively used, the limit on maximum ion current can be increased. At lower voltages, though, where the electron backflow is required for ionization, the maximum permissible ion current appears to be fundamentally independent of thruster size.

If thruster size can vary widely for the same ion-beam current, some basis other than ion-beam current should be used to select thruster size. For a more compact design, and probably also a lower thruster mass, a smaller size is preferred. It can also be shown that propellant utilization will tend to increase as thruster size is decreased.

From Eq. (5), the equivalent current density of the escaping neutrals varies as

$$j_o \sim B . \tag{13}$$

To maximize propellant utilization, j_i/j_o should be maximized. From relations (10), (11), and (13)

$$j_i/j_o \sim 1/L \ . \qquad (14)$$

That is, propellant utilization is maximized by using the smallest possible thruster size.

There are other considerations in selecting thruster size. A thruster should be large enough to reject the waste energy (probably by radiation). It also appears likely that larger thrusters would tend to have longer lifetimes. As a general conclusion, then, the smallest possible thruster size should be used, consistent with heat rejection and lifetime requirements.

Thruster Performance

In evaluating the suitability of closed-drift thrusters for particular missions, knowledge of their performance is essential. A procedure for predicting performance is presented in this section, together with available experimental data.

The general configuration assumed for calculation is a short single-stage closed-drift thruster, with only one major power circuit. The magnetic field is assumed to be supplied either by a field winding with negligible power requirements, or by permanent magnets. The electron emitting cathode is assumed to be a hollow cathode, properly sized so that external power is not required for cathode heating or otherwise sustaining the discharge after it is started.

Having assumed a hollow cathode, a cathode-to-plume potential drop is also assumed with a value equal to the first ionization potential of the gas used. It is true that the ionization process is more complicated than simply injecting electrons at this potential, but experimental potential differences for hollow cathodes approximate this value. The required electron emission from the cathode will equal the electron backflow through the accelerating region plus the neutralizing current for the accelerated ions.

The electron backflow will be set by the maximum of two conditions. One is the minimum electron current required to produce the ions by a discharge process. The other is the minimum electron-to-ion current ratio.

From an earlier discussion, a discharge loss of 70 eV/ion was assumed for argon, krypton, and xenon. For cesium and cadmium, which have lower ionization potentials, 50 eV/ion was assumed. At low applied voltages, the electron backflow is set by this discharge-loss requirement.

As indicated earlier, when the applied voltage is increased, a constant discharge loss per ion results in a decreased requirement for electron backflow. Eventually, a minimum electron-to-ion current ratio is reached. Present experimental evidence indicates a minimum value for J_e/J_i of about 0.5.[6,9,14,15,28]

To summarize the procedure for inert gases, the electron emission process was assumed to result in a potential-difference loss equal to the first ionization potential. The electron backflow to the anode was then taken to be the largest of two values. One was the electron backflow required to produce ions at 70 eV/ion. The other was a minimum electron backflow equivalent to half the ion current. Using this procedure, together with a thrust coefficient of 0.90, power efficiencies were calculated. The assumed utilization efficiencies of 0.80, 0.85, and 0.90 are believed to be consistent with the limited experimental closed-drift thruster data,[14,28] and were used to convert power efficiencies into thruster efficiencies. These thruster efficiencies are plotted against specific impulse in Fig. 9. The break in each efficiency curve corresponds to the minimum specific impulse at which J_e/J_i reaches 0.5.

As shown in Fig. 9, the efficiency is highest with xenon. The difference between different propellants is small above about 2000 s. But in the 1000 to 2000 s range of specific impulse, which is believed to be particularly suited to closed-drift thrusters, the effect of propellant atomic weight is important.

Limited experimental data are available for comparison with this theoretical approach. The most complete data appear to be for cesium propellant.[28,30] These data are presented in Fig. 10, together with a theoretical prediction. This theoretical prediction was similar to that carried out for Fig. 9, except that the discharge loss was dropped to 50 eV/ion and the propellant utilization was increased to 0.95. These changes are believed to be consistent with the extremely low ionization potential and large ionization cross section of cesium, as well as the limited experimental closed-drift thruster data.[28]

The calculated performance is in excellent agreement with all experimental performance except the data point near 4000 s. To provide the necessary exhaust velocity, the 4000-s point is at roughly 1000 V. With this high a discharge voltage, there would be a large fraction of the propellant that would be multiply ionized, resulting in increased thruster losses. Alternatively, the 4000-s point may not have been experimentally optimized. In the 1000-2000 s range of most interest, though, the calculation procedure appears to represent the experimental values with sufficient accuracy for a rough estimate of performance.

Limited data are also available for xenon propellant, and are shown in Fig. 11, together with the calculated xenon curve from Fig. 9. The thruster used in this case was a two-stage anode-layer type. It appears that this thruster was not designed to operate efficiently at low specific impulse. The maximum efficiency in the 3500-4000-s range, though, is in reasonable agreement with the calculated performance.

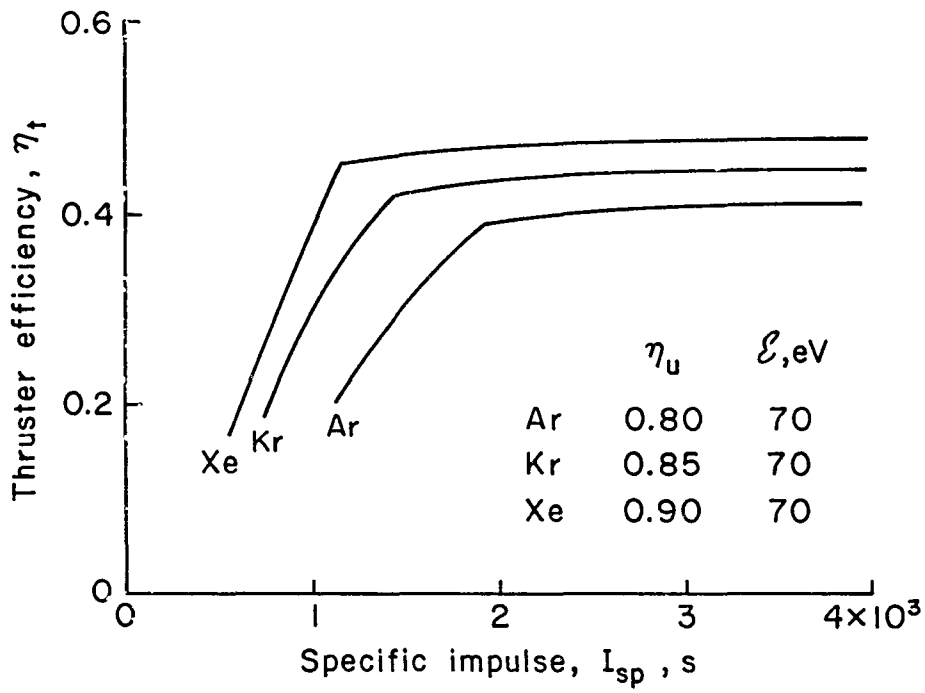

Fig. 9. Theoretical performance for single-stage closed-drift thruster with inert-gas propellants.

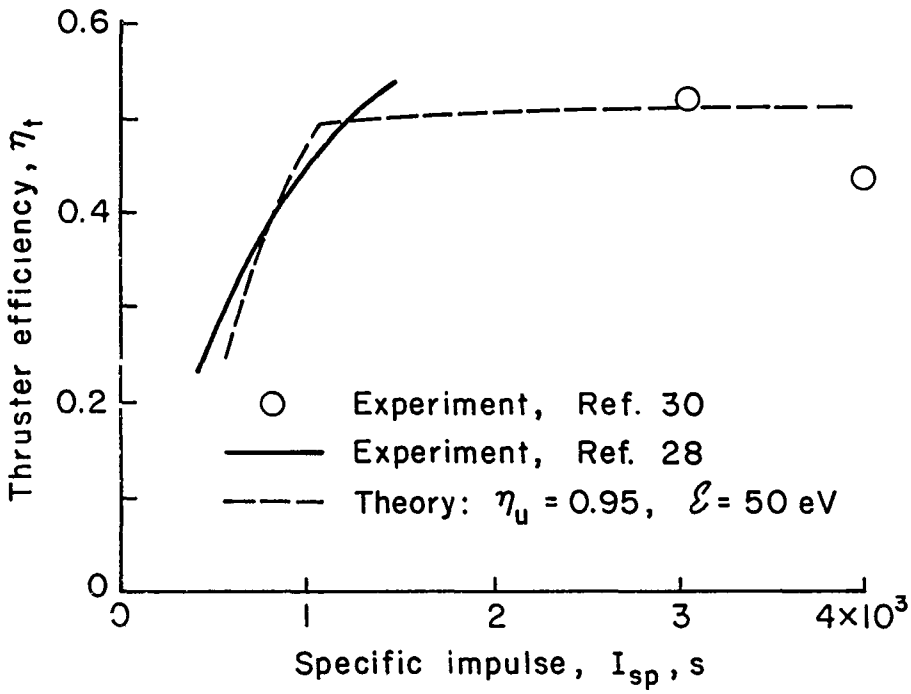

Fig. 10. Comparison of theory and experiment for cesium propellant. (A single-stage anode-layer thruster was used in Ref. 28, and a two-stage anode-layer thruster was used in Ref. 30.)

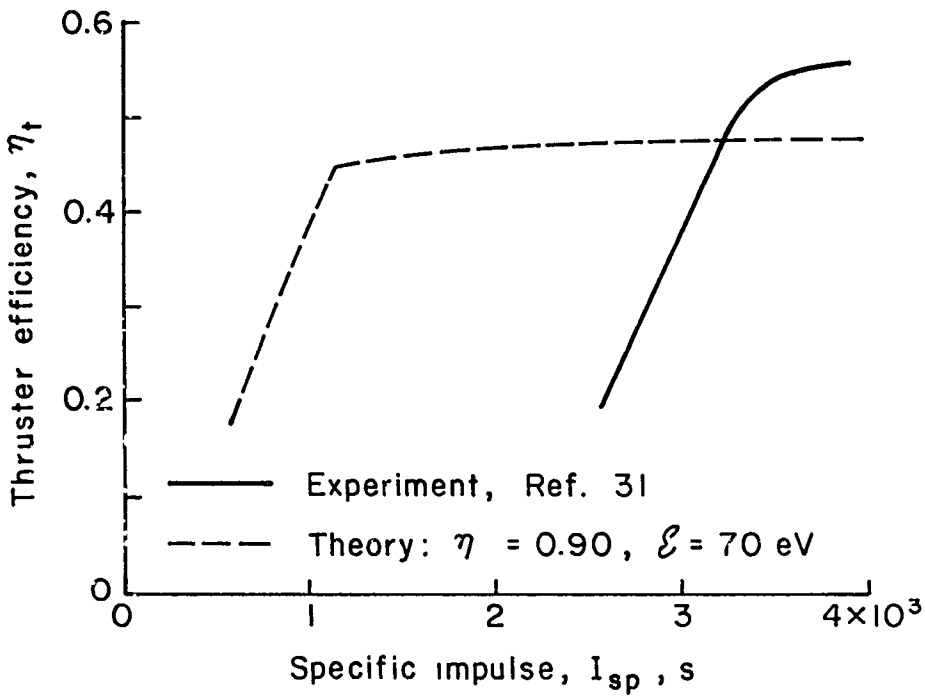

Fig. 11. Comparison of theory and experiment for xenon propellant. (A two-stage anode-layer thruster was used in Ref. 31.)

A final comparison can be made for cadmium propellant in a CDEA thruster. In this case, a fairly deep ($L/W \gtrsim 3$) channel is believed to be the cause of the experimental performance being significantly lower than the calculated performance (see Fig. 12).

Concluding Remarks

The technology of closed-drift thrusters was reviewed. This type of thruster appears to have inherent advantages over both electrothermal and gridded-electrostatic thrusters in the 1000 to 2000 s range of specific impulse.

Electron diffusion across a magnetic field is a crucial aspect of closed-drift thruster operation. Experimental electron-diffusion data have been reviewed and compared with diffusion theory. A normalized magnetic-field integral has been defined as the experimental integral, $\int Bdx$, divided by the minimum integral that will prevent an initially motionless electron from reaching the anode at the discharge voltage used. Experimental electron diffusion was found to be within a factor of about 3 of the Bohm diffusion value over a range of normalized magnetic-field integral from about 3 to 50. Above about 50, the experimental diffusion rose sharply, relative to the Bohm diffusion value. This sharp rise in electron diffusion was found to be related to the minimum electron-to-ion current ratio in the acceleration process.

The ion-production process was also analyzed. Because of the shallow depth of the ion production region, a closed-drift thruster (particularly of the anode-layer type) is essentially a high current-density device. To obtain useful propellant utilizations, the ion current densities should be in the A/cm^2 range. On the other hand, the discharge losses appear to be as low, or lower, than any competitive ion-beam sources.

A calculation procedure was presented for estimating the performance of a closed-drift thruster. Limited experimental data indicated that this procedure is adequate for rough performance estimates of single-stage thrusters with short acceleration channels.

The experimental and calculated performance indicate thruster efficiencies of about 0.5 are practical in the 1000 to 2000 s range of specific impulse, when using high ($\gtrsim 100$) atomic mass propellants.

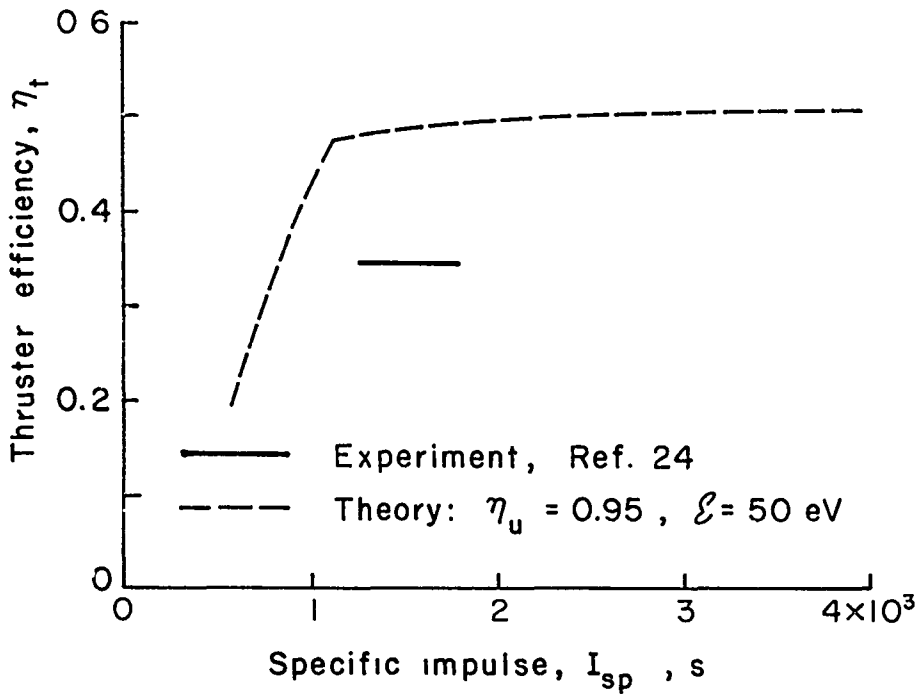

Fig. 12. Comparison of theory and experiment for cadmium propellant (A single-stage CDEA thruster with a relatively deep (L/W $\gtrsim$ 3) channel was used in Ref. 24.)

References

1. G. R. Seikel and E. Reshotko, "Hall Current Ion Accelerator," Bull. Am. Phys. Soc., Ser. II, Vol. 7, p. 414, June 1962.
2. E. C. Lary, R. C. Meyerand, Jr., and F. Salz, "Ion Acceleration in a Gyro-Dominated Neutral Plasma - Theory," Bull. Am. Phys. Soc., Ser. II, Vol. 7, p. 441, July 1962.
3. F. Salz, R. G. Meyerand, Jr., and E. C. Lary, "Ion Acceleration in a Gyro-Dominated Neutral Plasma - Experiment," Bull. Am. Phys. Soc., Ser. II, Vol. 7, p. 441, July 1962.
4. G. R. Seikel, "Generation of Thrust - Electromagnetic Thrusters," Proc. of the NASA-University Conf. on the Science and Technology of Space Exploration, Vol. 2, pp. 171-176, Nov. 1962.
5. M. C. Ellis, Jr., "Survey of Plasma Accelerator Research," Proc. of the NASA-University Conf. on the Science and Technology of Space Exploration, Vol. 2, pp. 171-176, Nov. 1962.
6. E. A. Pinsley, C. O. Brown, and C. M. Banas, "Hall-Current Accelerator Utilizing Surface Contact Ionization," J. Spacecraft and Rockets, Vol. 1, pp. 525-531, Sept./Oct. 1964.
7. C. O. Brown and E. A. Pinsley, "Further Experimental Investigations of a Cesium Hall-Current Accelerator," AIAA J., Vol. 3, pp. 853-859, May 1965.
8. R. X. Meyer, "A Space-Charge-Sheath Electric Thruster," AIAA J., Vol. 5, pp. 2057-2059, Nov. 1967.
9. R. X. Meyer, "Laboratory Testing of the Space-Charge-Sheath Electric Thruster Concept," J. Spacecraft and Rockets, Vol. 7, pp. 251-255, March 1970.
10. E. Zeyfang, "Investigations on Ion Sources for Hall Ion Accelerators," First Internat. Conf. on Ion Sources, Saclay, June 1969.
11. E. Zeyfang, "A Plasma Source with Annular Slit Hollow Cathode for Hall Ion Thrusters," III European Electric Propulsion Conf., Oct. 1974.
12. A. V. Zharinov and Yu. S. Popov, "Acceleration of Plasma by a Closed Hall Current," Sov. Phys.-Tech. Phys., Vol. 12, pp. 208-211, Aug. 1967.
13. I. P. Zubkov, A. Ya. Kislov, and A. I. Morozov, "Experimental Study of a Two-Lens Accelerator," Sov. Phys.-Tech. Phys., Vol. 15, pp. 1796-1800, May 1971.
14. A. I. Morozov, Yu. V. Esipchuk, G. N. Tilinin, A. V. Trofimov, Yu. A. Sharov, and G. Ya. Shchepkin, "Plasma Accelerator with Closed Electron Drift and Extended Acceleration Zone," Sov. Phys.-Tech. Phys., Vol. 17, pp. 38-45, July 1972.
15. A. I. Morozov, Yu. V. Esipchuk, A. M. Kapulkin, V. A. Nerovskii, and V. A. Smirnov, "Effect of the Magnetic Field on a Closed-Drift Accelerator," Sov. Phys.-Tech. Phys., Vol. 17, pp. 482-487, Sept. 1972.
16. Yu. V. Epsichuk, A. I. Morozov, G. N. Tilinin, and A. V. Trofimov, "Plasma Oscillations in Closed-Drift Accelerators with an Extended Acceleration Zone," Sov. Phys.-Tech. Phys., Vol. 18, pp. 928-932, Jan. 1974.

17. N. A. Kervalishvili and V. P. Kortkhondzhiya, "Low-Pressure Discharge in a Transverse Magnetic Field," Sov. Phys.-Tech. Phys., Vol. 18, pp. 1203-1205, March 1974.
18. I. V. Melikov, "Experimental Investigation of Anode Processes in a Closed Electron-Drift Accelerator," Sov. Phys.-Tech. Phys., Vol. 19, pp. 35-37, July 1974.
19. V. S. Yerofeyev and L. V. Leskov, "Hall-Accelerator of Plasma with Anode Layer" (in Russian), in Physical Principles of Plasma Accelerators (A. I. Morozov, ed.), pp. 18-47, Nauka, Minsk, 1974.
20. V. N. Dem'yanenko, I. P. Zubkov, and A. I. Morozov, "Open Single-Lens Hall-Current Accelerator," Sov. Phys.-Tech. Phys., Vol. 21, pp. 987-988, Aug. 1976.
21. I. V. Melikov, "Point and Jet Ionization in a Hall Plasma Accelerator," Sov. Phys.-Tech. Phys., Vol. 22, pp. 452-453, Apr. 1977.
22. S. N. Askhabov, I. V. Melikov, and V. V. Fishgoit, "Electric Discharge in Direct-Flow Hall Accelerator," Sov. Phys.-Tech. Phys., Vol. 22, pp. 453-458, Apr. 1977.
23. G. N. Tilinin, "High-Frequency Waves in a Hall Accelerator with an Extended Acceleration Zone," Sov. Phys.-Tech. Phys., Vol. 22, pp. 975-978, Aug. 1977.
24. A. V. Trofimov, "Hall Accelerator with Cadmium Vapor," Sov. Phys.-Tech. Phys., Vol. 22, pp. 1280-1282, Oct. 1977.
25. G. N. Tilinin, 'Modulation of the Ion Stream at the Exit from a Hall Plasma Accelerator with an Extended Acceleration Zone," Sov. Phys.-Tech. Phys., Vol. 22, pp. 1422-1423, Nov. 1977.
26. A. M. Bishaev and V. Kim, "Local Plasma Properties in a Hall-Current Accelerator with an Extended Acceleration Zone," Sov. Phys.-Tech. Phys., Vol. 23, pp. 1055-1057, Sept. 1978.
27. S. S. Ivashchenko, A. S. Parshchik, V. A. Tkachenko, and Yu. V. Shipilov, "Operational Characteristics of an Anode-Layer Accelerator in Low-Voltage Modes" (in Russian), Abstracts for IV All-Union Conference on Plasma Accelerators and Ion Injectors, pp. 23-24, Moscow, 1978.
28. V. I. Garkusha, V. S. Yerofeyev, Ye. A. Lyapin, and S. P. Chugina, "Characteristics of a Single-Stage Cesium Anode-Layer Accelerator" (in Russian), Abstracts for IV All-Union Conference on Plasma Accelerators and Ion Injectors, pp. 25-26, Moscow, 1978.
29. V. S. Yerofeyev and I. N. Safronov, "Operational Characteristics of a Double-Stage Cesium Anode-Layer Accelerator" (in Russian), Abstracts for IV All-Union Conference on Plasma Accelerators and Ion Injectors, pp. 27-28, Moscow, 1978.
30. O. N. Mironov, "Investigation of the Operation of a Cesium Accelerating Stage in a Double-Stage Anode-Layer Accelerator" (in Russian), Abstracts for IV All-Union Conference on Plasma Accelerators and Ion Injectors, pp. 29-30, Moscow, 1978.
31. A. T. Artipov, A. D. Grishkevich, V. V. Ignatenko, A. M. Kapulkin, V. F. Prisnyakov, and V. V. Statsenko, "Double-Stage Closed Electron Drift Accelerator," (in Russian), Abstracts for IV All-Union Conference on Plasma Accelerators and Ion Injectors, pp. 66-67, Moscow, 1978.
32. N. A. Bardadymov, A. B. Ivashkin, L. V. Leskov, and A. V. Trofimov, "Hybrid Closed Electron Drift Accelerator," (in Russian), Abstracts for IV All-Union Conference on Plasma Accelerators and Ion Injectors, pp. 68-69, Moscow, 1978.

33. A. I. Morozov, Physical Principles of Cosmic Electro-Jet Engines, Vol. I, (in Russian), pp. 8-16, Atomizdat, Moscow, 1978.
34. V. P. Shadov, A. A. Porotnikov, U. P. Rilov, and V. P. Kim, "Plasma Propulsion Systems: Present State and Development," 30th Internat. Astron. Congress, Sept. 1979.
35. W. Knauer, 'Mechanism of the Penning Discharge at Low Pressures," J. Appl. Phys., Vol. 33, pp. 2093-2099, June 1962.
36. W. Knauer and M. A. Lutz, "Measurement of the Radial Field Distribution in a Penning Discharge by Means of the Stark Effect," Appl. Phys. Lett., Vol. 2, pp. 109-111, March 1963.
37. D. G. Dow, "Electron-Beam Probing of a Penning Discharge," J. Appl. Phys., Vol. 34, pp. 2395-2400, Aug. 1963.
38. W. Knauer, A. Fafarman, and R. L. Poeschel, "Instability of Plasma Sheath Rotation and Associated Microwave Generation in a Penning Discharge," Appl. Phys. Lett., Vol. 3, pp. 111-112, Oct. 1963.
39. N. A. Kervalishvili and A. V. Zharinov, "Characteristics of a Low-Pressure Discharge in a Transverse Magnetic Field," Sov. Phys.-Tech. Phys., Vol. 10, pp. 1682-1687, June 1966.
40. Yu. S. Popov, "Low-Pressure Cold-Cathode Penning Discharge," Sov. Phys.-Tech. Phys., Vol. 12, pp. 81-86, July 1967.
41. N. A. Kervalishvili, "Effect of Anode Orientation on the Characteristics of a Low-Pressure Discharge in a Transverse Magnetic Field," Sov. Phys.-Tech. Phys., Vol. 13, pp. 476-482, Oct. 1968.
42. N. A. Kervalishvili, "Instabilities of a Low-Pressure Discharge in a Transverse Magnetic Field," Sov. Phys.-Tech. Phys., Vol. 13, pp. 580-582. Oct. 1968.
43. G. V. Smirnitskaya and Nguen Khyu Ti, "The Center Potential and Electron Density in a Penning Discharge," Sov. Phys.-Tech. Phys., Vol. 14, pp. 783-788, Dec. 1969.
44. [illegible] M. Reikhrudel', G. V. Smirnitskaya, and Nguen Khyu Ti, "Dependence of Current on Parameters in a Penning Discharge," Sov. Phys.-Tech. Phys., Vol. 14, pp. 789-795, Dec. 1969.
45. Yu. S. Popov, "Anode Sheath in a Strong Transverse Magnetic Field," Sov. Phys.-Tech. Phys., Vol. 15, pp. 1311-1315, Feb. 1971.
46. V. [illegible] Profeev and Yu. V. Sanochkin, "Ionization Instability of a Self-Sustaining Low-Pressure Discharge in a Strong Transverse [illegible] Field," Sov. Phys.-Tech. Phys., Vol. 15, pp. 1413-1417, [illegible]97[illegible].
47. [illegible] Smirnitskaya and I. A. Nosyreva, "Oscillations in a Low-[illegible] Penning Discharge," Sov. Phys.-Tech. Phys., Vol. 15, pp. [illegible], May 1971.
48. [illegible]rov, N. A. Kervalishvili, and V. P. Kortkhondzhiya, "[illegible] Instability and High-Energy Electrons in a Low-[illegible] Discharge in a Transverse Magnetic Field," Sov. Phys.-[illegible], Vol. 17, pp. 1526-1529, March 1973.
49. [illegible]dov, "Similitude Criteria in the Penning Discharge," [illegible]-Tech. Phys., Vol. 20, pp. 1254-1256, Sept. 1975.
50. [illegible]ufman, "Theory of Ion Acceleration with Closed Electron [illegible]," AIAA Paper No. 82-1919, Nov. 1982.
51. H. R. Kaufman and R. S. Robinson, "Plasma Processes in Inert-Gas Thrusters," J. Spacecraft and Rockets, Vol. 18, pp. 470-476, Sept./Oct. 1981.

52. R. S. Robinson and H. R. Kaufman, "Ion Thruster Technology Applied to a 30-cm Multipole Sputtering Ion Source," AIAA J., Vol. 15, pp. 702-706, May 1977.
53. R. S. Robinson, "Physical Processes in Directed Ion Beam Sputtering," NASA Contr. Rep., CR-159567, Appendix A, March 1979.
54. L. Spitzer, Jr., Physics of Fully Ionized Gases, 2nd ed., Interscience Publishers, N.Y., pp. 47-48, 1962.
55. F. F. Chen, Introduction to Plasma Physics, Plenum Press, N.Y., p. 169, 1974.
56. G. M. Plank, H. R. Kaufman, and R. S. Robinson, "Experimental Investigation of a Hall-Current Accelerator," AIAA Paper No. 82-1920, Nov. 1982.
57. H. E. Wilhelm, "Anomalous Correlation and Diffusion in Microfields of Magnetoactive Plasmas," Nuclear Technology/Fusion, Vol. 3, pp. 144-148, Jan. 1983.
58. H. R. Kaufman, R. S. Robinson, and L. E. Frisa, "Ion Flow Experiments in a Multipole Discharge Chamber," AIAA Paper No. 82-1930, Nov. 1982.
59. H. R. Kaufman and R. S. Robinson, "Ion Source Design for Industrial Applications," AIAA J., Vol. 20, pp. 745-760, June 1982.

ELECTRIC THRUSTER PERFORMANCE FOR ORBIT RAISING AND MANEUVERING

Abstract

Several electric thrusters are compared to chemical rockets for orbit-raising and in-orbit maneuvering applications. For power intensive payloads and satellites, electric propulsion can show substantial performance advantages over chemical propulsion. The arcjet is promising for near-future applications because of its low power requirements. The electrostatic thruster offers additional performance advantages over the arcjet, but with added power requirements. The performance of the electrostatic thruster can be enhanced considerably if the power processing requirements can be reduced. A performance gap exists between the specific impulse of an arcjet ($\sim$1000 sec) and the minimum practical specific impulse of an electrostatic thruster ($\sim$2000 sec). A high performance ($\eta \geq 0.5$) thruster in this specific impulse range, with minimal power processing requirements, would offer time-payload compromises intermediate of those possible with either the arcjet or the electrostatic thruster.

Introduction

The objective of this paper is to assess the degree to which present electric thruster technology satisfies orbit raising and maneuvering needs. In those areas where needs are not being met, the further objective is to indicate the research directions that appear most promising for satisfying those needs.

Electric propulsion is, at present, not being used for the primary propulsion applications of orbit raising and large-scale maneuvering in the near-earth environment. To replace chemical propulsion in these applications with a new technology will require the demonstration of major advantages. An apparent 10 or 20% advantage can easily disappear when a new technology is used to replace a well developed existing technology. When the advantage appears to be 50 or 100%, though, it is far more likely that a significant advantage will remain when the new technology is actually applied.

The mission and system analysis presented herein is simple, when compared to the sophisticated studies often presented in the aerospace sciences. The reasons for this simplicity are twofold. First, a sophisticated study is not required to show a major difference, if it exists. Second, the very complexity of a sophisticated study often

serves to obscure some results, when substantially different approaches with different levels of development are compared.

Propulsion System Performance

For chemical propulsion, a specific impulse of 500 sec was assumed in orbit-raising applications. Such a specific impulse requires cryogenic storage of propellant during the launch up to the low orbit start of an orbit raising mission, but such storage is well within the present state of the art. For maneuvering needs, a reduced specific impulse of 425 sec was assumed to be more consistent with the possible long-term storage requirements. A specific impulse of 500 sec is also included for maneuvering with mission durations consistent with cryogenic storage.

For electric propulsion, both electrostatic (electron-bombardment) and MPD (magneto-plasma-dynamic) thrusters were considered. These are the two main types of ion and plasma thrusters being studied in the U.S. Both of these were evaluated over a range of specific impulse. An H_2 arcjet was also included for a specific impulse of 1000 sec.

Short descriptions of these electric thrusters are included here for those unfamiliar with electric propulsion. Ions are generated in the electrostatic thruster by a low pressure discharge. The propellant pressure is sufficiently low in this discharge that a magnetic field is required to contain and efficiently utilize the energetic electrons. The ions are electrostatically extracted at one end of the discharge chamber by ion-optics "grids". These grids are thin, closely spaced sheets, usually of molybdenum, with many small holes in each sheet. The grid closest to the discharge chamber is at a sufficiently negative potential to reflect discharge electrons, and serves to form the ions into many small beams, or beamlets. The second grid is far more negative and provides the majority of the potential difference for ion acceleration. The holes in the second grid are aligned with those in the first so that, although the ions are attracted by the second grid, they do not strike it. A third grid may be added to reduce the ion beam divergence when the second grid is at a large negative potential. To provide both space-charge and current neutralization of the overall ion beam as it leaves the thruster, electrons are added by a neutralizer located downstream of the ion optics. Power processing is normally required for the voltages and currents for the various electrostatic thruster functions. This power processing requirement entails both losses and the heat rejection capability for these losses. Despite the apparent complexity of the electrostatic propulsion system, tests of thousands of hours duration have been successfully conducted.

MPD thruster operation consists of a single discharge between concentric electrodes, with the interaction of the discharge current and a magnetic field providing the thrust. More efficient operation is obtained at high power and thrust densities so that, for most applications, pulsed operation is required to reduce the average power to an achievable value. At high power, the magnetic field involved in thrust

generation is usually provided by the discharge current, rather than a separate field coil or permanent magnets. The pulsed operation requires an energy storage form of power processing between the power source and the thruster, as well as some mechanism for generating and controlling pulses of propellant flow. The MPD thruster is generally at a much lower level of development than the electrostatic thruster. Fewer duration tests have been conducted, and no flight-weight power processing and propellant flow controls exist.

The arcjet uses electrical energy to heat a propellant, which then expands through a nozzle to generate thrust, similar to the expansion process in a chemical rocket. The propellant temperature is limited by the temperature limits of the materials involved and the need to limit dissociation and ionization frozen flow losses in the propellant. With a rough temperature limit due to these considerations, the highest exhaust velocity is obtained with the propellant having the lowest molecular weight. Early studies with hydrogen propellant 10 to 20 years ago showed no particular thruster problems, but the cryogenic storage of hydrogen at that time was difficult. As a result, interest in the arcjet thruster waned after the initial studies. Recent advances in cryogenic storage have been the cause of much of the renewed interest in the arcjet thruster.

The electrostatic, MPD, and arcjet thrusters do not by any means complete the list of electric thrusters available. These three, however, should provide a performance matrix for discussing most of the advantages and disadvantages of electric propulsion. Other types of electric thrusters will also be included in the subsequent discussions.

The performance of an electric thruster is defined by its weight, specific impulse, and efficiency for converting electric power to thrust. The electrostatic thruster performance used herein was obtained from a parametric study of performance for both argon and xenon propellants,[1,2] and is presented in summary form in Table I. The only modifications made to the results of this study were a reduction of the specific impulse by a factor of 0.975 and a reduction of efficiency by a factor of 0.95, both to account for the "cosine loss" of off-axis components that were not included in the original study. The optimum thruster size was used for the data of Table I, which ranged from several KW at low specific impulses to several MW at high specific impulses. Larger than optimum thruster power can be accommodated with an array of thrusters. Smaller than optimum power can be accommodated by a size reduction, with only small performance losses as long as the size reduction is moderate. In practice, at least two electrostatic thrusters will normally be required to provide full three-axis attitude control during thrusting. Unlike a chemical rocket, a "swirl" component can be significant from a single electrostatic thruster with two or three grids. Because of the high specific impulses, it is desirable to offset this swirl with components from at least two thrusters.

Table I. Electrostatic Thruster Performance*

I_{sp}, sec	Ar Propellant		Xe Propellant	
	η_T	Kg/KW	η_T	Kg/KW
975			0.324	12.49
1462	0.251	4.34	0.469	7.12
1950	0.328	3.32	0.589	3.36
2438	0.400	2.47	0.672	2.68
2925	0.466	1.88	0.731	2.16
3900	0.570	1.57	0.806	1.50
4875	0.647	1.30	0.848	1.11
5850	0.704	1.11	0.874	0.90
6825	0.746	0.96	0.891	0.73
7800	0.779	0.84	0.902	0.61
9750	0.824	0.67	0.918	0.47

*Performance values from Ref. 2.

The efficiency of an electrostatic thruster increases with increasing atomic mass of the propellant. This effect accounts for the difference shown for Ar (40 amu) and Xe (131 amu) in Table I. The most completely developed electrostatic thruster[3] uses Hg (201 amu) as the propellant. From a propulsion viewpoint, Hg is the preferred propellant because it is easily stored with a low tankage fraction and gives high thruster efficiency. Environmental considerations, however, would probably prevent its use in large quantities in the near-earth environment. Xe is also an excellent electrostatic thruster propellant. It has a high enough atomic mass to give high efficiency, and its moderate critical temperature permits noncryogenic storage with tankage mass fractions of 0.05-0.10. It has a shortcoming of being costly and somewhat limited in supply. For mass requirements of at least several tons per year, though, the cost and limited supply should not be serious limitations. For larger quantities, Ar offers much lower cost with the shortcomings of reduced thruster performance and a need for cryogenic storage to reduce tankage mass fractions to a reasonable level. Both Xe and Ar are environmentally "clean" in the sense that they are inert and are obtained from the atmosphere, hence would be partially returned to their source if used in the near-earth environment. If used in sufficiently large quantities, however, they could still have an adverse impact on the upper atmosphere.

As indicated, the electrostatic thruster data of Table I are optimized performance data. For example, the efficiency of an electrostatic thruster can be increased by increasing the fraction of propellant that is ionized. This increase can be accomplished by using a deeper discharge chamber, resulting in a greater neutral residence time, hence a greater

probability of being ionized. Such a chamber shape, however, will also result in a smaller fraction of the ions being extracted into the ion beam. This last effect will result in increased discharge energy being required per beam ion. For the data in Table I, the chamber depth was selected to maximize overall thruster efficiency.

The data of Table I thus represent a reasonable upper limit for what may be expected from an electrostatic thruster. If significantly better performance is assumed, it should be justified on the basis of completely new design and/or theory.

As mentioned above, the Hg electrostatic thruster has been the subject of considerable development.[3] As a check on the calculation procedures used for the data of Table I, the performance of the existing 30 cm thruster with Hg at 3000 sec closely approximates the calculated performance of the same size of thruster at the same specific impulse with Xe as the propellant. If a Hg thruster were optimized in the manner described for Ar and Xe thrusters, it is expected that the Hg thruster would show performance superior to either Ar or Xe.

The electrostatic thruster requires electric power at a variety of voltages and currents. When the electric power is supplied at a somewhat arbitrary bus voltage, there is, as discussed previously, a need for power processing between the electric power source and the electric thruster. The most fully developed power processing is that for the 30 cm Hg thruster mentioned previously.[3] For power processing herein, an efficiency of 0.9 and a mass of 10 kg/KW will be assumed. These values are close to the actual values obtainable for the 30 cm Hg power processor.[3] As will be shown, the need for power processing is a critical factor in the evaluation of electrostatic thrusters.

The MPD thruster has not been evaluated in the same parametric manner as the electrostatic thruster. The best performance estimates to date appear to be from experimental evaluations.[4] Tabulated efficiencies for two high performance MPD thrusters are presented in Table II. The propellant for both of these thrusters is Ar. Although the effect of propellant atomic mass is not as straightforward as for an electrostatic thruster, there appears to be a general shift to higher efficiency with higher atomic mass in an MPD thruster. The efficiencies shown in Table II may, therefore, be somewhat limited by the choice of propellant.

As discussed previously, most applications of the MPD thruster assume pulsed operation. Neither the MPD thrusters nor the required power processing for pulsed operation have been studied sufficiently to provide estimates of flight hardware masses. With a view towards selecting optimistic numbers to avoid penalizing the MPD thruster, a power processing efficiency of 0.9 was assumed, together with a power-processing mass of 2.5 kg/KW, based on input electric power from the power source. The specific mass for the MPD thruster was assumed to be 2.5 kg/kW based on the power from the power source (2.25 kg/kW based on power from the power processor).

Table II. MPD Thruster Efficiency*

I_{sp}, sec	Benchmark Thruster	Improved Thruster
1000	0.18	
1200	0.20	
1500	0.22	0.20
2000	0.25	0.26
2500		0.29
3000		0.31
3500		0.32

*Efficiencies from Ref. 4.

The arcjet thruster was also included in this electric thruster performance comparison. If H_2 propellant is assumed, an efficiency of about 0.5 is possible at 1000 sec.[5] The use of H_2 implies, of course, efficient cryogenic propellant storage. Other propellants result in sharply reduced efficiency or specific impulse.

The arcjet was the subject of considerable work in the past, but receives no mention in recent surveys.[6,7] To obtain reasonable efficiencies, it is necessary to avoid significant dissociation and ionization. For H_2 propellant, this means limiting specific impulses to a maximum of roughly 1000 sec. Because of the higher atomic weights of other propellants, the maximum specific impulses for these other propellants are considerably lower. The specific mass of the arcjet was assumed to be 2.5 kg/kW.

Mission Analysis Assumptions

Performance was evaluated in terms of payload and mission time for two missions. The first was an orbit raising mission from a geocentric radius of 7.25×10^6 m (low earth orbit) to a radius of 4.23×10^7 m (geosynchronous earth orbit), with a plane change of 28.5 degrees. For high-thrust chemical propulsion, the Δv for orbit raising was about 5.2 km/sec. For low-thrust electric propulsion, the Δv was about 5.9 km/sec. The second mission was in-orbit maneuvering, with the total velocity change of the maneuvers equal to geosynchronous orbital velocity, 3.07 Km/sec.

A structural/tankage/guidance/reserve propellant mass of 0.10 m_o was assumed for all orbit raising, with m_o the initial low orbit mass. A similar fixed mass of 0.05 m_o was assumed for in-orbit maneuvering, with m_o the vehicle mass before maneuvering. These fixed masses are indicated as vehicle assumptions in Table III.A.

Table III. Mission Analysis Assumptions

	A. Vehicle	
Orbit Raising	Fixed Mass	0.10 m_o
Maneuvering	Fixed Mass	0.05 m_o
	B. Propulsion System	
Chemical		None
Electro-static	Thruster	m and η, Table I
	Power Processor	10 kg/kW, η=0.9*
	Power Source	15 kg/kW**
	Other	5 kg/kW
MPD	Thruster	2.25 kg/kW; η, Table II
	Power Processor	2.5 kg/kW, η=0.9
	Power Source	15 kg/kW**
	Other	2.5 kg/kW
Arcjet	Thruster	2.5 kg/kW, η=0.5
	Power Source	15 kg/kW**
	Other	2.5 kg/kW

*Power processor mass and losses omitted from some mission calculations for electrostatic thruster.

**A specific mass of 15 kg/kW was used for the power source when it was part of the propellant system. As part of the payload, 15 kg/kW was the lower limit.

For the chemical propulsion system, the mass of the rocket engine was assumed to be negligible, hence included within the fixed mass of either 0.10 m_o or 0.05 m_o.

All electric propulsion systems require an electric power source. When that source was considered to be part of the propulsion system mass, it had an assumed specific mass of 15 kg/kW exclusive of power processing. When included in the payload, the power source specific mass ranged upwards from 15 kg/kW. The value of 15 kg/kW is typical of either solar-cell arrays or nuclear-electric power sources,[8,9] although the solar-cell array value has also been supported by hardware tests. For orbit raising, starting from the assumed low orbit, the solar-cell is probably excluded because of earth shadowing. For higher level orbit raising or in-orbit maneuvering, both power sources are possible alternatives. Within the VanAllen belts, the effects of radiation from those belts on solar-cell efficiency must be considered.

For the electrostatic propulsion system, the thruster mass and efficiency were obtained from Table I, with the specific mass based on thruster input power (after power processing losses). The power processor specific mass was 10 kg/kW and the efficiency was 0.9, as discussed earlier. An additional mass of 5 kg/kW (based on power source output) was assumed for all cables, support structure, etc. that are peculiar to an electrostatic propulsion system. These assumptions are indicated in Table III.B. Although these assumptions are simple compared to more detailed mass studies made previously,[10,11] the predicted total propulsion system mass is in reasonable agreement with the more detailed studies.

The assumptions for the MPD and arcjet propulsion systems are also indicated in Table III.B. The "other" mass is cut in half for these propulsion systems because they are felt to be more compact than the electrostatic system. The thruster and power processor masses for the MPD system are both felt to be optimistically light considering the unresolved problems of pulsed propellant and power flow.

For the arcjet propulsion system, the masses are also uncertain. But the uncertainty should be small compared to power-source mass, so that the impact on arcjet mission performance of any errors should also be small.

As indicated in the Introduction, the mission analysis approach used herein is simple. The intent is not to calculate refined mission performance, but to compare broad characteristics of different propulsion systems. Further, for the comparison to indicate that electric propulsion should supplant chemical propulsion for any of the missions under consideration, large and clearcut advantages should be demonstrable for electric propulsion.

Propulsion System Thrust-to-Mass Ratio

The relative evaluation of different propulsion systems must rest ultimately on thorough mission analyses. For various electric propulsion systems, however, it is possible to compare performance at the same specific impulse by comparing the thrust-to-mass ratios for the different systems. Using the mass and efficiency assumptions outlined in the previous section, with the power source assumed to be part of the propulsion system, the thrust-to-mass ratios shown in Fig. 1 were obtained. Thrusting time is usually a parameter of interest for electric propulsion, so any comparison should be made for the same thrusting time, hence the same vehicle acceleration for a given mission. For a given acceleration (F/m_o) the system with the highest thrust-to-mass ratio will have the minimum mass for the propulsion system, resulting in maximum payload mass.

$$m_{prop}/m_o = (F/m_o)/(F/m_{prop}) \qquad (1)$$

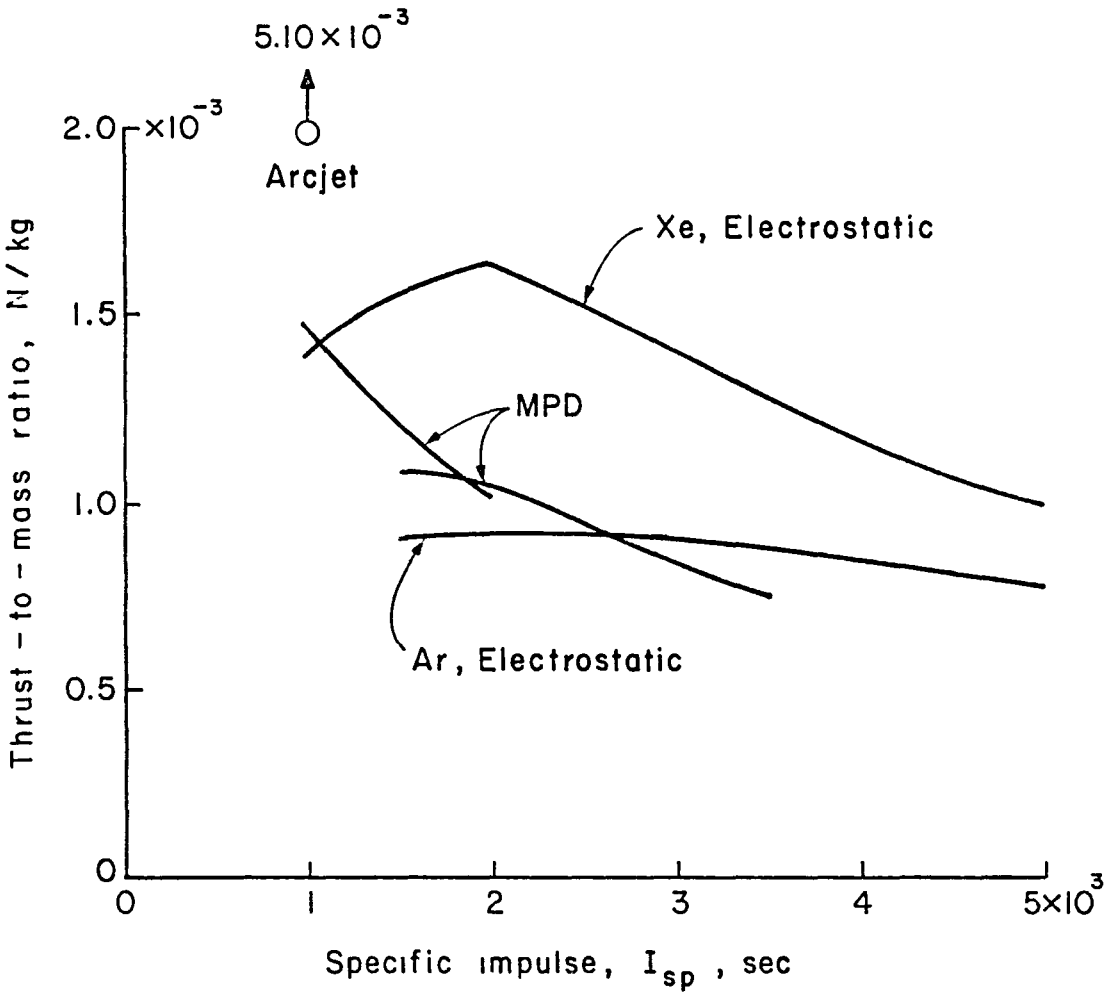

Fig. 1. Comparison of thrust-to-mass ratios for different electric propulsion systems Mass of system as shown includes 15 kg/kW power source, but does not include propellant mass.

The propellant mass is not included in the propulsion system mass as defined for Fig. 1, but it should be evident that this mass should be the same for two vehicles with the same initial mass, the same thrust, the same acceleration, and the same thrusting time. Unless there are other considerations such as cost or reliability, then, the electric propulsion system with the highest thrust-to-mass ratio should always be chosen.

The foregoing applies strictly to a comparison at the same specific impulse. It is possible, though, to make limited comparisons at different specific impulses. Given data over a range of specific impulse for a particular thruster type, with a maximum in the thrust-to-mass ratio, operation at a specific impulse below the peak in this ratio should not be of interest. This is because such operation would result in both increased propellant mass for a given mission and increased propulsion system mass exclusive of propellant. It follows that, in comparing two different electric propulsion systems with the same thrust-to-mass ratio, the one with the higher specific impulse should be preferred.

Returning to Fig. 1, it should be apparent that operation of an electrostatic thruster with Xe is preferred over Ar from a performance viewpoint. Further, operation with Xe below about 2000 sec is undesirable because the thrust-to-mass ratio decreases in that region. Next, the performance of the MPD thruster is inferior to that of the Xe electrostatic thruster, except near 1000 sec, where the arcjet is superior to both. Even at 1000 sec, the MPD performance is not equal to Xe electrostatic performance at 2000 sec, and, because of increased propellant consumption, would be considered definitely inferior. This result was obtained despite some very favorable assumptions for the MPD thruster.

The comparison between the Xe electrostatic and MPD thrusters can perhaps be made more clear with numerical values. At 1950 sec, the maximum for Xe in Fig. 1, the total system mass of the Xe electrostatic thruster is 33.7 kg per kW of electric power from the power source. For the MPD thruster the same system mass is only 22.5. The Xe electrostatic system is clearly much heavier than the MPD system, with less than half of its weight consisting of power source.

When the specific masses of the two systems are divided by the efficiency of converting electric power to thrust, the relative values are reversed. For the electrostatic thruster, the efficiency product (power conditioning times thruster) is 0.530, giving a mass of 63.6 kg per kW of useful beam kinetic energy. For the MPD thruster, the efficiency product is 0.225 (2000 sec), giving 100.0 kg per kW of useful beam energy. It is clear then, that despite optimistic mass assumptions, the low efficiency of the MPD thruster results overall in reduced system performance.

There are, of course, a number of caveats in interpreting Fig. 1. H_2 is required for the arcjet performance shown. If cryogenic storage of H_2 is not possible for the mission lifetime under consideration, the

arcjet would have to operate at either a much lower efficiency or a much lower specific impulse. Further, the MPD performance might be much improved by using other propellants. Finally, the electrostatic thruster is more fully developed than most ion and plasma thrusters, and may therefore be closer to its ultimate capability.

Orbit Raising

Three basic types of orbit-raising or maneuvering missions were considered. One-way missions with the power source included in the propulsion system constituted one basic type, and are shown in Fig. 2. One-way missions in which the power source is considered part of the payload are shown in Figs. 3 and 4. Finally, ten-trip missions with a reusable tug are shown in Fig. 5.

The one-way missions with the power source included in the propulsion system mass, Fig. 2, reflect strongly the thrust-to-mass ratios of Fig. 1. The minimum mission time is roughly inverse to maximum thrust-to-mass ratio. At longer mission times, the thrust-to-mass ratios at higher specific impulses determine the relative order. A 20% payload advantage over chemical propulsion (at 0.247 payload fraction) is possible with a 65 day mission time for an arcjet, while a 50% payload advantage is possible at 126 days. The Xe electrostatic thruster shows a 50% advantage over chemical propulsion at the same 126 day mission time, but cannot match the arcjet at shorter mission times. For a 50% payload advantage over chemical, the Ar electrostatic thruster requires 192 days and the MPD 202 days.

The results shown in Fig. 2 are similar to results shown many times previously. That is, electric propulsion requires mission times of the order of 100-200 days for significant (in this case 50%) payload advantages over chemical propulsion.

Similar calculations with the power source included in the payload are shown in Fig. 3. A power supply being included in the payload might be considered a fortuitous coincidence. However, a little reflection should show that many activities in space will be power intensive, resulting in the frequent need to transport power supplies. For the 15 kg/kW specific mass assumed for the power source, sharp increases are shown for all payload ratios. These increases result, of course, from the shifting of the power source mass to the payload category. Note that the MPD thruster approaches Xe thruster performance for mission times longer than about 90 days. This is because so much power is assumed to be available from the payload, that the low efficiency of the MPD thruster is not much of a penalty. With more limited availability of power, the MPD thruster would not fare as well.

A significant result from Fig. 3, compared to Fig. 2, is the greatly reduced mission times possible for the same payload advantage over chemical propulsion. For the arcjet thruster, a 50% advantage is possible in 30 days, while for the Xe electrostatic thruster a 50% advantage is possible in 68 days.

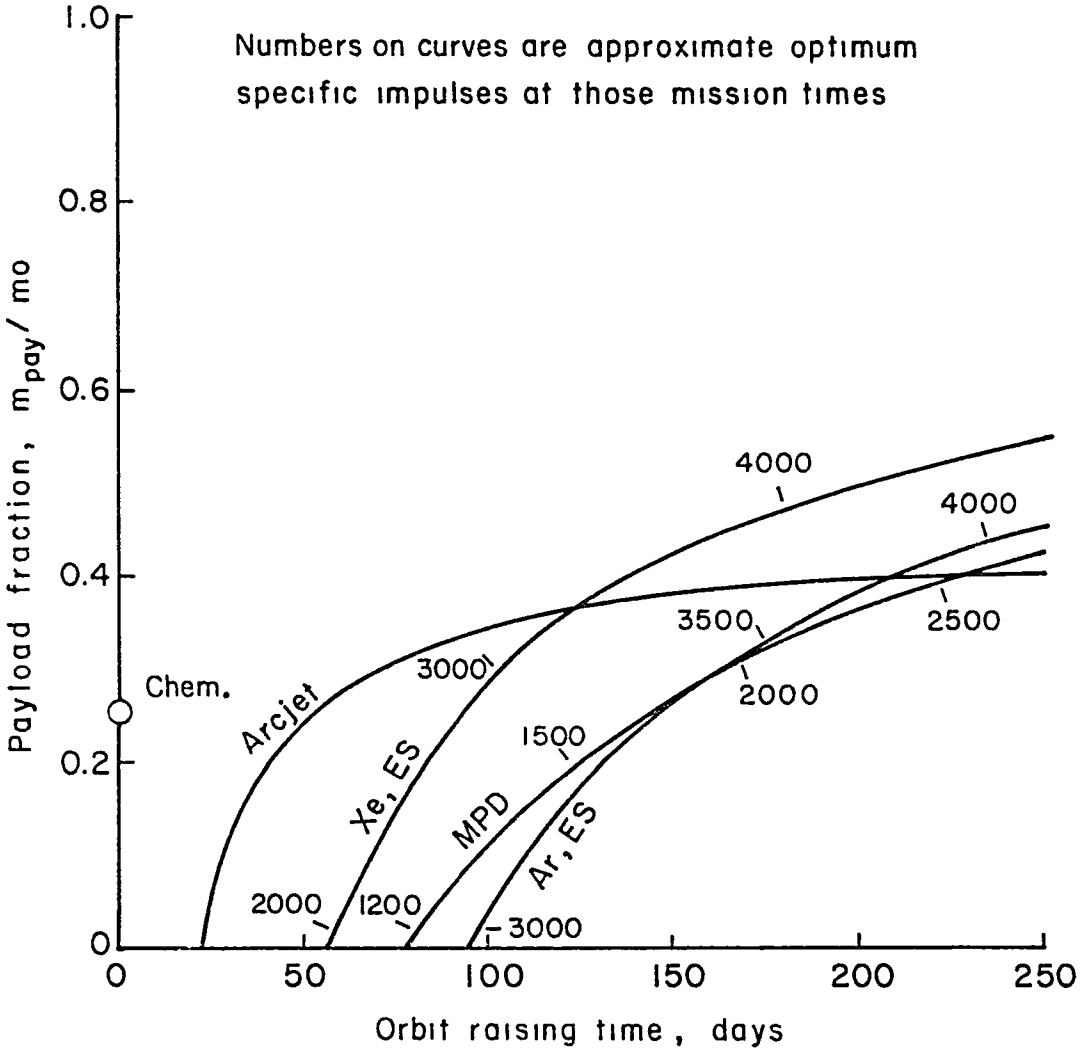

Fig 2. One-way orbit raising mission Power source (15 kg/kW) included in propulsion system mass.

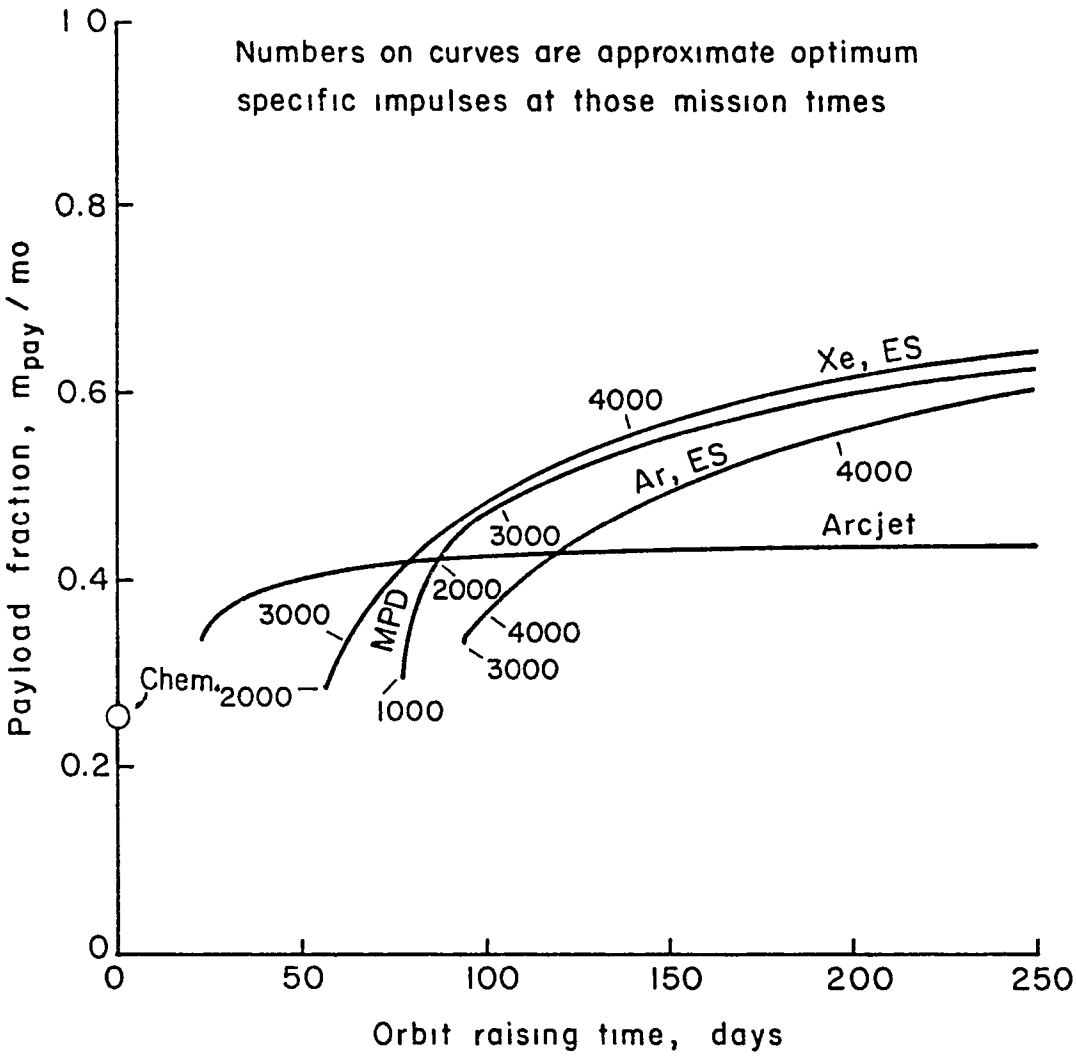

Fig. 3. One-way orbit raising mission. Power source (15 kg/kW) included in payload.

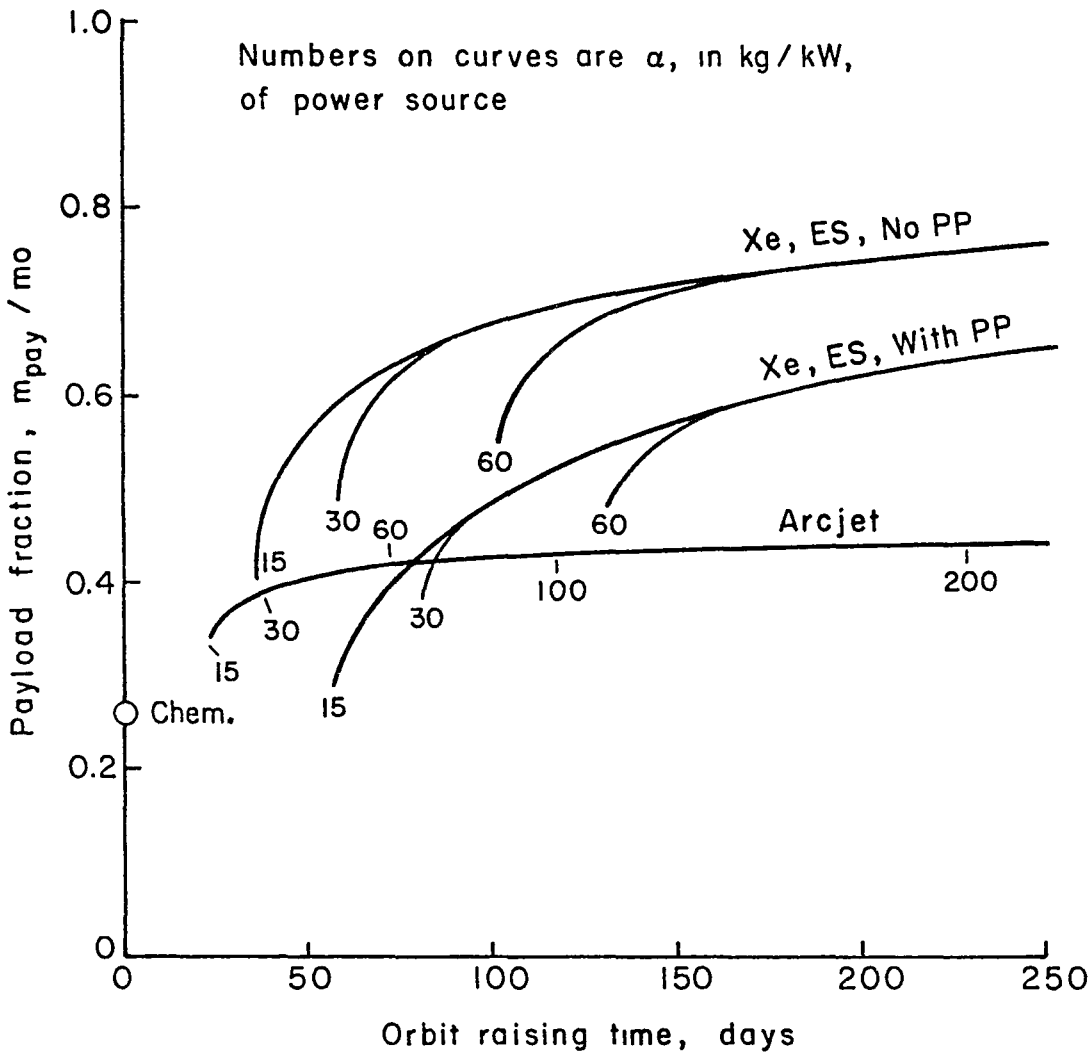

Fig 4. One-way orbit raising mission. Power source (variable kg/kW) included in payload.

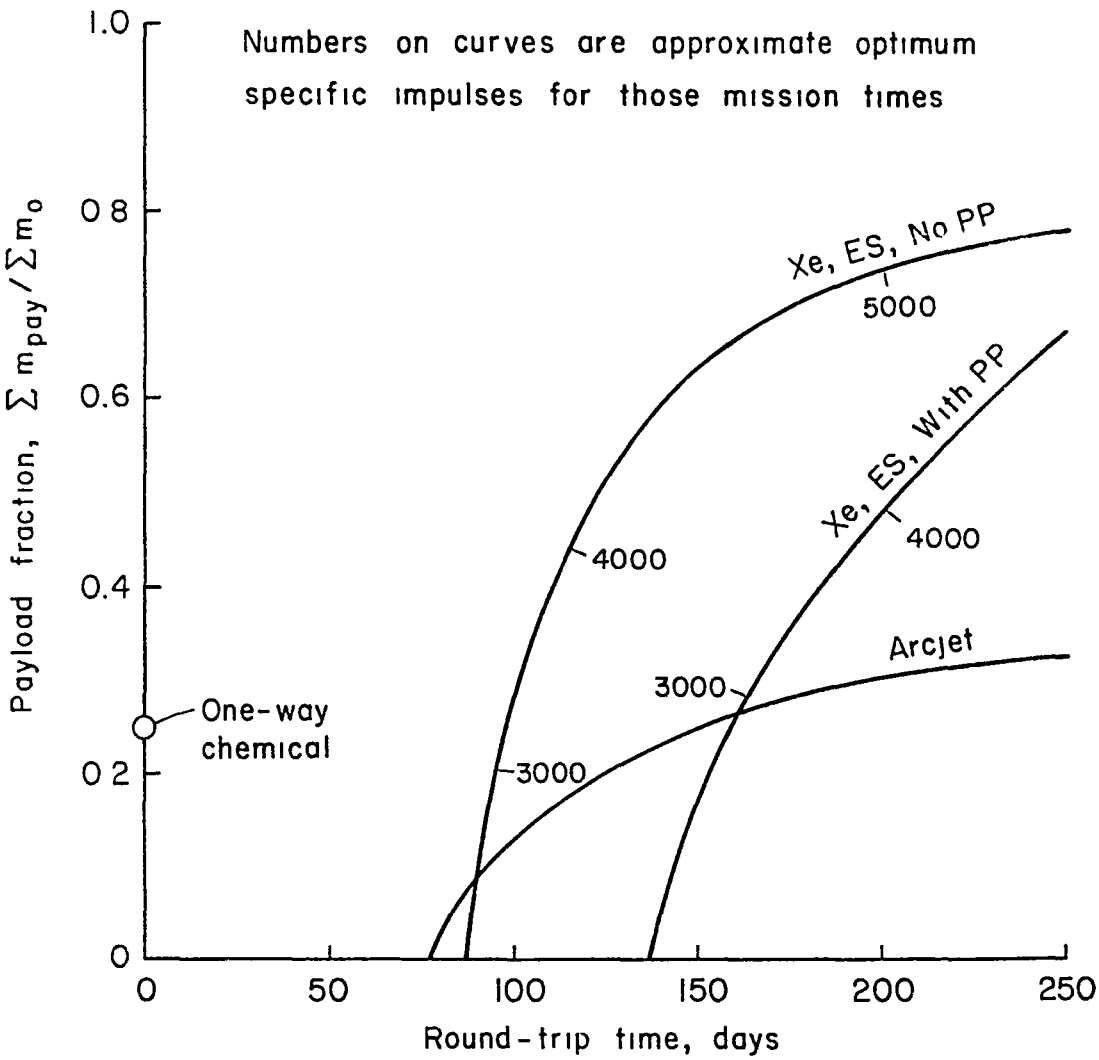

Fig. 5. Ten-trip orbit raising mission. Power source (15 kg/kW) included in propulsion system mass.

A payload that generates power with a specific mass of 15 kg/kW is obviously very power intensive, and probably almost all power source. The more frequent expectation would be that only a fraction of the payload would be power source and the specific mass of the overall payload would be much larger. This situation is indicated in Fig. 4. Because of the added variables included, only curves for the arcjet and Xe electrostatic thruster are shown.

Considering first the Xe electrostatic thruster with power processing, the 15 kg/kW curve for this thruster and the arcjet curve are the same as shown in Fig. 3. The arcjet curve is notable in that increasing the specific mass of the payload has no effect except to limit the minimum mission time. This is because the mission time determines the thruster power level, and with specific impulse limited to 1000 sec, additional power cannot be utilized. For the 50% payload advantage over chemical propulsion cited in connection with Fig. 3, the requirement for the payload is actually about 23 kg/kW, or less. For payloads with higher specific masses, the arcjet mission time would simply stretch out beyond 30 days. To a close approximation, the arcjet mission time is proportional to the specific mass for the payload at these higher values.

For the Xe electrostatic thruster, there are different branches for different payload specific masses. At long mission times, though, the different branches come together. Comparison of the 30 kg/kW Xe curve in Fig. 4 (with power processing) with the 15 kg/kW MPD curve of Fig. 3 will show they are almost identical. What this comparison means is that, for minimum mission times, the MPD thruster requires a more power intensive payload (by about a factor of two) for the same performance. For longer mission times, the specific mass of the payload is not as important, due to possible tradeoffs between specific impulse and efficiency.

Another Xe electrostatic curve is also shown in Fig. 4, for no power processing. The 10 kg/kW power processing mass, together with the efficiency of 0.9, serves to reduce payload capability substantially from that which would otherwise be possible. Reduced power processing requirements have already been investigated,[12] so that the improvement shown in Fig. 4 is based on a present trend. Furthering this present trend would clearly be advantageous in terms of mission capability.

Using a 60 kg/kW specific mass for the payload as a basis of comparison, the arcjet thruster shows a 68% payload advantage over a chemical propulsion, with the mission time for the arcjet about 73 days. For the Xe electrostatic thruster with power processing, the payload advantage is about 96% with a 131 day mission time. Without power processing, the payload advantage is increased to 150% while the mission time is reduced to 103 days. The Xe electrostatic thruster, with or without power processing, shows substantial additional payload advantages for longer mission times.

Performance for the ten-trip tug is indicated in Fig. 5. The power source must here be a part of the propulsion system in order for the tug to make the return trip to low orbit. A greater number of round trips per vehicle would, of course, have shown a greater advantage for this variation. It was felt, though, that a significant advantage, if it exists, should be evident for a ten-trip lifetime.

The chemical rocket is really not practical for a ten-trip tug under the assumptions herein. (Only about 2% of the low orbit mass can be delivered to a geosynchronous orbit, if propellant for the return trip must also be carried along.) The one-way payload capability for a 500 sec chemical rocket is still included, however, as a basis of comparison.

Although readily capable of appreciable payload as a ten-trip tug, the arcjet shows only marginal advantages over one-way chemical propulsion. For a 20% advantage, a round-trip time of about 170 days is required, while for a 50% advantage about 600 days is required. The 1000 sec specific impulse of the arcjet is clearly a limitation for the ten-trip tug mission.

For the Xe electrostatic ten-trip tug, with power processing, a 20% advantage is obtained with a round-trip time of about 164 days, while a 50% advantage requires about 176 days. In 250 days, the advantage can be about 163%.

Without a power processor, the Xe electrostatic thruster shows a 50% advantage in under 110 days. For a 250-day round-trip time, the advantage would be about 216%.

In the interest of simplicity, considerations such as thruster refurbishing have been ignored. It should be clear, though, that significant payload advantages should still be possible using a multiple-trip tug with a Xe electrostatic thruster. These advantages can be enhanced if power processing requirement can be reduced.

In-Orbit Maneuvering

The propulsion system mass fraction required for maneuvering was calculated for a Δv of 3.07 km/sec. If a single large maneuver were required, the Δv requirement for a chemical rocket could be smaller by a few percent. Both storable (425 sec) and cryogenic (500 sec) propellants were considered for chemical propulsion.

The chemical propulsion system is compared to arcjet propulsion in Fig. 6. If an electric power source must be carried along for the exclusive use of the arcjet, equal propulsion system mass requires a cumulative thrusting time of about 24 days (@ 425 sec) and 32 days (@ 500 sec). For a 20% advantage, these times stretch out to about 46 days and 64 days.

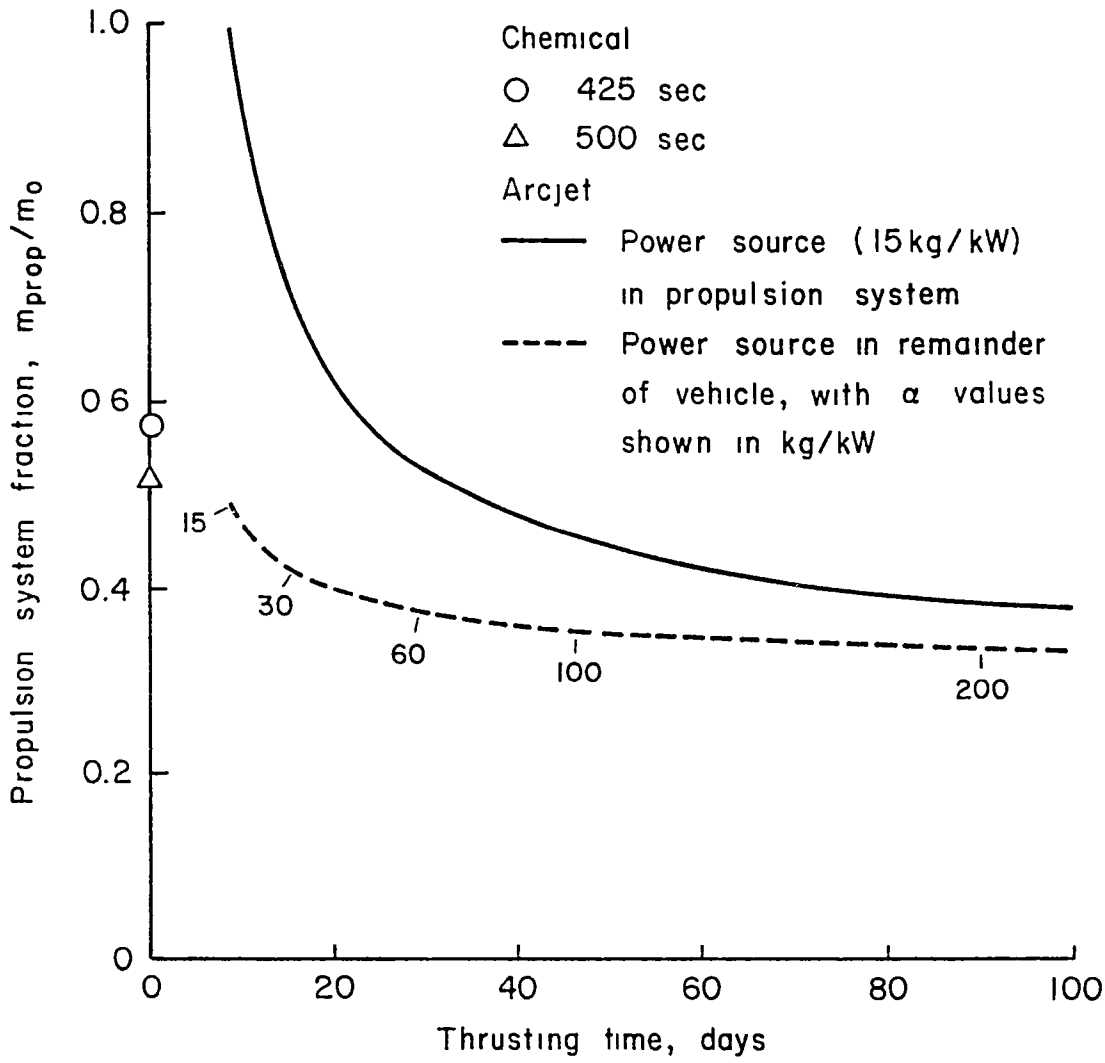

Fig. 6. In-orbit maneuvering capability of arcjet system (Chemical system shown for comparison.)

If the power is assumed to be available from an onboard power source, then the power source does not need to be included in the propulsion system mass. The arcjet performance then becomes dependent on the amount of power available. If the remainder of the satellite, other than the maneuvering propulsion system, has a specific mass of 60 kg/kW, the mass advantage is about 35% (425 sec) and 28% (500 sec) for a thrusting time of about 29 days. Longer thrusting times result in only small decreases in arcjet propulsion mass, but do permit less power intensive satellites to be used effectively. As with orbit raising, the thrusting time varies roughly proportionally with specific mass (kg/kW) of the remainder of the satellite.

The in-orbit maneuvering capability of the Xe electrostatic thruster is shown in Fig. 7. Even with the power processing mass and losses omitted, the Xe thruster requires thrusting times in excess of 50 days to match the mass of the arcjet - when both systems include the power source mass.

If the power source is assumed to be part of the remainder of the satellite, propulsion system advantages can be shown relative to the arcjet, but only for relatively more power intensive satellites.

A point should be made concerning specific impulse of the Xe electrostatic thruster. With thrusting time, propulsion system mass, and specific mass (kg/kW) of the rest of the satellite all variable, a simple optimum in performance is not possible in all cases without additional restrictions. For the lower values of specific mass shown in Fig. 7, a specific impulse of 1950 sec actually gave optimum performance in all respects. For the higher specific masses, the shortest thrusting times were obtained with 1950 sec, with only small mass penalties compared to higher specific impulses.

If higher thrust to mass ratios were possible for the Xe electrostatic thruster below 1950 sec (see Fig. 1), then clearly that performance would be advantageous for some in-orbit maneuvering applications. With the moderate maneuvering Δv assumed herein, the need appears to be for a thruster that can operate efficiently at a specific impulse between the 1000 sec of the arcjet and the minimum practical value of 1950 sec for the Xe electrostatic.

Concluding Remarks

A number of significant conclusions can be drawn from the study presented herein. For orbit raising missions in the next few years, with power sources included in the payloads, the arcjet could show significant 60-70% payload advantages over chemical propulsion. The mission time with an arcjet is primarily dependent on the power available from the payload, but can be well under 100 days for payload specific masses of 60 kg/kW, or less.

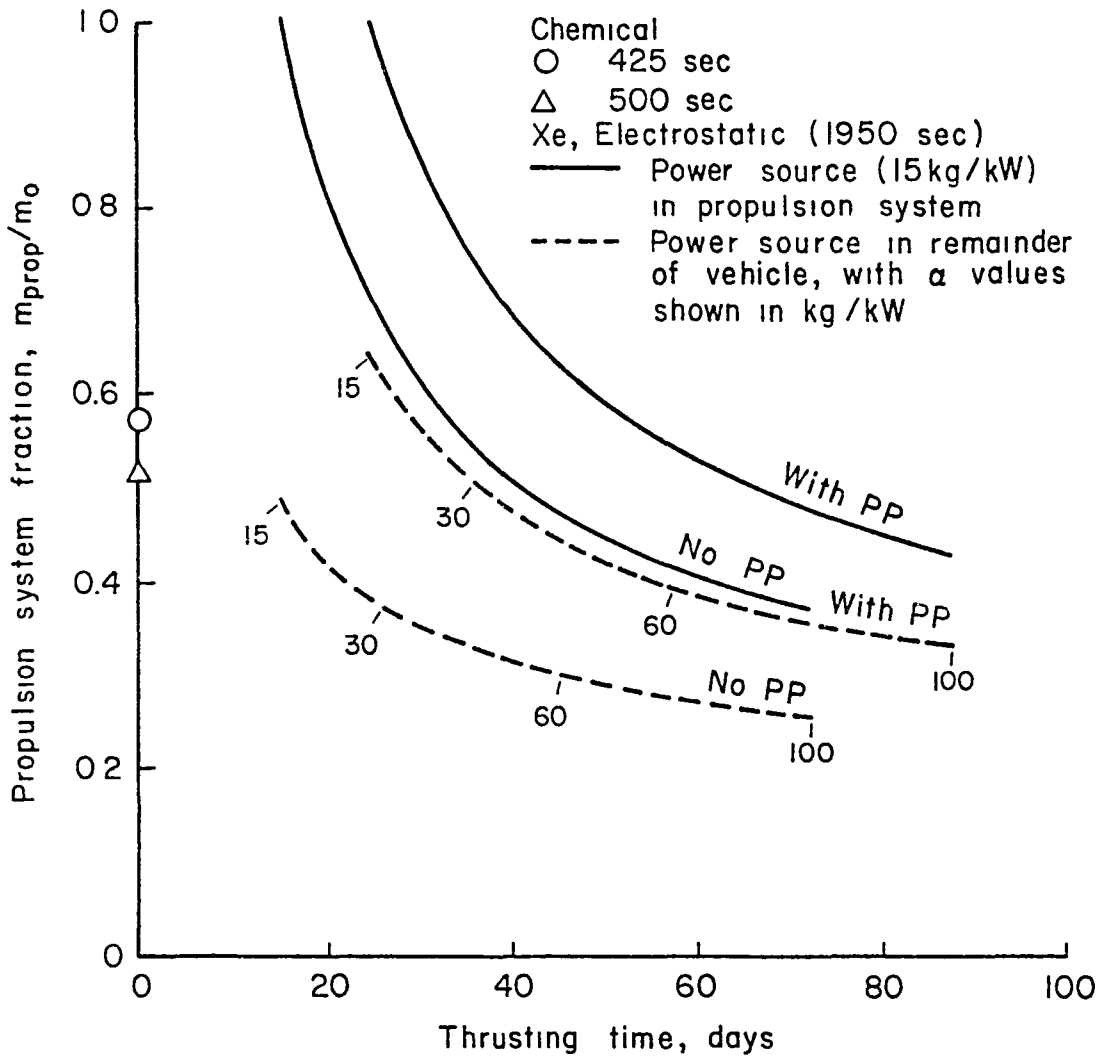

Fig. 7. In-orbit maneuvering capability of Xe electrostatic system. (Chemical system shown for comparison.)

The Xe electrostatic thruster can show further payload gains over the arcjet, presumably for the more distant future. The degree of advantage over the arcjet will depend in a large measure on the power processing required.

Although not calculated in detail, the present 30-cm Hg electrostatic thruster would be expected to approximate the optimized Xe electrostatic thruster in mission capability.

The MPD thruster is penalized by having a very low efficiency. This problem appears to be more serious than the absence of well-developed propellant controls and power processing for pulsed operation.

Multiple-trip orbit raising tugs appear to be practical only for high-efficiency electrostatic thrusters (Xe in this study, but presumably also Hg). Reduction of power processing requirements will greatly increase the practicality of multiple-trip tugs.

There is no clearcut advantage for either the arcjet or the Xe electrostatic thruster in the in-orbit maneuvering application, but the arcjet is generally more promising where short thrusting times are desired and the on-board electric power is limited. It does not appear promising to use either electric thruster type if a power supply must be dedicated solely to maneuvering propulsion.

For future research, it is clear that the arcjet should have a high priority. Actually, this type of thruster should be considered a class, rather than a single type. The tradeoff between additional losses and higher specific impulses should be explored above 1000 sec. The resistojet is also a promising alternative for many arcjet applications. Other alternatives may also exist.

Despite its well developed state, the electrostatic thruster still shows promise of future efficiency improvements. The "ion reflection" technique, in particular, offers a possibility of reduced ion losses to discharge-chamber walls, hence higher electrical efficiency.[13] The advantage of higher efficiency is two-fold. It would permit the substitution of a lighter atomic weight propellant with smaller performance penalties. It would also further reduce the power processing needs, in that a larger fraction of the total power would go into the beam, with the possibility of supplying beam energy by direct coupling to the power source. Note that for the Xe electrostatic thruster, the efficiency is not, in itself, a problem. That is, in the usable range above 1950 sec, the efficiency ranges upwards of 67%.

Although efficient, the Xe electrostatic thruster is not practical for applications below about 2000 sec. The limitation in thrust-to-mass ratio below this specific impulse results primarily from limitations in the electrostatic acceleration process. Some other acceleration process, such as Hall-current acceleration, may permit efficient ion thrusters in the 1500-2000 sec range. Such alternative electric thrusters appear to be desirable research objectives, to permit time-payload compromises intermediate of those possible with either the arcjet or the Xe electrostatic thruster, or their closely related types.

References

1. H. R. Kaufman, "Performance of Large Inert-Gas Thrusters," AIAA Paper No. 81-0720, Apr. 1981.
2. H. R. Kaufman and R. S. Robinson, "Large Inert-Gas Thrusters," AIAA Paper No. 81-1540, July 1981.
3. Lewis Research Center, "30-Centimeter Ion Thrust Subsystem Design Manual," NASA Tech. Mem. TM-79191, June 1979.
4. R. L. Burton, K. E. Clark, and R. G. Jahn, "Thrust and Efficiency of a Self-Field MPD Thruster," AIAA Paper No. 81-0684, Apr. 1981.
5. J. H. Childs and R. J. Cybulski, "SERT and Early Electric Propulsion Systems," Astro. Aerosp. Eng., pp. 112-117, May 1963.
6. W. R. Hudson, "NASA Electric Propulsion Technology Program," AIAA Paper No. 79-2118, Oct./Nov. 1979.
7. H. W. Loeb, et al., "European Electric Propulsion Activities," AIAA Paper, No. 79-2120, Oct./Nov. 1979.
8. L. E. Young, "Solar Array Technology for Solar Electric Propulsion Missions," AIAA Paper, 79-2086, Oct./Nov. 1979.
9. D. Buden, "100-kW_e Nuclear Space Electric Power Source," AIAA Paper, No. 79-2089, Oct./Nov. 1979.
10. D. C. Byers, F. F. Terdan, and I. T. Myers, "Primary Electric Propulsion for Future Space Missions," AIAA Paper No. 79-0881, May 1979.
11. D. C. Byers, "Characteristics of Primary Electric Propulsion Systems, AIAA Paper No. 79-2041, Oct./Nov. 1979.
12. V. K. Rawlin, "Reduced Power Processor Requirements for the 30-cm Diameter Hg Ion Thruster, AIAA Paper No. 79-2081, Oct./Nov. 1979.
13. H. R. Kaufman and R. S. Robinson, "Electric Thruster Research," NASA Contr. Rep. CR-165603, Dec. 1981.

APPENDIX A

Poisson's equation (in SI units) is used to relate the electric potential ϕ to the charge density ρ due to electron and ions.

$$\nabla^2\phi = -\rho/\varepsilon_o \tag{A1}$$

This equation is applied in the pre-sheath region, where the large potential differences relative to plasma potential (which are common in the sheath region) have not been established. It is, however, assumed that any potential difference compared to plasma potential will establish a general streaming of ions in the direction of the electric field, because the energy available is of the order of the electron temperature which is generally much greater than the random ion energy.

The charge density ρ is given by

$$\rho = en_i - en_e \tag{A2}$$

where e is a unit charge and n_i and n_e are the ion and electron concentrations, respectively.

Equilibrium statistical mechanics requires

$$n_e = n_o \exp[e\phi/kT_e] , \tag{A3}$$

where n_o is the concentration of electrons in the unperturbed bulk plasma, T_e is the local electron temperature and k is the Boltzmann constant.

There is a magnetic field present in the sheath region under consideration, i.e., near the outer wall of a multipole discharge chamber. There is some evidence from studies of closed-drift accelerators that

the electron temperature will change with potential in such a region. As a simple first approximation, it will be assumed that the temperature decreases linearly with potential such that

$$T_e(\phi) = T_o - \frac{Re}{k}\,\phi \tag{A4}$$

where T_o is the electron temperature in the bulk plasma and R is a constant of proportionality. Thus,

$$n_e = n_o \exp[e\phi/(kT_o - Re\phi)] \tag{A5}$$

in the region under consideration.

The ion density is given by the streaming condition and the conservation of charge and energy

$$n_i = n_o\,(v_r/v_i) \tag{A6}$$

where v_i is the local ion streaming velocity and v_r is the ion velocity at a reference condition near plasma potential. If variation is only considered in one dimension, Poisson's equation becomes:

$$\frac{d^2\phi}{dx^2} = -\frac{en_o}{\varepsilon_o}\left\{\frac{v_r}{v_i} - \exp[e\phi/(kT_o - Re\phi)]\right\} \quad . \tag{A7}$$

Conservation of energy for the ions requires

$$\frac{1}{2}\,m_i v_r^{\,2} = \frac{1}{2}\,m_i v_i^{\,2} + e\phi \tag{A8}$$

where $\phi = 0$ when $v_i = v_r$. This yields

$$v_i = \left(v_r^{\,2} - \frac{2e\phi}{m_i}\right)^{1/2} , \tag{A9}$$

and Poisson's equation is written as

$$\frac{d^2\phi}{dx^2} = -\frac{en_o}{\varepsilon_o}\left\{v_r\,(v_r^2 - \frac{2e\phi}{m_i})^{-1/2} - \exp[e\phi/(kT_o - Re\phi)]\right\} . \qquad (A10)$$

If $Re\phi/kT_o < 1$, the exponential can be written as

$$\exp[e\phi/(kT_o - Re\phi)] = \exp[\sum_{j=1}^{\infty} \frac{1}{R}\,(Re\phi/kT_o)^j] . \qquad (A11)$$

Expanding the factors of the infinite product and keeping terms to third order in $(e\phi/kT_o)$,

$$\frac{d^2\phi}{dx^2} \approx -\frac{en_o}{\varepsilon_o}\left[v_r(v_r^2 - \frac{2e\phi}{m_i})^{-1/2} - 1 - \frac{e\phi}{kT_o} - (R + \frac{1}{2})\,\frac{e^2\phi^2}{k^2T_o^2}\right.$$

$$\left. - (R^2 + R + \frac{1}{6})\,\frac{e^3\phi^3}{k^3T_o^3}\right] . \qquad (A12)$$

Let the origin of the coordinates be located at the reference position. Integrating the equation:

$$\int_o^x \frac{d^2\phi}{dx^2}\,\frac{d\phi}{dx}\,dx = -\frac{en_o}{\varepsilon_o}\int_{\phi(o)}^{\phi(x)}\left[v_r(v_r^2 - \frac{2e\phi}{m_i})^{-1/2}\right.$$

$$\left. - 1 - \frac{e\phi}{kT_o} - (R + \frac{1}{2})\,\frac{e^2\phi^2}{k^2T_o^2} - (R^2 + R + \frac{1}{6})\,\frac{e^3\phi^3}{k^3T_o^3}\right] d\phi , \qquad (A13)$$

$$\frac{1}{2}\left(\frac{d\phi}{dx}\right)^2\Bigg|_o^x = -\frac{en_o}{\varepsilon_o}\left[-\frac{m_i v_r}{e}\left(v_r^2 - \frac{2e\phi}{m_i}\right)^{1/2} - \phi - \frac{e\phi^2}{2kT_o}\right.$$

$$\left. - \left(R + \frac{1}{2}\right)\frac{e^2\phi^3}{3k^2T_o^2} - \left(R^2 + R + \frac{1}{6}\right)\frac{e^3\phi^4}{4k^3T_o^3}\right]\Bigg|_{\phi(o)}^{\phi(x)} \tag{A14}$$

Letting $\left.\frac{d\phi}{dx}\right|_{x=o} \approx 0$,

$$\frac{1}{2}\left(\frac{d\phi}{dx}\right)^2 = -\frac{en_o}{\varepsilon_o}\left[-\frac{m_i v_r}{e}\left(v_r^2 - \frac{2e\phi}{m_i}\right)^{1/2} + \frac{m_i v_r^2}{e} - \phi - \frac{e\phi^2}{2kT_o}\right.$$

$$\left. - \left(R + \frac{1}{2}\right)\frac{e^2\phi^3}{3k^2T_o^2} - \left(R^2 + R + \frac{1}{6}\right)\frac{e^3\phi^4}{4k^3T_o^3}\right]. \tag{A15}$$

Letting $e\phi < \frac{1}{2}m_i v_r^2$ and keeping terms of order ϕ^3,

$$\frac{1}{2}\left(\frac{d\phi}{dx}\right)^2 \approx -\frac{en_o}{\varepsilon_o}\left\{\frac{m_i v_r^2}{e}\left[\frac{1}{2}\left(\frac{e\phi}{\frac{1}{2}m_i v_r^2}\right) + \frac{1}{8}\left(\frac{e\phi}{\frac{1}{2}m_i v_r^2}\right)^2 + \frac{1}{16}\left(\frac{e\phi}{\frac{1}{2}m_i v_r^2}\right)^3\right]\right.$$

$$\left. - \phi - \frac{e\phi^2}{2kT_o} - \left(R + \frac{1}{2}\right)\frac{e^2\phi^3}{3k^2T_o^2}\right\}. \tag{A16}$$

Then let $E_r \equiv \frac{1}{2}\, m_i v_r^2$,

$$\frac{1}{2}\left(\frac{d\phi}{dx}\right)^2 = -\frac{en_o}{\varepsilon_o}\left[\frac{1}{4}\frac{e\phi^2}{E_r} + \frac{1}{8}\frac{e^2\phi^3}{E_r^2} - \frac{e\phi^2}{2kT_o} - \left(R + \frac{1}{2}\right)\frac{e^2\phi^3}{3k^2T_o^2}\right]. \quad \text{(A17)}$$

Because the left-hand side is the square of the electric field, it must be positive so the factor in brackets must be negative.

$$\frac{1}{4}\frac{e\phi^2}{E_r} + \frac{1}{8}\frac{e^2\phi^3}{E_r^2} - \frac{e\phi^2}{2kT_o} - \left(R + \frac{1}{2}\right)\frac{e^2\phi^3}{3k^2T_o^2} < 0 \quad \text{(A18)}$$

As a check on the procedure, for the moment keep only terms to second order in ϕ,

$$\frac{1}{4}\frac{e\phi^2}{E_r} < \frac{e\phi^2}{2kT_o} \quad \text{(A19)}$$

or,

$$E_r > \frac{kT_o}{2}, \quad \text{(A20)}$$

$$\frac{1}{2}m_i v_r^2 > \frac{kT_o}{2}, \quad \text{(A21)}$$

$$v_r > \sqrt{\frac{kT_o}{m_i}}. \quad \text{(A22)}$$

Thus, to second order in ϕ the Bohm velocity is recovered as the streaming velocity.

Consider now the expression with terms to third order in ϕ.

$$\frac{1}{8}\left(\frac{e\phi}{E_r}\right)^2 + \frac{1}{4}\left(\frac{e\phi}{E_r}\right) < \frac{(R+\frac{1}{2})}{3}\left(\frac{e\phi}{kT_o}\right)^2 + \frac{1}{2}\left(\frac{e\phi}{kT_o}\right) \tag{A23}$$

Completing the square on each side,

$$\left[\sqrt{\frac{1}{8}}\ \frac{e\phi}{E_r} + \sqrt{\frac{1}{8}}\ \right]^2 - \frac{1}{8} \left[\sqrt{\frac{(R+\frac{1}{2})}{3}}\ \frac{e\phi}{kT_o} + \sqrt{\frac{3}{16(R+\frac{1}{2})}}\right]^2 - \frac{3}{16(R+\frac{1}{2})}$$

$$\frac{1}{8}\left(\frac{e\phi}{E_r}+1\right)^2 - \frac{1}{8} < \frac{(R+\frac{1}{2})}{3}\left[\frac{e\phi}{kT_o} + \frac{3}{4(R+\frac{1}{2})}\right]^2 - \frac{3}{16(R+\frac{1}{2})} \quad . \tag{A24}$$

Let $x = kT_o/e\phi$ and $y = E_r/e\phi$. Solving for the limiting condition of equality yields

$$\frac{1}{8}\left(\frac{1}{y}+1\right)^2 - \frac{1}{8} = \frac{(R+\frac{1}{2})}{3}\left[\frac{1}{x} + \frac{3}{4(R+\frac{1}{2})}\right]^2 - \frac{3}{16(R+\frac{1}{2})} \quad . \tag{A25}$$

Setting R = 0 yields a value for the Bohm velocity including third order corrections v_B . Results are stated in dimensionless form as $v_B(R,x)/v_B(0,x)$ to show the effect of various constants of proportionality in the electron temperature variation. This is shown in Fig. A1 as a function of the rate of temperature change R.

From the limiting results, it is clear that a reduction in electron temperature yields a boundary condition modification in terms of reduced ion velocity approaching the sheath. Larger values of R correspond to more abrupt changes in electron temperature. These results are valid only in the transition region from plasma to sheath and should not be extrapolated deep into the sheath. The qualitative trends are in agreement with experimental observations of ion flow.

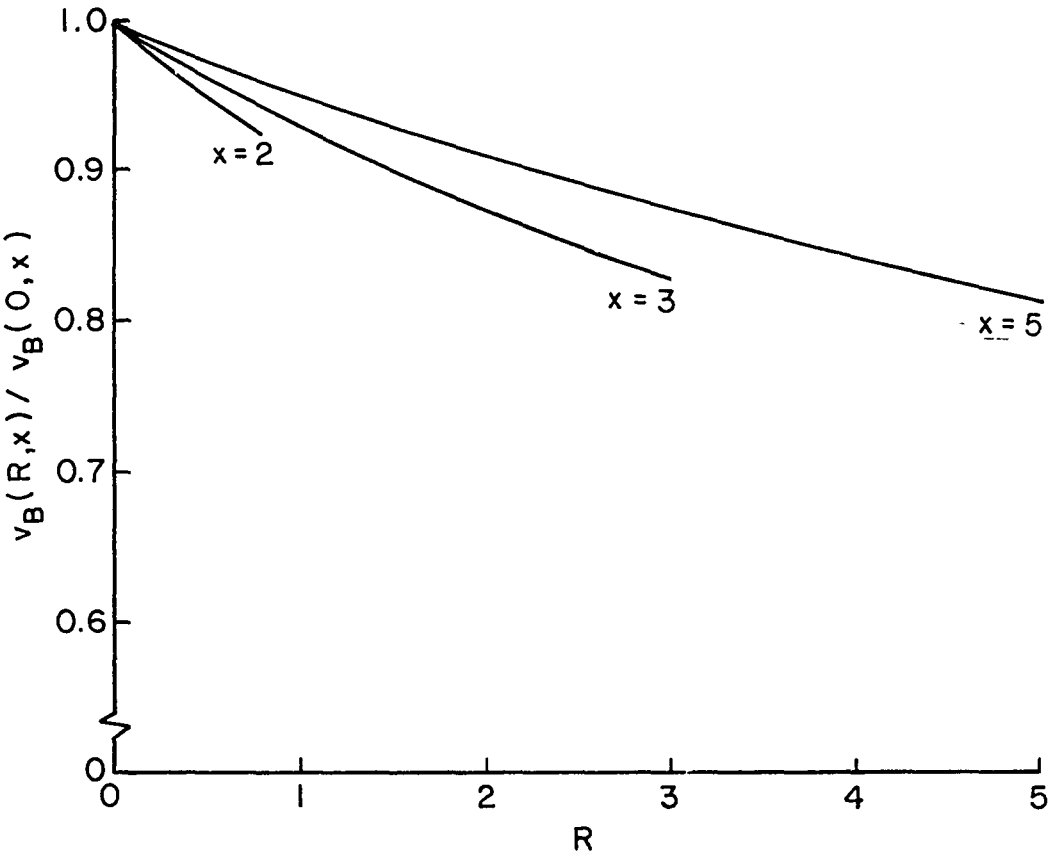

Fig. A1. Ion approach velocity as a function of the rate of electron temperature variation.

APPENDIX B

Optical Pyrometer Measurements

In the hollow cathode studies, temperature measurements were made with an optical pyrometer. The use of the pyrometer required corrections to be made to the pyrometer readings. The corrections were for emissivity (nonblackbody) and the absorption by the vacuum facility glass. The correction for the emissivity is given by[b1]

$$\frac{1}{T_{t,1}} = \frac{1}{T_{obs,1}} + \lambda \frac{\ell n(\varepsilon_\lambda)}{c} \quad , \tag{B1}$$

where $T_{t,1}$ is the true temperature, $T_{obs,1}$ is the observed temperature, λ is the wavelength of the filter in the pyrometer (0.653 μ), ε_λ is the spectral emissivity of the material, and c is a natural constant ($1.4388 \times 10^{+4}$ μ °K).

Temperature measurements were made with three materials, graphite, W, and Ta. Their spectral emissivities at a wavelength of 0.653 μ are given in Table B-1.[b2,b3,b4] It should be noted that the expression for the spectral emissivity of tantalum was a least-squares fit of experimental data.[b4] The correlation coefficient of the fit was 0.734.

The correction for the intensity absorption by the vacuum facility glass is given by[b5]

$$\frac{1}{T_{t,2}} = \frac{1}{T_{obs,2}} + A \quad , \tag{B2}$$

where $T_{t,2}$ is the true temperature of a black body, $T_{obs,2}$ is the observed temperature of a black body and A is the correction for the glass absorption. The temperature of the facility wall should not change significantly during tests, so the value of A should be expected to be independent of the facility-wall temperature.

Combining Eqs. (B1) and (B2) yields

$$\frac{1}{T_t} = \frac{1}{T_{obs}} + \lambda \frac{\ell n(\varepsilon_\lambda)}{c} + A \quad . \tag{B3}$$

Equation (B3) incorporates both temperature corrections. T_t is the true temperature of the nonblackbody material with the glass absorption correction, and T_{obs} is the observed temperature using the pyrometer.

Table B-1. Spectral emissivities of graphite, tungsten, and tantalum at a wavelength of 0.653 μ.

Material	Spectral Emissivity
Tungsten[b2]	$0.4757-2.095\times10^{-5}$ T
Graphite[b3]	$0.745-1.88\times10^{-5}$ T
Tantalum[b4]	$0.5353-5.655\times10^{-5}$ T

To determine the value of A, a thermocouple was spot-welded to a Ta wire. The wire was heated and values of A were calculated from Eq. (B3). The measured values of A are shown in Table B-2. An average value of $A = -3.70 \times 10^{-5}\ ^{\circ}K^{-1}$ was felt to be adequate for all corrections.

Table B-2. Measurements taken to determine the glass absorption at a wavelength of 0.653 μ.

True Temperature (°K)	Correction for Glass Absorption, A ($°K^{-1}$)
1290	-5.08×10^{-5}
1369	-5.49×10^{-5}
1403	-5.79×10^{-5}
1505	-4.79×10^{-5}
1528	-4.52×10^{-5}
1618	-3.32×10^{-5}
1691	-3.39×10^{-5}
1763	-1.52×10^{-5}
1872	-1.92×10^{-5}
1959	-1.16×10^{-5}

References

b1. H. J. Kostkowski and R. D. Lee, "Theory and Methods of Optical Pyrometry," NBS Monograph 41, in Precision Measurements and Calibration, Vol. 2, J. F. Swindelly, ed., NBS SP-300, pp. 361-390, 1968.

b2. R. D. Larrabee, "Spectral Emissivity of Tungsten," J. Opt. Soc. of Amer. 49, p. 619, 1959.

b3. R. J. Thorn and O. C. Simpson, "Spectral Emissivities of Graphite and Carbon," J. Appl. Phys. 24, p. 633, 1953.

b4. W. J. Parker and G. L. Abbott, "Theoretical and Experimental Studies of the Total Emittance of Metals," in Symposium on Thermal Radiation of Solids, S. Katzoff, ed., NASA SP-55, pp. 11-28, 1965.

b5. P. D. Foote, C. O. Fairchild, and T. R. Harrison, "Pyrometric Practice," NBS Technological Paper No. 170, 1921.

End of Document